Ab initio calculation of intermolecular potentials, prediction of second virial coefficients for dimers H_2-H_2, H_2-O_2, F_2-F_2 and H_2-F_2, and Monte Carlo simulations of the vapor-liquid equilibria for hydrogen and fluorine

Inaugural-Dissertation zur Erlangung des Doktorgrades
der Mathematisch-Naturwissenschaftlichen Fakultät

Universität zu Köln

vorgelegt von

Tat Pham Van

aus Vietnam

Köln, Germany

October 2006

Berichterstatter: Prof. Dr. U. K. Deiters

Institut für Physikalische Chemie,

Universität zu Köln

PD. Dr. Thomas Kraska

Institut für Physikalische Chemie,

Universität zu Köln

Tag der letzten mündlichen Prüfung: 6.12.2006

Acknowledgements

ii

Huu Hoa who gave me much help with correcting several computer programs. I got a lot of encouragement from Vietnamese students in Germany, especially from my friends in Aachen.

Finally, I am forever indebted to my parents, Mr. Pham Gia Trieu and Mrs. Ngo Thi Lua, my brothers, sisters, and especially to my wife, Pham Nu Ngoc Han, and my children, Pham Gia Huan and Pham Ngoc Gia Bao for their understanding, endless patience and encouragement.

Köln, September 2006

Tat Pham Van

Institute of Physical Chemistry
University of Cologne
Köln, Germany

Zusammenfassung

Die reinen Elemente Wasserstoff, Fluor und Sauerstoff sowie die Mischungen Wasserstoff-Sauerstoff und Wasserstoff-Fluor besitzen zahlreiche industrielle Anwendungen. Wasserstoff könnte ein erneuerbarer Energieträger bei Brennstoffzellen-Technologien werden und könnte die anderen wichtigen Brennstoffe verdrängen. Daher ist die Berechnung der thermodynamischen Daten der oben genannten Systeme ein wichtiges Anliegen für die praktische Anwendung.

Diese Arbeit enthält die Ergebnisse der Berechnungen der vier *Ab-initio*-Paarpotentiale für die Dimere H_2-H_2, H_2-O_2, F_2-F_2 und H_2-F_2, der daraus abgeleiteten zweiten Virialkoeffizienten einschließlich der Quantenkorrekturen 1. Ordnung sowie der thermodynamischen Phasengleichgewichtsdaten der Reinstoffe Wasserstoff und Fluor, wobei letztere mit der Gibbs-Ensemble-Monte-Carlo-Methode (GEMC) berechnet wurden.

Die neuen intermolekularen Wechselwirkungspotentiale der Dimere H_2-H_2, H_2-O_2, F_2-F_2 und H_2-F_2 wurden mit quantenmechanischen Methoden berechnet, und zwar mit Hilfe der Coupled-cluster-Theorie CCSD(T) und unter Verwendung korrelationskonsistenter Basissätze aug-cc-pVmZ (m = 2, 3, 4); die Ergebnisse wurden zum Basissatzlimit extrapoliert (hier mit aug-cc-pV23Z bezeichnet) und bezüglich des "basis set superposition error" (BSSE) korrigiert. Die so erhaltene Potentialhyperfläche für das H_2-H_2-Dimer stimmt gut mit der von Diep und Johnson [25] vorgeschlagenen Hyperfläche überein. Zum Vergleich wurden auch störungstheoretische Rechnungen mit der Møller–Plesset-Theorie zweiter und vierter Ordnung angestellt sowie Rechnungen mit den Basissätzen 6-31G und 6-311G, aber die Ergebnisse waren schlechter. Für die Abschätzung der Genauigkeiten der theoretischen Methoden und der Basissätze wurden verschiedene molekulare Parameter berechnet.

Die quantenmechanischen Ergebnisse wurden für die Erstellung von vier neuen analytischen Paarpotential-Funktionen verwendet. Die anpassbaren Parameter dieser Funktionen wurden durch Anpassung an die *Ab-initio*-Wechselwirkungsenergien durch eine globale Minimierung der Fehlerquadrate bestimmt, und zwar durch eine Kombination des Levenberg-Marquardt-Verfahrens und eines genetischen Algorithmus. Aus diesen Funktionen wurden die zweiten Virialkoeffizienten von Wasserstoff und Fluor sowie die Kreuz-Virialkoeffizienten der Systeme Wasserstoff–Sauerstoff und Wasserstoff–Fluor durch Integration ermittelt; dabei wurden Quantenkorrekturen berücksichtigt. Die Ergebnisse stimmen mit experimentellen Daten—soweit vorhanden—oder mit empirischen Korrelationen überein.

Monte-Carlo-Simulationen unter Verwendung der Gibbs-Ensemble-Technik (GEMC) wurden eingesetzt, um mit Hilfe der analytischen Paarpotentiale den Dampfdruck von Wasserstoff und Fluor, die Dichten der koexistierenden flüssigen und gasförmigen Phasen, die Verdampfungsenthalpie und -entropie im Temperaturbereich 18–32 K für Wasserstoff und 60–140 K für Fluor zu berechnen. Diese Temperaturintervalle reichen nahe an die kritischen Gebiete der Substanzen heran. Aus den berechneten orthobaren Dichten konnten die kritische Temperatur, der kritische Druck und das kritische Molvolumen abgeschätzt werden. Die Ergebnisse stimmen gut mit experimentellen Daten sowie mit Berechnungen mit Hilfe von Zustandsgleichungen überein. Ferner wurden zur Charakterisierung der Strukturen von Wasserstoff und Fluor die Site-site-Paarkorrelationsfunktionen $g(r)$ ermittelt.

Abstract

The pure elements hydrogen, fluorine and oxygen and the mixtures hydrogen-oxygen and hydrogen-fluorine are used in several industrial applications nowadays. Hydrogen might become a renewable energy carries in fuel cell technologies [122, 16]. Hydrogen is considered a fuel which can replace all the major fuels [46, 95]. Consequently, the estimation of thermodynamic data for the mentioned systems over a wide range of temperature and pressure is a need for future practical applications.

This thesis presents the results of the calculations of four new *ab initio* intermolecular pair potentials, the second virial coefficients with first-order quantum corrections of the dimers H_2-H_2, H_2-O_2, F_2-F_2 and H_2-F_2, and thermodynamic properties of phase equilibria for the pure fluids hydrogen and fluorine derived from the Gibbs ensemble Monte-Carlo simulation techniques.

The new intermolecular interaction potentials of the dimers H_2-H_2, H_2-O_2, F_2-F_2 and H_2-F_2 were developed from quantum mechanics, using coupled-cluster theory CCSD(T) and correlation-consistent basis sets aug-cc-pVmZ (m = 2, 3, 4); the results were extrapolated to the complete basis set limit (denoted aug-cc-pV23Z). The constructed potential energy surface of the dimer H_2-H_2 turned out to be in good agreement with that proposed by Diep [25]. The interaction energies were corrected for the basis set superposition error (BSSE) with the counterpoise scheme. For comparison also Møller-Plesset perturbation theory (at levels 2 to 4) as well as the basis sets 6-31G and 6-311G were investigated, but the results proved inferior. Molecular properties were calculated for assessing the accuracy level of each theoretical method and the basis set, respectively. The quantum mechanical results were used to establish four new analytical pair potential functions. The adjustable parameters of these functions were determined by global least square fits to the *ab*

initio interaction energy values by means of the Levenberg-Marquardt (LM) and the Genetic algorithm (GA). From these functions the second virial coefficients of hydrogen and fluorine as well as the cross virial coefficients of the systems hydrogen-oxygen and hydrogen-fluorine were obtained by integration; corrections for quantum effects were included. The results agree well with experimental data, if available, or with empirical correlations.

Gibbs ensemble Monte Carlo (GEMC) simulation techniques were used to examine the ability of analytical intermolecular pair potential functions constructed from quantum mechanical calculations. Four intermolecular potential functions of hydrogen and fluorine developed in present thesis, were used for these GEMC-simulations to obtain the densities of the vapor-liquid coexisting phases, the vapor pressure, the enthalpy of vaporization, the entropy of vaporization and the boiling temperature in the temperature range from 18 K to 32 K for hydrogen and from 60 K to 140 K for fluorine. These temperature ranges come close to the critical region of the substances. The structural properties of the pure fluid hydrogen and fluorine were characterized with the site-site pair correlation functions $g(r)$. The critical temperature, density, pressure and volume of hydrogen and fluorine were estimated from the densities of vapor-liquid equilibria, and the vapor pressures were derived from the GEMC-NVT simulations. The obtained results agree with experimental data and with computed data resulting from the equations of state and the simulations using the Lennard-Jones potentials.

Contents

List of Figures

List of Tables

Chapter 1

Introduction

Hydrogen, fluorine and the mixtures hydrogen-oxygen and hydrogen-fluorine are used in several industrial areas. Hydrogen in its liquid form has been used as a fuel in space vehicles for years [95]. It could become the most important energy carrier of tomorrow [59]. Liquid hydrogen, oxygen and fluorine are the usual liquid fuels for rocket engines [122, 58, 2, 3]. The National Aeronautics and Space Administration (NASA) is the largest user of liquid hydrogen in the world [16, 41]. The knowledge of thermodynamic properties of the pure substances hydrogen, fluorine and the mixtures hydrogen-oxygen and hydrogen-fluorine are important for practical applications. It is also necessary for their safe use [46, 76].

Computer simulations have expanded in number, complexity, and importance over the last many years [4]. Computers permit the study of systems for which analytical solutions are not available or require approximation techniques. Molecular simulations have been used for various studies [35]. The properties of the studied systems are determined solely by the intermolecular forces and energies [35, 4]. Therefore, simulations have become a necessary tool for studying fluids and fluid mixtures. They can generate structural and thermodynamic as well as transport properties consistently without the need to introduce artificial simplifications as required by integral equation techniques, and statistical thermodynamic perturbation theory [35, 4]. Computer simulation techniques, Monte Carlo as well as Molecular Dynamics, cannot work without some input. It is necessary to know the interaction potentials of the systems under study.

Monte Carlo simulation is used to calculate widely phase equilibria of both poly-
meric and low molecular organic substances. The field of phase equilibria simulation
is now highly developed and very broad in techniques and applications. Some re-
cently published works, are de Pablo et al. (1998 and 2000) [87, 86], Delhommelle et
al. (2000) [123], Martin and Siepmann (1998 and 1999) [71, 72] and Spyriouni et al.
(1998) [112]. Gibbs ensemble simulation had been developed by Panagiotopoulos
(1987) [91]. The basic idea in the Gibbs ensemble method is to simulate phase co-
existence properties by following the evolution in phase space of a system composed
of two distinct regions. The two regions in the simulation system represent the two
coexistence phases, e.g. a vapor in equilibrium with a liquid at saturation. However,
there are no physical interfaces between the two regions. In general, the two regions
have different densities and compositions, while they are at thermodynamic equilib-
rium with each other. Although the Gibbs ensemble simulation considers chemical
equilibria between coexisting phases, it does not require an explicit calculation of
the chemical potential. Due to its simplicity, the Gibbs ensemble method became
the choice for simulating phase equilibria in the past decade.

Gibbs Ensemble Monte Carlo simulation has become a useful tool to estimate the
phase equilibria of several pure substances and their binary and ternary mixtures.
Gibbs ensemble Monte Carlo simulation technique was used for

- Pure components: It permits simulation of vapor-liquid coexistence points for
  any pure component system at a given temperature.

- Mixtures: It permits simulation of vapor-liquid and liquid-liquid coexistence
  points for binary and ternary systems at any given temperature and pressure.

- Critical constants: It permits prediction of critical points based on a supplied
  set of pure component coexistence points.

Vapor-liquid equilibria can also be estimated with several equations of state and
with Monte Carlo simulation using analytic potential functions, in which the usual
procedure is to assume a simple model potential, e.g., the Lennard-Jones pair po-
tential (1924) [63] and the Morse potential (1929) [81], fit its parameters to suitable
experimental data, and then to perform the simulation. Such a simulation is no
longer predictive, because it requires an experimental input of the same kind that it

produces. This can sometimes be a severe limitation, namely if experimental data are scarce.

Recently an alternative approach has become feasible, for which the name "global simulation" has been coined by H. Popkie et al. (1973) [97]. It consists of a calculation of intermolecular potentials by quantum mechanical methods, followed by computer simulations and eventually calculations with equations of state fitted to the simulation results, in order to obtain properties that are not accessible to simulations. Such global simulations have been reported for the noble gases, where it is now possible to predict the vapor-liquid phase equilibria without recourse to experimental data with an accuracy comparable to the experimental uncertainty. One of the first attempts that achieved near-experimental accuracy was that of Deiters, Hloucha and Leonhard (1999) [23] for neon. Further global simulation attempts for noble gases were published by the groups of Eggenberger and Huber [29, 126, 96], Sandler [37], and Malijevský [69]. Using a functional form for the dispersion potentials of argon and krypton proposed by Korona et al. [56], Nasrabad and Deiters (2003, 2004) even predicted phase high-pressure vapour–liquid phase equilibria of noble-gas mixtures [84, 85]. Other mixed-dimer pair potentials for noble gases were published by López Cacheiro et al. (2004) [7], but they were not used for phase equilibria predictions, yet.

The development of *ab initio* pair potentials for molecules is much more complicated because of the angular degrees of freedom of molecular motion, but for some simple molecules such potentials have already been constructed: Leonhard and Deiters (2002) used a 5-site Morse potential to represent the pair potential of nitrogen [65] and were able to predict vapour pressures and orthobaric densities. Bock et al. (2000) also used a 5-site pair potential for carbon dioxide [5]. There have been other attempts to develop a pair potential function for hydrogen. Recently such a potential was published by Diep and Johnson (2000) [25, 26], who performed calculations with post-SCF methods MP2, MP3, MP4, and CCSD(T) and with the basis sets aug-cc-pVmZ (m=2, 3, 4), including extrapolation to the basis set limit. This pair potential, however, uses a spherical harmonics expansion to account for the anisotropy of interaction. Such an approach can become problematic, however, if repulsion at short ranges becomes the dominant feature of a fluid, e.g., in a dense

liquid state; they furthermore applied the first-order quantum correction to the 2nd virial coefficients developed by Pack (1983) [89] and Wang Chang [45]. Naicker et al. (2003) [83] used SAPT (symmetry-adapted perturbation theory) to develop a 3-site pair potential for hydrogen chloride, based on Korona's function and a modified Morse potential; they then successfully predicted the vapour–liquid phase equilibria of hydrogen chloride with GEMC (Gibbs ensemble Monte Carlo [92]) simulations.

Research objectives

The *ab initio* intermolecular pair potentials of the dimers H_2-H_2, F_2-F_2, H_2-O_2 and H_2-F_2 should be calculated from quantum mechanics, using the level of theory CCSD(T) and correlation-consistent basis sets aug-cc-pVmZ (m = 2, 3, 4). Then the quantum mechanical results should be used to construct four new analytical potential functions of these dimers. The second virial coefficients of the dimers H_2-H_2, F_2-F_2 and the cross second virial coefficients of the dimers H_2-O_2 and H_2-F_2 have to be determined by integration of these functions. The thermodynamics of vapor-liquid equilibria as well as the structural properties of pure fluids hydrogen and fluorine should be derived from GEMC simulations using those potentials.

To achieve these goals, the thesis has the following four specific objectives:

- Calculations from quantum mechanics: Constructing the angular orientations of the dimers H_2-H_2, H_2-O_2, F_2-F_2 and H_2-F_2; calculating the *ab initio* intermolecular energies for all built orientations, and single-molecule properties of some representational orientations from quantum chemical methods CCSD(T), MPn (n =2, 3, 4) and basis sets; correcting the energy results for the basis set superposition error (BSSE) with the counterpoise method; extrapolating the interaction energies to the complete basis set limit aug-cc-pV23Z.

- Construction of analytical potential functions: Developing four new 5-site *ab initio* intermolecular potentials of the dimers H_2-H_2, H_2-O_2, F_2-F_2 and H_2-F_2 along the proposed potentials of carbon dioxide [5], nitrogen [65] and hydrogen chloride [83]; estimating the adjustable parameters of these analytical potential functions with the fit to *ab initio* intermolecular energies combining the Levenberg-Marquardt (LM) and the Genetic Algorithm (GA); evaluating the accuracy of the fit upon the statistical results of analysis.

- Prediction of virial coefficients: Calculating the second virial coefficients of hydrogen, fluorine and the cross second virial coefficients of the dimers hydrogen–oxygen and hydrogen-fluorine by 4D numerical integrals for the constructed potential functions; eventually including corrections for quantum effects; comparing the accuracy of the obtained virial coefficients of this work with the experimental data and with results from the correlation equations and equations of state.

- Simulation of the phase equilibria: Carrying out GEMC-NPT and NVT simulations using the four developed *ab initio* 5-site intermolecular potentials of hydrogen and fluorine for the temperature range from 18 K to 32 K for hydrogen and from 60 K to 140 K for fluorine; calculating the thermodynamic properties and the critical point of the fluids hydrogen and fluorine from the obtained densities of coexisting phases and vapor pressures; comparing the results in this work with experimental data and with results from equations of state.

Outline of the thesis

This thesis consists of five chapters and five appendices.

Chapter 1: This chapter gives an introduction to important applications and properties of hydrogen, oxygen and fluorine, and their mixtures; it presents the simulation methods are being used recently for the prediction of the thermodynamic properties of several systems; also the major objectives of this thesis are shown in here.

Chapter 2: This chapter describes the theoretical background for the *ab initio* calculations, the basis sets and the intermolecular pair potentials, for the calculations of the second virial coefficients with quantum effects, the equations of state, Levenberg-Marquardt (LM) and the Genetic Algorithm (GA) used for the least-square fit, the Metropolis algorithm, and the Gibbs ensemble Monte Carlo simulations.

Chapter 3: This chapter contains the methodologies, requirements and means of

calculation, in which all are extracted upon the theoretical background; the computer programs and materials used for this thesis are shown here; the four new intermolecular potentials used for the calculation of the virial coefficients and GEMC simulations are shown here too; this chapter also contains the simulation details which are needed for the prediction of the vapor liquid equilibria.

Chapter 4: This chapter presents the discussion following the calculation results which have been obtained from the performing stages. The results are compared with experimental data.

Chapter 5: This chapter summarizes and discusses the achievements of the thesis, and gives recommendation for future work.

Chapter 2

Theoretical Background

2.1 *Ab initio* implementations

Quantum mechanics (QM) provides an accurate mathematical description of the
behavior of electrons. QM is used in chemistry to predict many properties of an
individual atom or molecule. In practice, the QM equations can only be solved ex-
actly for one-electron systems. QM methods have been developed for approximating
the solutions for multiple-electron systems. The energies and wave-functions of a
system are given by the solutions of the Schrödinger Equation [43, 14]:

$$\widehat{H}\Psi = E\Psi \tag{2.1}$$

where $\widehat{H}$ is the Hamiltonian operator, which in this case gives the kinetic and po-
tential energies of atomic nuclei and electrons. The wave-function Ψ depends on the
coordinates of the electrons and the nuclei. The Hamiltonian consists of kinetic and
potential energy terms, in general,

$$\widehat{H} = -\frac{h^2}{8\pi^2} \sum_i^{\text{particles}} \frac{1}{m_i}\left(\frac{\partial^2}{\partial x_i^2} + \frac{\partial^2}{\partial y_i^2} + \frac{\partial^2}{\partial z_i^2}\right) + \frac{1}{4\pi\varepsilon_0} \sum^{\text{particles}} \sum_{i<j} \frac{q_i q_j}{r_{ij}} \tag{2.2}$$

where m_i and q_i are the mass and charge of particle i, and r_{ij} is the distance of be-
tween particles. The first term gives the kinetic energy of the particle. The second
term represents the Coulombic attraction or repulsion of particles.

The Born-Oppenheimer approximation simplifies Eq. 2.3 by separating the nuclear

and electron motions. The Hamiltonian for a molecule with stationary nuclei is

$$\widehat{H} = -\frac{1}{2} \sum_{i}^{\text{electrons}} \left(\frac{\partial^2}{\partial x_i^2} + \frac{\partial^2}{\partial y_i^2} + \frac{\partial^2}{\partial z_i^2} \right)^2 - \sum_{i}^{\text{nuclei}} \sum_{j<i}^{\text{electrons}} \frac{Z_i}{r_{ij}} + \sum^{\text{electrons}} \sum_{i<j} \frac{1}{r_{ij}} \quad (2.3)$$

Here the first term corresponds to the kinetic energy of the electrons, the second to the attraction of electrons to nuclei, and the third to the repulsion between electrons. The repulsion between nuclei is defined at the end of the calculation [43, 14, 13, 48].

2.1.1   Electron correlation methods

The Hartree-Fock method provides approximate solutions to the Schrödinger equation by replacing the real electron-electron interaction with an average interaction. The Electron Correlation (EC) energy is the energy difference between the HF and the lowest possible energy in each basis set. It is due to a correlation between the motion of electrons. For systems and states where correlation effects are important, the Hartree-Fock results will not be satisfactory [34]. QM methods have been developed to include some effects of electron correlation [13, 48, 34].

Three main correlation correction methods are Configuration Interaction (CI), Many Body Perturbation Theory (MBPT), and Coupled-Cluster (CC). The Coupled-Cluster method presents the most successful approach to accurate many-electron molecular solutions. It might applied to relatively large systems and is capable of recovering a large part of the correlation energy [13, 48, 34].

In practice the Coupled-Cluster method is restricted to large systems with multi-electron configurations. However the Coupled-Cluster wave function provides an accurate correlation to the Hartree-Fock description [13, 48, 34].

Configuration Interaction (CI)

Configuration Interaction (CI) methods constructed by replacing one or more occupied orbitals in Hartree-Fock determinant with a virtual orbital. The wave function

of the system is represented as the linear combination of these multiple determinants [13].

$$\Psi = c_0\Psi_{\text{HF}} + c_1\Psi_1 + c_2\Psi_2 + ... \tag{2.4}$$

Here the coefficients c_i are the weights of each determinant in the expansion and ensure normalization.

The full CI method builds wave-functions by the linear combination of the Hartree-Fock determinant and all possible substituted determinants [48, 13];

$$\Psi = c_0\Psi_{\text{HF}} + \sum_{s>0} c_s\Psi_s \tag{2.5}$$

Here the first term in right side is the Hartree-Fock determinant, and s runs over all possible substitutions.

Møller–Plesset perturbation theory

Møller and Plesset (1934) [48, 13] proposed a convection for correlation as a perturbation from the Hartree-Fock wave-function. It is called Møller–Plesset perturbation theory. The minimal correlation is the second-order MP2 method. Third-order MP3 and fourth-order MP4 calculations are also possible. The results of an MP4 calculation is equivalent to a CISD calculation. MP5 and higher calculations are seldom carried out due to the high computation time [62, 48].

In the Møller–Plesset perturbation theory the perturbed Hamiltonian, H_λ is defined as

$$H_\lambda = H_0 + \sum_{i=1}^{\infty} \lambda^i H_i \tag{2.6}$$

Here λ is an expansion coefficient. The n-electron integral over H_0 is equal to the sum over the one-electron eigenvalues of the Fock Operator.

The exact ground-state wave function and energy Ψ_λ and E_λ of a system described

by the full Hamiltonian H_λ can be expanded in powers of λ [62, 34].

$$\Psi_\lambda = \Psi^{(0)} + \lambda\Psi^{(1)} + \lambda^2\Psi^{(2)} + ...$$
$$E_\lambda = E^{(0)} + \lambda E^{(1)} + \lambda^2 E^{(2)} + ... \tag{2.7}$$

Insertion of the exact wave function and energy into the Schrödinger equation yields

$$(H_0 + \lambda V)(\Psi^{(0)} + \lambda\Psi^{(1)} + ...) = (E^{(0)} + \lambda E^{(1)} + ...)(\Psi^{(0)} + \lambda\Psi^{(1)} + ...) \tag{2.8}$$

After expanding the results, the coefficients on each side of the equation can be equated for each power of λ, leading to a set of relations representing successively higher orders of perturbation.

$$(H_0 + \lambda E^{(0)})\Psi^{(0)} = 0$$
$$(H_0 + E^{(0)})\Psi^{(1)} = (E^{(1)} - V)\Psi^{(0)} \tag{2.9}$$
$$(H_0 + E^{(0)})\Psi^{(2)} = (E^{(1)} - V)\Psi^{(1)} + E^{(2)}\Psi^0$$

The correction of energy and wave function at corresponding order can be obtained by solving the equation for each order of λ, [13, 34].

Coupled-Cluster theory

Today, Coupled-Cluster (CC) theory is probably the most accurate and best applicable approach for the treatment of molecular systems. The Coupled Cluster (CC) method was developed in the late 1960s by Cizek (1966) [11, 13, 48], but it was not until the late 1970s that the practical implementation began to take place and until 1982 that the key stone of modern implementation, CCSD (Coupled Cluster with single and double excitation) [98], was presented.

The size consistency problem of CI is solved by using the CC method to form a wave-function where the excitation operators are exponentiated [11, 13, 48]

$$\psi_{CC} = \exp(T)\psi_C \tag{2.10}$$

The cluster operator T is defined as $T = T_1 + T_2 + T_3 + ... + T_n$
and T_n is a linear combination of all n-type excitations. n the total number of

electrons and the various T_i operators generate all possible determinants having i excitations from the reference.

$$T_1 \Psi_C = \sum_i \sum_a C_i^a \Psi_i$$
$$T_2 \Psi_C = \sum_{i>j} \sum_{a>b} C_{ij}^{ab} \Psi_{ij}^{ab}$$

(2.11)

Here C_i^a and C_{ij}^{ab} are the coefficients to be determined

$$\Psi_{CCSD} = \Psi_0 + \sum_a \sum_i C_i^a \Psi_i^c + \sum_{i>j} \sum_{a>b} C_{ij}^{ab} \Psi_{ij}^{ab}$$
$$+ \frac{1}{2} \sum_{cb} \sum_{ij} C_i^c C_j^b \Psi_{ij}^{cb} + \frac{1}{2} \sum_{a>b} \sum_{c>d} \sum_{i>j} \sum_{k>l} C_{ab}^{ij} C_{cd}^{kl} \Psi_{ijkl}^{abcd} + \dots$$

(2.12)

This appears to be the advantage of CC theory: Higher excitations are included, but their coefficients may be determined by the excitations of lower order. The coefficients are determined by projecting Schrödinger's equation on the left with the configurations generated by the $\hat{T}$ operator. This replaces the eigenvalue problem by a non-linear simultaneous system [39].

Coupled cluster calculations can be similar to configuration interaction calculations, in which the wave function is a linear combination of many determinants [13, 34, 48]. The method used in this work, CCSD(T), includes triple excitations perturbatively rather than exactly. Coupled Cluster calculations give variational energies as long as the excitations are included successively [13, 34, 48].

2.1.2 Basis sets

Ab initio methods try to get accurate information by solving the Schrödinger equation without fitting parameters to experimental data. Actually, *ab initio* methods also make use of experimental data in a rather subtle way. These methods use several approximations for solving the Schrödinger equation. One of the approximations inherent in essentially all *ab initio* methods is the use of basis sets [13, 48].

An individual molecular orbital is defined as [34]:

$$\psi_i = \sum_{\mu=1}^{N} c_{\mu i} \Phi_\mu \tag{2.13}$$

here the coefficients $c_{\mu i}$ are known as the molecular orbital expansion coefficients. The basis functions $\Phi_{1...N}$ are assumed to be normalized. Thus Φ_μ refers to an arbitrary basis function in the same way that ψ_i refers to an molecular orbital.

In HF calculations the wave function need to be described by mathematical functions, which are known well for a few one-electron systems only. This is the second approximation of the HF calculation. The functions used most often are linear combinations of Gaussian-type orbitals $\exp(-ar^2)$, denoted GTO. Amongst the used split-valence basis sets are those of Pople et al. [13] including the basis sets 3-21G, 6-21G, 4-31G, 6-31G, and 6-311G. The first number indicates the number of primitives used in the contracted core functions. The numbers after the hyphen indicate the numbers of primitives used in the valence functions. If there are two numbers, it is a valence-double-ζ basis, is there are three, valence-triple-ζ [13, 34, 48].

Split-valence basis set: the 6-31G basis sets

For the basis set 6-31G the core orbitals are a contraction of six primitive GTOs (PGTOs), the inner part of the valence orbitals is a contraction of three PGTOs and outer part of the valence is represented by one PGTO. The designation of the carbon/hydrogen 6-31G basis is (10s4p/4s) $\rightarrow$ [3s2p/2s]. This basis set is only strictly defined for hydrogen through fluorine [48, 13].

The basis set 6-31G(p1,p2) where p1 can be d, 2d, 3d, f, df, 2df or 3df and p2 can be p, 2p, 3p, d, pd, 2pd or 3pd. 6-31G* can be used instead of 6-31G(d) and 6-31G** is the same as 6-31G(d,p). The 6-31+G basis will add diffuse s- and p-orbitals on all non-hydrogen atoms and 6-31++G also adds diffuse s-functions on all hydrogen atoms [48].

Split-valence basis set: the 6-311G basis sets

For the basis set 6-311G the core orbitals are also a contraction of six primitive GTOs (PGTOs); This basis set is only strictly defined for hydrogen through fluorine [48, 13].

The general form of the basis set is 6-311G(p1,p2) where p1 can be d, 2d, 3d, f, df, 2df or 3df and p2 can be p, 2p, 3p, d, pd, 2pd or 3pd. 6-311G* can be used instead of 6-311G(d) and 6-311G** is the same as 6-311G(d,p). The 6-311+G basis will add diffuse s- and p- orbitals on all non-hydrogen atoms and 6-311++G also adds diffuse s-functions on all hydrogen atoms [48, 13].

Correlation consistent basis sets

A set of basis sets for correlated calculations has also been developed by Dunning et al (1970) [51, 52, 53]. These basis sets are called as correlation consistent (or *cc*) and are designed as a base set of sp functions combined with correlation functions.

Several basis sets of different sizes are available. These are known by their abbreviation: cc-pVDZ, cc-pVTZ, cc-pVQZ, and cc-pV5Z, where D, T and Q indicate the number of contracted functions. The terms of primitive and contracted functions are shown below [48, 13].

Basis	Primitive functions	Contracted functions
cc-pVDZ	9s,4p,1d/4s,1p	3s,2p,1d/2s,1p
cc-pVTZ	10s,5p,2d,1f/5s,2p,1d	4s,3p,2d,1f/3s,2p,1d
cc-pVQZ	12s,6p,3d,2f,1g/6s,3p,2d,1f	5s,4p,3d,2f,1g/4s,3p,2d,1f
cc-pV5Z	14s,9p,4d,3f,2g,1h/8s,4p,3d,2f,1g	6s,5p,4d,3f,2g,1h/5s,4p,3d,2f,1g

The energy–optimized cc basis sets are augmented by additional diffuse functions, denoted by the prefix *aug-* to the abbreviation. The augmentation involves inserting one extra function with a smaller exponent for each angular momentum [48].

2.1.3 Supermolecule approach

In calculations for dimers, basis functions of one molecule can be contribute to the basis set of the other. The effect is known as Basis Set Superposition Error (BSSE).

In the limit of a complete basis set, the BSSE would be zero [48, 13, 43]. An approximate method of assessing BSSE is the counterpoise (CP) correction. The BSSE is estimated from the monomer energies with the regular basis and the energies calculated with the full set of basis functions for the whole complex. The geometries of the two separated molecules A and B, and the complex AB are optimized. The energy difference between those is calculated with following formula [48, 13, 60, 43]

$$\Delta E = E(AB)^*_{ab} - E(A)_a - E(B)_b \tag{2.14}$$

Here basis set a for A and basis set b for B, and basis set ab for complex AB. Two energy calculations of the fragments in the complex are carried out with the full ab basis set. The energy of A is calculated in the presence of both the normal a basis functions and with the b basis functions of fragment B located at the corresponding nuclear positions, but without the B nucleus present. Such basis functions located at fixed points in space are referred to as ghost orbitals. The CP correction is calculated as [48, 13, 43]

$$\Delta E_{\text{CP}} = E(A)^*_{ab} + E(B)^*_{ab} - E(A)^*_a - E(B)^*_b \tag{2.15}$$

The counterpoise corrected ΔE energy is given as $\Delta E - \Delta E_{\text{CP}}$ [48, 13, 43].

2.1.4   Symmetry-adapted perturbation theory

This perturbational method was proposed by Jeziorski et al. [49, 50, 120]. It computes the interaction energy E_{int} directly from a sum of physical contributions

$$E_{\text{int}} = E^{(1)}_{\text{pol}} + E^{(1)}_{\text{exch}} + E^{(2)}_{\text{pol}} + E^{(2)}_{\text{exch}} + \cdots \tag{2.16}$$

where $E^{(1)}_{\text{pol}}$ is the damped classical electrostatic interaction energy, $E^{(2)}_{\text{pol}}$ is a sum of the damped classical induction and quantum mechanical dispersion energies

$$E^{(2)}_{\text{pol}} = E^{(2)}_{\text{ind}} + E^{(2)}_{\text{disp}} \tag{2.17}$$

and $E^{(n)}_{\text{exch}}$, $n = 1,2$, are exchange corrections defined by the symmetry-adapted perturbation theory (SAPT) [49, 50, 120].

2.1.5 Extrapolation to the basis set limit

Many attempts were to extrapolate the interaction energies of weakly bound molecular system at the basis set limit from correlation-consistent basis sets and an extrapolation scheme. The relationship between the correlation-consistent energies and the energy in the basis-set limit may now be written as [43, 138, 55, 10]

$$\Delta E_{\text{exact}} = \Delta E_X + AX^{-3} \tag{2.18}$$

Using this formula, the correlation energy E_{exact} can be extrapolated from the correlation-consistent energies E_X for small cardinal numbers X. To apply Eq. 2.18, only two energies are needed. From the cardinal numbers X and Y, the energies E_X and E_Y can be obtained. From these energies, the extrapolated basis-set limit E_{XY}^* and the parameter A_{XY} can be determined with the following two equations satisfied [43, 138, 55, 10, 33]

$$E_{XY}^* = E_X + A_{XY}X^{-3} \tag{2.19}$$

$$E_{XY}^* = E_Y + A_{XY}Y^{-3} \tag{2.20}$$

The extrapolated correlation energy and the linear parameter A_{XY} can be calculated from the following formulae [43, 10]:

$$E_{XY}^* = \frac{X^3 E_X - Y^3 E_Y}{X^3 - Y^3} \quad \text{and} \quad A_{XY} = \frac{E_X - E_Y}{X^{-3} - Y^{-3}} \tag{2.21}$$

2.1.6 Electrostatic interactions

Electrostatics is the study of interactions between charged positions. It is necessary for understanding the interactions of electrons, which is described by a wave function or electron density. The Coulomb's law equation for the energy of interaction between two particles with charges e_a and e_b at a distance r_{ab} is [114]

$$E = \frac{1}{4\pi\epsilon_0} \sum_{a \in A} \sum_{b \in B} \frac{e_a e_b}{r_{ab}} \tag{2.22}$$

2.2 Intermolecular potential functions

2.2.1 Lennard-Jones potential

The total intermolecular pair potential is obtained by summing the attractive and repulsive potentials. One of them is the Lennard-Jones (1924) 6-12 potential [63]. This potential function was used successfully for noble gases, but also in simulations of molecules, by using 2-site models [9, 79] by adding quadrupole moments [8, 57]. The Lennard-Jones potential can be written as

$$E_{ij} = 4\epsilon \left[\left(\frac{\sigma}{r_{ij}} \right)^{12} - \left(\frac{\sigma}{r_{ij}} \right)^{6} \right] \tag{2.23}$$

where ϵ characterises the well depth of the pair interaction and σ is the hard sphere radius of the atom (the distance at which E_{ij} is zero). r_{ij} is the distance between i and j ($r_{ij} = |\vec{r}_i - \vec{r}_j|$).

In 1987 the Gibbs ensemble Monte Carlo technique was proposed by Panagiotopoulos [91]. The phase properties of several systems have been obtained successfully by these techniques using Lennard-Jones 6-12 potentials.

2.2.2 Morse potential

The harmonic potential is a starting point for a discussion of vibrating molecules. A potential that is suitable for cases when attractive interaction comes from the formation of a chemical bond was proposed by Morse (1930) [81]:

$$E_{ij} = D \left[e^{-2\alpha \left(\frac{r_{ij} - r_e}{r_e} \right)} - 2e^{-\alpha \left(\frac{r_{ij} - r_e}{r_e} \right)} \right], \tag{2.24}$$

The Morse potential is usually written as [44]

$$E_{ij} = D(1 - \exp(-\alpha r_{ij}))^2 \tag{2.25}$$

where D is the depth of the interaction potential, r_{ij} is the interaction distance and α denotes the range of the interaction. This potential is widely used to model covalently diatomic molecules. Both potentials Eq. 2.23 and 2.24 are scalable. The

total energy scales linearly with ϵ or D, and the distances scale linearly with σ and r_{e}.

The Morse potential therefore has an important parameter, α, which can be used to study the effect of the range of the potential on the properties of a molecular system. In recent years the Morse potential were modified in several ways to study the effects of intermolecular interactions. The modified Morse functions can be constructed using either experimental measurements or theoretical calculations. They were used successfully for the prediction of thermodynamic properties of several systems.

2.2.3 Korona potential

Korona et al. (1997) [56] worked out an analytical representation for helium dimers which includes a repulsive exponential component and an attractive damped dispersion component of the form

$$E(r) = A e^{-\alpha r + \beta r^2} + \sum_{n=3}^{8} f_{2n}(r,b) \frac{C_{2n}}{r^{2n}} \tag{2.26}$$

where A, α, β and b denote adjustable parameters, the C_{2n} denote dispersion coefficient, and f_{2n} is the damping function of Tang and Toennies [121]

$$f_{2n}(r,b) = 1 - e^{-br} \sum_{k=0}^{2n} \frac{(br)^k}{k!} \tag{2.27}$$

2.2.4 Special potentials

For the prediction of the thermodynamic properties for hydrogen chloride and fluorinated compounds with Monte Carlo simulation, pair potentials were developed from symmetry-adapted perturbation theory (SAPT) by Naicker (2002) [117, 118, 83], one of them was written as

$$E_{AB}^{\mathrm{int}} = \sum_{a \in A} \sum_{b \in B} \left[\alpha_{ab} e^{-\beta_{ab} r_{ab}} + f_m(\delta_n^{ab} r_{ab}) \left(\sum_{n=6,8,10,12} \frac{C_n^{ab}}{r_{ab}^n} + \frac{q_a q_b}{r_{ab}} \right) \right] \tag{2.28}$$

Where $f_m(\delta_n^{ab} r_{ab})$ $(m = 10)$ is a damping function proposed by Tang and Toennies (1984) [121] and has form like Eq. 2.27. The second virial coefficients, vapor pressure and the phase coexistence diagram for halogenated compounds obtained with

this potential function, were in a good agreement with experimental data.

A new four-dimensional intermolecular pair potential for dimer carbon dioxide was proposed by Bock (2000) [5]:

$$E(r_{ij}) = D_{ij} \exp(-\alpha_{ij} r_{ij}) + \left[\frac{C_{ij}^{(12)}}{r_{ij}^{12}} + \frac{C_{ij}^{(10)}}{r_{ij}^{10}} + \frac{C_{ij}^{(8)}}{r_{ij}^{8}} + \frac{C_{ij}^{(6)}}{r_{ij}^{6}} + \frac{q_i q_j}{r_{ij}} \right] f(r_{ij}) \quad (2.29)$$

Here $f(r_{ij}) = (1 + e^{-2(\delta_{ij} r_{ij} - 2)})^{-15}$ is a damping function. The results of the virial coefficients for the dimer carbon dioxide agreed well with experimental data.

For prediction also of thermodynamic properties of vapour liquid equilibria for nitrogen using Gibbs ensemble Monte Carlo simulation a new *ab initio* pair potential was developed at the CCSD(T) level of theory with aug-cc-pVmZ ($m = 2, 3$) correlation-consistent basis sets by Leonhard and Deiters. (2001) [65]:

$$E_{ss} = \sum_{i=1}^{5} \sum_{j=1}^{5} (E_{ij}^{\mathrm{M6}} + D^{\mathrm{CC}}(r_{ij}) \frac{q_i q_j}{4\pi\epsilon_0 r_{ij}})$$

with

$$E_{ij} = D_{\mathrm{e},ij} \{ (1 - e^{-\alpha_{ij}(r - r_{\mathrm{m},ij})})^2 - 1 \} + D_{ij}^{\mathrm{M6}}(r) \frac{C_{6_{ij}}}{r^6}$$

$$D_{ij}^{\mathrm{M6}}(r) = e^{-f_{ij}^d (1 - r_g)^2}$$

$$r_g = r/(r_{ij}^d r_{\mathrm{m},ij}); \quad D^{\mathrm{CC}}(r) = 1 - e^{-r_{ij}}$$

$$(2.30)$$

where $D^{\mathrm{CC}}(r)$ and $D_{ij}^{\mathrm{M6}}(r)$ are damping functions. This potential used successfully for the prediction of the thermodynamic behavior of phase equilibria of nitrogen.

2.2.5   Damping functions

Damping is important for site-site potentials in which the sites can get much closer than the center of mass separation used in the angular expansion while the dimer is still in an important region.

The theory gives the dispersion energy between two atoms as [114]

$$E_{\text{disp}} = -\frac{C_6}{r^6} - \frac{C_8}{r^8} - \frac{C_{10}}{r^{10}} - \ldots \tag{2.31}$$

This cannot be correct with $r \rightarrow 0$. The electronic energy remains finite in limit $\overrightarrow{r}^0$, and the nucleus-nucleus repulsion behaves correctly as $1/r$.

For atoms the dispersion energy can be described by a modified expression [114]:

$$E_{\text{disp}} = -f_6(r)\frac{C_6}{r^6} - f_8(r)\frac{C_8}{r^8} - f_{10}(r)\frac{C_{10}}{r^{10}} - \ldots \tag{2.32}$$

where the $f_n(r)$ are damping functions. These functions must satisfy the following conditions:

- $f_n(r) \rightarrow 1$ as r $\rightarrow \infty$, to recover the long-range formula.

- $f_n(r) \rightarrow R^n$ as r $\rightarrow 0$, to suppress the singularity

2.2.6 Fitting the potential energy surface

Levenberg-Marquardt algorithm

The Levenberg-Marquardt algorithm provides a numerical solution to the mathematical problem for minimizing a sum of squares of several nonlinear functions that depend on a common set of parameters. This minimization problem occurs especially in least-squares curve fitting [135]. It is assumed that there are m functions $f_1, .., f_m$ of n parameters $\boldsymbol{p}_1, ..., \boldsymbol{p}_n$ with $m \geq n$ can be written in vector notation

$$\mathbf{f}^T = (f_1, ..., f_m) \quad \text{and } \mathbf{p}^T = (\boldsymbol{p}_1, ..., \boldsymbol{p}_n) \tag{2.33}$$

The least-squares problem is to find the parameter vector $\mathbf{p}$ which minimizes the function

$$S(\mathbf{p}) = f^T f = \sum_{i=1}^{m} [f_i(\mathbf{p})]^2 \tag{2.34}$$

Given a set of observation data pairs (t_i, y_i), and a model $c(t|\mathbf{p})$ the residuals $f_i(\mathbf{p})$ are defined as

$$f_i(\mathbf{p}) = y_i - c(t_i|\mathbf{p}) \tag{2.35}$$

For the Levenberg-Marquardt algorithm it is necessary to provide an initial value for the parameter vector $\mathbf{p}$. In most cases, an standard value like $\mathbf{p}^{\mathrm{T}} = (1, 1, ..., 1)$ is appropriate for the curve fits; in other cases, the initial guess has to be already close to the final solution. The Levenberg-Marquardt algorithm then iteratively constructs new vectors. In each iteration, the parameter vector $\mathbf{p}$ is replaced by a new evaluation $\mathbf{p} + \mathbf{q}$. The functions $f_i(\mathbf{p} + \mathbf{q})$ are approximated to determine $\mathbf{q}$

$$\mathrm{f}(\mathbf{p} + \mathbf{q}) \approx \mathrm{f}(\mathbf{p}) + \mathrm{J}\mathbf{q} \tag{2.36}$$

where $\mathbf{J}$ is the Jacobian of $\mathbf{f}$ at $\mathbf{p}$. At a minimum of the sum of squares S, its gradient with respect to $\mathbf{q}$, $\nabla_{\mathrm{q}}S$, is equal to zero. Differentiating the square of the right hand side of the equation above and setting the results to zero gives

$$(\mathbf{J}^{\mathrm{T}}\mathbf{J})\mathbf{q} = -\mathbf{J}^T\mathbf{f} \tag{2.37}$$

From this equation $\mathbf{q}$ can be obtained by inverting $\mathbf{J}^T\mathbf{J}$. The idea of the Levenberg-Marquardt algoritm is to replace this equation by a damped version

$$(\mathbf{J}^{\mathrm{T}}\mathbf{J} + \lambda\mathbf{I})\mathbf{q} = -\mathbf{J}^T\mathbf{f} \tag{2.38}$$

The damping factor λ is adjusted at each iteration step. A large value makes the Levenberg-Marquardt algorithm behave like the gradient method (method of Steepest Descent), which converges slowly, but with high probability; a value of zero makes the Levenberg-Marquardt algorithm behave like the Gauss-Newton method, which converges quickly, but also tends to diverge instead.

Genetic algorithm

Genetic algorithms are global optimization methods which are based on the mechanisms of natural selection described by genetics and the Darwinian theory of evolution. This is especially useful for searching parameter spaces in which there are many

local minima. The Genetic algorithm (GA) proposed by D. A. Goldberg (1989) [38] has been applied successfully to the description of a variety of global minimization problems. In 1998 the potential energy surfaces were fitted with genetic programming in searching the function space proposed by Makarov and Metiu [68]. In recent years the genetic algorithm has been used to find the solutions for many chemistry problems.

The GA was proposed by Wiliam Ferreira (2005) [134]. It is assumed that there is a function $V([a], \vec{r})$ in some set of n_p points $(\vec{r}_p, e_p)$. The least-square problem is to find the parameter vectors $[a] = [a_1, a_2, .., a_m]$ which minimizes function

$$S = \sum_p^{n_p} \delta_p^2 = \sum_p^{n_p} (e_p - \bar{e}_p)^2 \tag{2.39}$$

with $\bar{e}_p \equiv V([a], \vec{r}_p)$.

Wiliam Ferreira (2005) [134] successfully fitted potential energy surfaces of reactive systems with this Genetic algorithm.

2.3 Second virial coefficients

The virial equation is a power series for the compressibility factor in the reciprocal molar volume, $1/V_n$ [42, 129, 136].

$$z = \frac{PV_n}{RT} = 1 + \frac{B_2}{V_n} + \frac{B_3}{V_n^2} + \dots \tag{2.40}$$

where z is the compressibility factor, B_2 is the second virial coefficient, and B_3 is the third virial coefficient. In a mixture the second virial coefficient has the form

$$B(T) = B_{aa}x_a^2 + 2B_{ab}x_a x_b + B_{bb}x_b^2 \tag{2.41}$$

where the x_i are mole fractions, B_{ii} are the virial coefficients of pure components, and B_{ab} is the cross second virial coefficient.

The virial coefficient can be calculated with the integral as [45]

$$B(T) = -2\pi \int_0^\infty [e^{-E(r)/kT} - 1] r^2 dr \tag{2.42}$$

where $E(r)$ is a spherically symmetric inter-particle potential obtained by integration over the angular coordinates.

2.3.1   Empirical correlation methods

For second virial coefficients a reliable correlation was proposed by Vetere (1999, 2005) [128, 129]. Its results agree well with experimental data for many substances. It can be derived from an eight-parameter equation of state as [128, 129]

$$B = \left(\frac{a}{1.987T} \exp(b - KT)\right) - \left(\frac{a}{1.987T_{B_0}}\right) \exp(b - KT_{B_0}) \tag{2.43}$$

where the second term on the right-hand site makes it possible to calculate B up to the Boyle temperature, T_{B_0}, and beyond. At temperatures appreciably below T_{B_0}, roughly $T \leq 0.85 - 0.9T_{B_0}$, Eq.2.43 reduces to

$$B = \left(\frac{a}{1.987T} \exp(b - KT)\right) \tag{2.44}$$

without loss of reliability. Eq. 2.44 can correlate with good accuracy all the experimental range of B for fluids, both polar and non-polar, using two empirical parameters. An equation for the cross second virial coefficient was proposed by Martin(1979) [70]

$$\frac{B_{ij}(P_c)_{ij}}{R(T_c)_{ij}} = K_1(T_b)_{ij}\left\{\frac{\exp[((T_b)_{ij} - T)]}{T} - \frac{\exp[K((T_b)_{ij} - T_{B_0})_{ij}]}{(T_{B_0})_{ij}}\right\} \tag{2.45}$$

where K_1 and K are two empirical constants. The T_c, P_c and T_b are the critical temperature and pressure, and the boiling temperature.

Recently Estela-Uribe and Jaramillo (2002, 2005) [31, 30] published empirical correlation equations for second virial coefficients which are based on the corresponding-states approach of Lee and Kesler [61]. In their work, the proposed correlations for

the second virial coefficients of binary interactions as

$$B = \left(\frac{RT_c}{p_c}\right)[B_0(T_r) + (\omega - \omega_0)B_1(T_r) \tag{2.46}$$

where B_0 the reduced second virial coefficient, B_1 represents for the contribution due to the non-spherical geometry of the fluid of interest and ω and ω_0 are, respectively, the acentric factors of the fluid of interest and the reference fluid. The second cross virial coefficient, B_{ij} can be calculated from Eq. 2.46 by replacing T_c, p_c and ω in Eq. 2.46 with $T_{c,ij}$, $p_{c,ij}$ and ω_{ij}, respectively, and use $T_{r,ij} = T/T_{c,ij}$. The empirical correlation equations are characterized by pseudo-critical parameters, which are interpolations of the pure-fluid critical temperatures and densities [30]:

$$p_{c,ij}^{-1/3} = \frac{1+d_{ij}}{2}(\rho_{c,i}^{-1/3} + \rho_{c,j}^{-1/3}); \quad T_{c,ij} = \frac{(1-k_{ij})(T_{c,i}T_{c,j})^{1/2}}{1 + c/(M_{ij}T)}$$
$$\text{with } M_{ij}^{-1} = \frac{1}{2}(M_i^{-1} + M_j^{-1}) \text{ and } k_{ij} = 1 - \frac{a_{ij}\rho_{c,ij}}{(\rho_{c,i}\rho_{c,j})^{1/2}} \tag{2.47}$$

Here the M_i denote molar masses of the pure components, M_{ij} an interaction molar mass, and c is a constant (21.8 K g/mol). It turns out that the adjustable parameters a_{ij} and d_{ij} are very close to zero for a large number of chemical compounds.

2.3.2   Calculation from Equations of State

For the second virial coefficients of several non-polar and polar substances a two-parameter corresponding-states model has been proposed by Mathias (2003) [73], which relates the reduced second virial coefficient to the critical properties T_c and P_c. This model is based on the Redlich-Kwong EOS [136] as

$$P = \frac{RT}{v-b} - \frac{a_c\alpha(T)}{v(v+b)}$$
$$\text{with } b = 0.08664035\frac{RT_c}{P_c} \tag{2.48}$$
$$a_c = 0.42748025\frac{R^2T_c^2}{P_c}$$

where the α-function improved to Redlich-Kwong EOS proposed by Mathias (2003) [73]. The result at the critical temperature agrees with experimental data.

In years (1981, 1981a, 1982) [19, 20, 21] Deiters constructed an EOS (equation of state) from perturbed hard chain theory with the aim to obtain an EOS which yields correct critical temperatures, pressures, and densities of pure components, because calculations of phase equilibria of mixtures under elevated pressure may be affected by the wrong representation of the critical points for pure components. However, the application of this EOS to mixtures is difficult—leading at first to an implementation for pure components, only. Deiters (1982) proposed an extension to binary mixtures, by exchanging a part of the equation of state by a polynomial series.

The Deiters equation of state (denoted D1) has been coded in program *ThermoC* [18, 22] and can be used to calculate the second virial coefficients, vapor pressure and vapor-liquid equilibria of pure components. This equation contains an ideal gas part, a hard-sphere term with the quantum correction and an attraction term:

$$
A_{\mathrm{m}} = + \mu^{\ominus} - RT \ln \frac{V_{\mathrm{m}}}{V_{\mathrm{m}}^{\ominus}} - RT + RTcc_0 \frac{4\xi - 3\xi^2}{(1-\xi)^2} + \Delta A_{\mathrm{m}}^{\mathrm{qc}}
$$
$$
- \frac{N_A}{c^2} \xi \Big[h_0 \chi(\rho, c) \widetilde{T}(e^{1/\widetilde{T}} - 1) + \sum_{k=0}^{3} \sum_{j=0}^{6} \sum_{i=0}^{10} f_{ijk}(c-1)^k \widetilde{T}^{-j} \xi^i \Big] \qquad (2.49)
$$
$$
\text{with} \quad \xi = \frac{N_A \pi \sigma^3}{6 V_{\mathrm{m}}}, \widetilde{T} = \frac{c k_{\mathrm{B}} T}{\epsilon}
$$

The symbol $\ominus$ refers to the reference state of the equation of state. The parameters ϵ (potential well depth), σ (hard-core diameter), and c (anisotropy parameter) are substance specific. The f_{ijk} are (universal) expansion coefficients, h_0 and c_0 are constants, $\chi(\rho, c)$ is a function of density, and N_A is Avogadro's constant.

2.3.3 Quantum corrections

In 1944 Chang [45] studied the influence of quantum effects on virial coefficients of linear molecules. Such molecules can be represented as rigid rotators, with three degrees of translational and two degrees of rotational freedom. The interaction potential for molecules is a function of the intermolecular distance and three angles which describe the relative orientation of the molecules.

The Hamiltonian of N rigid rotators of mass m and moment of inertia I is

$$H(q^N, p^N) = \sum_i \frac{1}{2m} p_i^2 + \sum_i \frac{1}{2I} \left(p_{\theta_i}^2 + \frac{p_{\phi_i}^2}{\sin^2 \theta_i} \right) + \Phi(q^N) \tag{2.50}$$

in which q represents the collection of five coordinates, $x, y, z, \phi,$ and q necessary to specify the location and orientation of a single molecule. The quantities p_θ and p_ϕ are the momenta conjugate to the coordinates θ and ϕ. The partition function is

$$\begin{aligned} Z_N &= \frac{1}{N! h^{5N}} \int \dots \int e^{-H(q^N, p^N)/kT} dp_{x_1} dp_{y_1} dp_{z_1} dp_{\theta_1} dp_{\phi_1} \\ &\quad \times dx_1 dy_1 dz_1 d\theta_1 d\phi_1 \dots \end{aligned} \tag{2.51}$$

Integration over the momenta leads to the expression

$$\begin{aligned} Z_N &= \frac{1}{N! \lambda_{tr}^{3N} \lambda_{rot}^{2N}} \int \dots \int e^{-\Phi(q^N)/kT} \{ \sin\theta_1 \sin\theta_2 \dots \} \\ &\quad \times d\theta_1 d\phi_1 dx_1 dy_1 dz_1 \dots d\theta_N d\phi_N dx_N dy_N dz_N \end{aligned} \tag{2.52}$$

in which $\lambda_{tr}^2 = h^2/2\pi mkT$ and $\lambda_{rot}^2 = h^2/2\pi IkT$. This expression is written in

$$Z_N = \frac{(4\pi)^N}{N! \lambda_{tr}^{3N} \lambda_{rot}^{2N}} \int \dots \int W_N(q^N) dq_1 \dots dq_N \tag{2.53}$$

in which $W_N(q^N)$ is the classical Boltzmann factor furthermore

$$dq_i = \frac{1}{4\pi} dx_i dy_i dz_i \sin\theta_i d\theta_i d\varphi_i \tag{2.54}$$

The formulas for the virial coefficients for angle dependent potentials are

$$\begin{aligned} B(T) &= \frac{-N}{32\pi^2 V} \int \int f_{12} dq_1 dq_2 \\ &= \frac{N}{4} \int_0^\infty \int_0^{2\pi} \int_0^\pi \int_0^\pi f_{12} \sin\theta_1 d\theta_1 \sin\theta_2 d\theta_2 d(\phi_2 - \phi_1) r_{12}^2 dr_{12} \end{aligned} \tag{2.55}$$

$$C(T) = -\frac{N^2}{192\pi^3 V} \int \int \int f_{12} f_{13} f_{23} dq_1 dq_2 dq_3 \tag{2.56}$$

$f_{ij} = \{\exp[-(\varphi_{ij}/kT)] - 1\}$. The f_{ij} are functions not only of the intermolecular distance, but also of the three angles needed to specify the orientation of two molecules. From the quantum statistical theory Chang (1944) [45] showed that the diatomic molecules may be represented by rigid three-dimensional rotators of mass m and moment of inertia I, each with five degrees of freedom: three translational and two rotational.

The Hamiltonian operator for a system of N such molecules is given in Eq. 2.50. The quantum effects on the virial coefficients of diatomic gases was obtained as

$$B(T) = B_{\mathrm{cl}} + \left[\left(\frac{h^2}{m} \right) B_I^{\mathrm{tr}} + \left(\frac{h^2}{m} \right)^2 B_{II}^{\mathrm{tr}} + ... \right] \\ + \left[\left(\frac{h^2}{I} \right) B_I^{\mathrm{rot}} + \left(\frac{h^2}{I} \right)^2 B_{II}^{\mathrm{rot}} + ... \right] \tag{2.57}$$

in which

$$B_{\mathrm{cl}}(T) = -\frac{N}{4} \int \int (e^{-\varphi/kT} - 1) r^2 \mathrm{d}r \mathrm{d}\Omega \tag{2.58}$$

$$B_I^{\mathrm{tr}}(T) = +\frac{N}{4} \left(\frac{1}{48\pi^2 k^3 T^3} \right) \int \int e^{-\varphi/kT} \left(\frac{\partial \varphi}{\mathrm{d}r} \right) r^2 \mathrm{d}r \mathrm{d}\Omega \tag{2.59}$$

$$B_I^{\mathrm{rot}}(T) = +\frac{N}{4} \left(\frac{1}{96\pi^2 k^3 T^3} \right) \int \int e^{-\varphi/kT} \left[\left(\frac{\partial \varphi}{\partial \theta_1} \right)^2 + \left(\frac{\partial \varphi}{\partial \theta_2} \right)^2 \\ + \csc^2\theta_1 \left(\frac{\partial \varphi}{\partial \phi_1} \right)^2 + \csc^2\theta_2 \left(\frac{\partial \varphi}{\partial \phi_2} \right)^2 \right] r^2 \mathrm{d}r \mathrm{d}\Omega \tag{2.60}$$

In this expressions:

$$\varphi = \varphi(r, \theta_1, \theta_2, \phi_2 - \phi_1) \\ \int ...\mathrm{d}\Omega = \int_0^{2\pi} \int_0^{\pi} \int_0^{\pi} ...\sin\theta_1 \mathrm{d}\theta_1 \sin\theta_2 \mathrm{d}\theta_2 \mathrm{d}(\phi_2 - \phi_1) \tag{2.61}$$

In 1984 Gray and Gubbins [40] proposed a semiclassical expansion in orders of $\hbar$ for the first-order translational and rotational quantum corrections

$$B_{QM}^{\text{trans}}(T) = \frac{\hbar^2}{24(k_{\text{B}}T)^3} \times \frac{\langle F^2 \rangle_0}{2M_r} \tag{2.62}$$

$$B_{QM}^{\text{rot}}(T) = \frac{\hbar^2}{24(k_{\text{B}}T)^3} \times \sum_{\alpha=x,y,z} \frac{\langle T_\alpha^2 \rangle_0}{I_\alpha} \tag{2.63}$$

where F is the force on each molecule, M_r is the reduced mass of the system, and T_α is the torque about the local molecular axis α with moment of inertia I_α. The notations $\langle F^2 \rangle_0$ and $\langle T_\alpha^2 \rangle_0$ represent integrations weighted with the zero-density pair distribution function. The rotational correction for a mixed system is the average of the two fragment contributions. The total first-order quantum-corrected second virial coefficient, $B_{QM}^{(1)}(T)$, is defined as the sum of the contributions from Eqs. 2.66, 2.62 and 2.63.

The first-order quantum correction to the virial coefficient of linear molecules was proposed by Pack (1983) [89] and Wang (2003) [132]. Recently the quantum correction has been presented in Wormer's work (2005) too [137]. Following the latter, the virial coefficient up to first order can be written

$$B(T) = \frac{N_A}{2u \iint d\Omega_1 d\Omega_2} \iiiint \left\{ 1 - \exp(-u/k_{\text{B}}T) \left[1 + \frac{1}{12(k_{\text{B}}T)^2} H_0 u \right] \right\} \\ \times \mathrm{d}r_1 \mathrm{d}r_2 \mathrm{d}\Omega_1 \mathrm{d}\Omega_2 \tag{2.64}$$

Here N_A is Avogadro's constant, k_{B} Boltzmann's constant, T the temperature, and $u(r, \alpha, \beta, \phi)$ the pair potential; its parameters, the center-center distance and the relative orientation angles are calculated from the center vectors $\vec{r_i}$ and the absolute orientations Ω_i. H_0 is the translation-rotation Hamiltonian of a molecular pair.

Eq. 2.64 can be broken down into a zeroth order (classical) term and first-order quantum corrections (radial part, angular part proportional to I^{-1} (moment of inertia), angular part proportional to μ^{-1} (reduced mass)):

$$B(T) = B_{\text{cl}}^0(T) + B_{\text{r}}^1(T) + B_{\text{aI}}^1(T) + B_{\text{a}\mu}^1(T) \tag{2.65}$$

The classical part is given by

$$B_{\mathrm{cl}}^0(T) = -\frac{N_A}{4} \int\limits_0^{2\pi} \mathrm{d}\phi \int\limits_0^{\pi} \sin\beta \,\mathrm{d}\beta \int\limits_0^{\pi} \sin\alpha \,\mathrm{d}\alpha \int\limits_0^{\infty} \left(\exp\left(-\frac{u}{k_{\mathrm{B}}T} \right) - 1 \right) \, r^2 \,\mathrm{d}r \quad (2.66)$$

The first-order correction terms can be written as:

$$
\begin{aligned}
B_{\mathrm{r}}^{(1)}(T) =& \frac{N_A \hbar^2}{96\mu(k_{\mathrm{B}}T)^3} \int\limits_0^{2\pi}\int\limits_0^{\pi} \sin\beta \int\limits_0^{\pi} \sin\alpha \int\limits_0^{\infty} \exp\left(-\frac{u}{k_{\mathrm{B}}T}\right)\left(\frac{\partial u}{\partial r}\right)^2 \\
&\times r^2 \,\mathrm{d}r \,\mathrm{d}\alpha \,\mathrm{d}\beta \,\mathrm{d}\phi
\end{aligned}
\quad (2.67)
$$

$$
\begin{aligned}
B_{\mathrm{a},I}^{(1)}(T) =& -\frac{N_A \hbar^2}{48(k_{\mathrm{B}}T)^2} \int\limits_0^{2\pi}\int\limits_0^{\pi} \sin\beta \int\limits_0^{\pi} \sin\alpha \int\limits_0^{\infty} \exp\left(-\frac{u}{k_{\mathrm{B}}T}\right) \\
&\times \sum_{l_1 l_2 l} u_{l_1 l_2 l}(r) A_{l_1 l_2 l}(\alpha,\beta,\phi)\left(\frac{l_1(l_1+1)}{2I_1} + \frac{l_2(l_2+1)}{2I_2}\right) r^2 \,\mathrm{d}r \,\mathrm{d}\alpha \,\mathrm{d}\beta \,\mathrm{d}\phi
\end{aligned}
$$
$$(2.68)$$

$$
\begin{aligned}
B_{\mathrm{a},\mu}^{(1)}(T) =& -\frac{N_A \hbar^2}{48(k_{\mathrm{B}}T)^2} \int\limits_0^{2\pi}\int\limits_0^{\pi} \sin\beta \int\limits_0^{\pi} \sin\alpha \int\limits_0^{\infty} \exp\left(-\frac{u}{k_{\mathrm{B}}T}\right) \\
&\times \sum_{l_1 l_2 l} u_{l_1 l_2 l}(r) A_{l_1 l_2 l}(\alpha,\beta,\phi)\frac{l(l+1)}{2\mu r^2} \, r^2 \,\mathrm{d}r \,\mathrm{d}\alpha \,\mathrm{d}\beta \,\mathrm{d}\phi
\end{aligned}
$$
$$(2.69)$$

The terms $u_{l_1 l_2 l}(r) A_{l_1 l_2 l}(\alpha,\beta,\phi)$ represent a spherical harmonics expansion of the interaction potential.

2.3.4   Numerical calculation of integrals

The Gauss quadrature method is an approximative numerical integration technique. The value of a one-dimensional integral is calculated as a weighted sum of integrand values. With each x_i there is an associated weight, w_i [67, 1, 15, 135, 99, 113].

$$\int_a^b f(x)\mathrm{d}x \simeq \sum_{i=1}^{n} w_i f(x_i) \tag{2.70}$$

The points x_i within the interval [a, b] are the abscissae, and the w_i are the weights [1]. Calculating a two-dimensional integral with the Gauss quadrature rule can be similarly described as

$$\int_{a_1}^{b_1} \int_{a_2}^{b_2} f(x, y) \mathrm{d}y \mathrm{d}x \simeq \sum_{i=1}^{n} w_i \left(\int_{a_2}^{b_2} f(x_i, y) \mathrm{d}y \right) \tag{2.71}$$

$$\int_{a_1}^{b_1} \int_{a_2}^{b_2} f(x, y) \mathrm{d}y \mathrm{d}x \simeq \sum_{i=1}^{n} \sum_{j=1}^{n} w_i v_j f(x_i, y_j) \tag{2.72}$$

where (w_i, x_i) and (v_i, y_j) are the weights and abscissae of the rules used in the respective dimensions. The one-dimensional rule may also be used similarly for multi-dimensional integral forms

$$\int_{a_1}^{b_1} \int_{a_2}^{b_2} \cdots \int_{a_n}^{b_n} f(x_1, x_2, \ldots, x_n) \mathrm{d}x_n \mathrm{d}x_{n-1} \cdots \mathrm{d}x_1 \tag{2.73}$$

In this work, 4D integrations were carried out with such a Gauss-Legendre quadrature method [113, 135, 67, 99]

2.4 Monte Carlo Simulation

2.4.1 Metropolis method

The Metropolis method is regarded as one of the 10 greatest numerical methods developed of the 20th Century [78]. In this method, points in the configuration space $\psi^{(l)}$ can be generated randomly according to the probability distribution $\exp(E\psi^{(l)}/(k_\mathrm{B}T))$. This means that, on average, the number of points generated per unit volume around a point $\psi^{(l)}$ is

$$\langle A \rangle = \frac{1}{M} \sum_{l=1}^{M} h(\boldsymbol{\psi}^{(l)}) \tag{2.74}$$

where M is the total number of points generated, so-called number of Monte Carlo cycles. In the case of random samples the suitable laws of large numbers was proposed by Markov chains [127]

$$\langle A \rangle = \frac{1}{M} \sum_{l=1}^{M} h(\boldsymbol{\psi}^{(l)}) \rightarrow \int_{\Re} h(\boldsymbol{\psi})\pi(\boldsymbol{\psi})\mathrm{d}\boldsymbol{\psi} \tag{2.75}$$

Another reason for the interest in Metropolis methods is that, it is rather straightforward to construct one or more Markov chains [127] whose limiting invariant distribution is the desired target distribution. In equilibrium, the average number of accepted moves from a state to any other state is equalled by the number of reverse moves. The advantage of this theory is that the algorithm to generate the configurations permits also the reverse moves.

$$u_i p_{ij} = u_j p_{ji}$$
$$u_i : \text{configurational probability } i \tag{2.76}$$
$$p_{ij} : \text{transition probability from state } i \text{ to state } j$$

If $X(i)$ is the number of states:

$$p_{ij} = \begin{cases} 0 & \text{for } \boldsymbol{\psi}_j \notin X(i); \\ \frac{1}{M} & \text{for } \boldsymbol{\psi}_j \in X(i) \text{ and } \rho(\boldsymbol{\psi}_j) \geq \rho(\boldsymbol{\psi}_i); \\ \frac{1}{M}\frac{\rho(\boldsymbol{\psi}_j)}{\rho(\boldsymbol{\psi}_i)} & \text{for } \boldsymbol{\psi}_j \in X(i) \text{ and } \rho(\boldsymbol{\psi}_j) < \rho(\boldsymbol{\psi}_i) \end{cases} \tag{2.77}$$

The reversibility can be demonstrated as follows:

- When $\boldsymbol{\psi}_j \notin X(i)$ is, then $\boldsymbol{\psi}_i \notin X(j)$ and $p_{ij} = 0 = p_{ji}$

- When $\rho(\boldsymbol{\psi}_j) \geq \rho(\boldsymbol{\psi}_i)$ then $p_{ij} = \frac{1}{M}$ and $p_{ji} = \frac{1}{M}\frac{\rho(\boldsymbol{\psi}_j)}{\rho(\boldsymbol{\psi}_i)} = \frac{1}{M}\frac{u_i}{u_j} \Rightarrow u_j p_{ji} = u_i p_{ij}$

and vice versa. To accept a move with the probability $p = \frac{\rho(\boldsymbol{\psi}_j)}{\rho(\boldsymbol{\psi}_i)}$, one evaluates p and compares this value with a random number $x \in [0,1]$. If $p > x$, the move is accepted and otherwise rejected.

2.4.2 The Gibbs ensemble

Gibbs ensemble simulations are carried out in two microscopic regions. Simulation is performed in each region within standard boundary conditions. Each region should

be in internal equilibrium, and temperature, pressure and the chemical potentials of all components should be the same in the two regions. In Monte Carlo simulations the system temperature is specified in advance. The remaining three conditions are satisfied by carrying out three types of moves, which are displacements of particles within each region, fluctuations in the volume of the two regions and transfers of particles [35, 4].

For theory foundations the Gibbs ensemble techniques have also been described the detail by Panagiotopoulos in the publication (1987, 1988) [91, 94]. The prediction and simulation of phase transitions in complex fluids were proposed by Panagiotopoulos (1994) [93]. In the following years a full development of the statistical mechanical definition of the ensemble was proposed by Smit et al. (1989) [109] and Smit (1989) and Frenkel (2002) [108, 35]. The main lines of reasoning were reproduced by Smit et al. (1988) [94] and Smit (1993) [107].
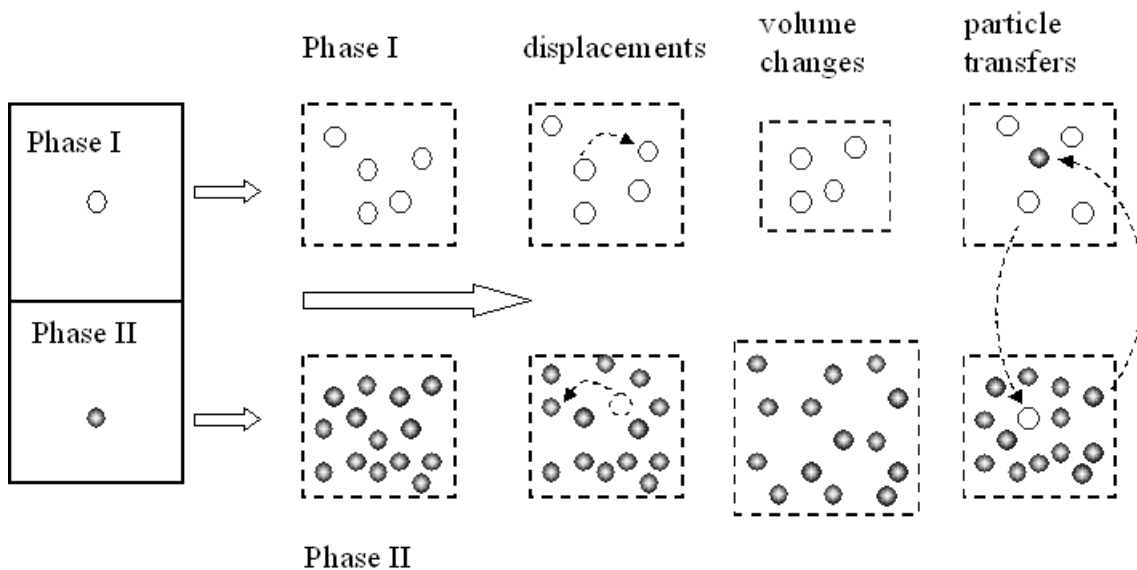
Figure 2.1: Scheme of the Gibbs ensemble technique [93]. Dotted lines indicate periodic boundary conditions.

For a system at constant temperature T, total volume V, and total number of particles N the system is divided into two regions with volumes V_I and $V_{II} (= V - V_I)$

and number of particles N_I and $N_\mathrm{II}(= N - N_\mathrm{I})$. The partition function is

$$
\begin{aligned}
Q_{NVT} = &\frac{1}{\Lambda^{3N} N!} \sum_{N_\mathrm{I}=0}^{N} \binom{N}{N_\mathrm{I}} \int_0^V \mathrm{d}V_I V_\mathrm{I}^{N_\mathrm{I}} V_\mathrm{II}^{N_\mathrm{II}} \int \mathrm{d}\xi_\mathrm{I}^{N_\mathrm{I}} \exp[-\beta U_\mathrm{I}(N_\mathrm{I})] \\
&+ \int \mathrm{d}\xi_\mathrm{II}^{N_\mathrm{II}} \exp[-\beta U_\mathrm{II}(N_\mathrm{II})]
\end{aligned}
\tag{2.78}
$$

where Λ is the de Broglie wavelength, $\beta = 1/k_\mathrm{B}T$, ξ_I and ξ_II are the scaled coordinates of the particles in the two regions. $U_{(N_\mathrm{I})}$ is the total intermolecular potential of N_I particles. Eq. 2.78 represents an ensemble with probability

$$
\wp(N_\mathrm{I}, V_\mathrm{I}; N, V, T) \propto \frac{N!}{N! N_\mathrm{II}!} \exp(N_\mathrm{I}\ln V_\mathrm{I} + N_\mathrm{II}\ln V_\mathrm{II} - \beta U_\mathrm{I}(N_\mathrm{I}) - \beta U_\mathrm{II}(N_\mathrm{II})) \tag{2.79}
$$

The partition function Eq. 2.78 was used by Smit et al. [110] for a system with a first-order phase transition. In a Gibbs ensemble simulation the two regions are expected to reach the correct equilibrium densities. The acceptance criteria for the three types of moves can be obtained from Eq. 2.79.

For a displacement step in one of the regions, the probability of acceptance is the same for conventional NVT simulations:

$$
\wp(\mathrm{move}) = \min[1, \exp(-\beta \Delta \mathrm{U})] \tag{2.80}
$$

where ΔU is the internal energy change resulting from the displacement.

For a volume change step the volume of region I is increased by ΔV with a corresponding decrease of the volume of region II,

$$
\wp(\mathrm{move}) = \min\left[1, \exp\left(-\beta\Delta U_\mathrm{I} - \beta\Delta U_\mathrm{II} + N_\mathrm{I}\ln\frac{V_\mathrm{I}+\Delta V}{V_\mathrm{I}} + N_\mathrm{II}\ln\frac{V_\mathrm{II}-\Delta V}{V_\mathrm{II}}\right)\right] \tag{2.81}
$$

Eq. 2.81 indicates that sampling is performed uniformly in the volume. Such sampling is performed by generating a uniformly distributed random number between 0 and 1, ξ, and obtaining ΔV as

$$
\Delta V = \xi \delta \nu_{\max} \min(V_\mathrm{I}, V_\mathrm{II}) \tag{2.82}
$$

where $\delta\nu_{\max}$ is the maximum fractional volume change. A parameter adjusted to obtain the desired acceptance rate of the volume changes. The acceptance criterion for particle transfers is written for transfer from region II to region I is

$$\wp_{\text{change}} = \min\left[1, \frac{N_{\text{II}}V_{\text{I}}}{(N_{\text{I}}+1)V_{\text{II}}}\exp(-\beta\Delta U_{\text{I}} - \beta\Delta U_{\text{II}})\right] \tag{2.83}$$

Eq. 2.83 can be readily applied to multi-component systems. Eq. 2.83 indicates that the probability of transfer out of an empty region is zero, which is the mathematical limit of the transfer probability, $\wp_{\text{transfer}}$, as N_{II} is continuously reduced towards zero. In such case, for all unsuccessful steps, the old configuration is counted once more for the calculation of any system property.

For pure component systems, one intensive, usually the temperature, variable can be independently specified when two phases coexist. The vapor pressure is then obtained from the simulation. For multi-component systems the pressure can be specified in advance, so that the total system is considered at NPT condition. The probability for this case is

$$\wp(N_{\text{I}}, V_{\text{I}}; N, P, T) \propto \frac{N!}{N_I N_{\text{II}}!}\exp\left(N_{\text{I}}\ln V_{\text{I}} + N_{\text{II}}\ln V_{\text{II}} - \beta U_{\text{I}}(N_{\text{I}})\right.$$
$$\left. - \beta U_{\text{II}}(N_{\text{II}}) - \beta P(V_{\text{I}} + V_{\text{II}})\right) \tag{2.84}$$

The volume changes in the two regions are done independently. The acceptance criterion for a volume change of region I is ΔV_{I} and of region II by ΔV_{II} is

$$\wp_{\text{volume}} = \min\left[1, \exp\left(-\beta\Delta U_{\text{I}} - \beta\Delta U_{\text{II}} + N_{\text{I}}\ln\frac{V_{\text{I}} + \Delta V_{\text{I}}}{V_{\text{I}}} + \right.\right.$$
$$\left.\left. N_{\text{II}}\ln\frac{V_{\text{II}} - \Delta V_{\text{II}}}{V_{\text{II}}} - \beta P(\Delta V_{\text{I}} + \Delta V_{\text{II}})\right)\right] \tag{2.85}$$

For a binary mixture with components A and B, in which B is much large the A, only component A is transferred directly between regions. Component B is transferred indirectly, by changing a particle of type A into one of type B in one of the two regions with a simultaneous reverse change in the other region. The move is accepted

with a probability (for a change of A into B in region II),

$$\wp_{\text{change}} = \min\left[1, \frac{N_{\text{II}}^{\text{A}} N_{\text{I}}^{\text{B}}}{(N_{\text{I}}^{\text{A}} + 1)(N_{\text{II}}^{\text{B}} + 1)} \exp(-\beta\Delta U_{\text{I}} - \beta\Delta U_{\text{II}})\right] \tag{2.86}$$

The chemical potentials of the two components in the two regions satisfied by these two sets of moves are

$$\begin{aligned}
\mu_{\text{I}}^{\text{A}} &= \mu_{\text{II}}^{\text{A}} \\
\mu_{\text{I}}^{\text{B}} - \mu_{\text{I}}^{\text{A}} &= \mu_{\text{II}}^{\text{B}} - \mu_{\text{II}}^{\text{A}}
\end{aligned} \tag{2.87}$$

This calculation is readily generalized for systems with more than two components.

Simulations of phase equilibria in the Gibbs ensemble do not require prior knowledge or calculation of the chemical potentials of components in a system. During the particle transfer steps, the change in internal energy of a region caused by addition of a particle is clearly related to the energies, U^+, used in the Widom equation for calculation of chemical potentials in NVT simulations:

$$\mu_i = -k_{\text{B}}T\ln\langle\exp(-\beta\Delta U^+)\rangle + k_{\text{B}}T\ln\rho_i \tag{2.88}$$

where μ_i is the chemical potential of component i and $\beta = 1/k_{\text{B}}T$, and ρ_i is the density of component i ($\rho_i = N_i/V$). Smit and Frenkel [109] obtained a similar expression for Gibbs ensemble simulations in region I:

$$\mu_i = -k_{\text{B}}T\ln\langle\frac{V_{\text{I}}}{N_{\text{I},1} + 1}\exp(-\beta\Delta U_1^+)\rangle \tag{2.89}$$

where U_1^+ is the internal energy change of region I during attempted transfers of particles of species i. The values of the chemical potentials resulting from Eqs. 2.88 and 2.89 differ less than simulation uncertainty [109], except when very few particles are present in one of the two regions.

2.4.3   Structural quantities

The structure of simple fluids is characterized by a set of distribution functions, the simplest of which is the site-site distribution function $g(r_{ij})$ or $g(r)$. It gives the

probability of finding a pair of atoms at a distance r, relative to the probability expected for a completely random distribution at the same density [4]. The site-site distribution functions, g(r) are defined by integrating over the positions of all atoms, and applying appropriate normalization factors. Obviously the choice i and j is arbitrary in a system of identical atoms. A equivalent expression is defined in [4]

$$g(r) = \rho^{-2} \left(\sum_i \sum_{j \neq i} \delta(r_i) \delta(r_j - r) \right) = \frac{V}{N^2} \left(\sum_i \sum_{j \neq j} \delta(r - r_{ij}) \right) \tag{2.90}$$

This formula could be used in the evaluation of g(r) by computer simulation. The ensemble average, $\langle a(r_i, r_j) \rangle$ of any site-site function may be expressed in

$$\langle a(r_i, r_j) \rangle = \frac{1}{V^2} \int \mathrm{d}r_i \mathrm{d}r_j g(r_i, r_j) a(r_i, r_j) \tag{2.91}$$

A set of site-site distribution function $g_{ab}(r_{ab})$ can be calculated in same way as the atomic g(r) for each type of site. The coordination number of atoms can be calculated by the following expression

$$N_c = 4\pi\rho \int_0^{r_{min}} r^2 g(r) dr \tag{2.92}$$

where N_c is the coordination number, and ρ is the density.

2.4.4 Boundary conditions

Monte Carlo and Molecular Dynamics simulations of a molecular system are to provide the properties of a macroscopic system. Most simulations investigate the structural and thermodynamic properties of a system with a few hundreds particles. In periodic boundary conditions, the simulation is carried out in a cubic box throughout space to form an infinite lattice. In the course of the simulation, when a molecule moves in the central box, its periodic image in every one of the other boxes moves with exactly the same orientation in exactly the same way. Thus, a molecule leaves the central box, one of its images will enter through the opposite face. There are no walls at the boundary of the central box, and the system has no surface [35, 4]. Boundary conditions are usually used in conjunction with the minimum image convention for short ranged forces. Here interactions between each
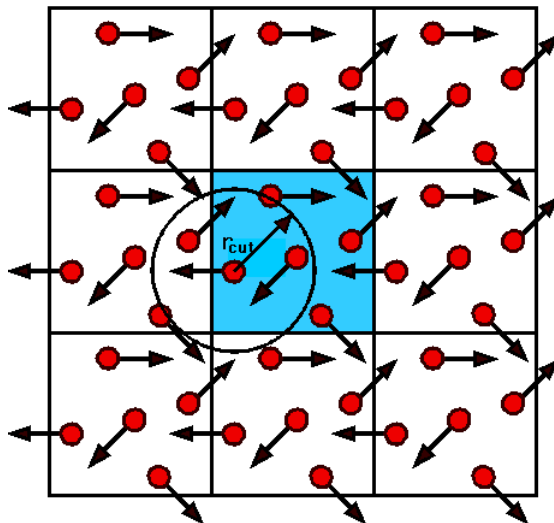
Figure 2.2: Periodic boundary conditions. The central box is outlined by a bolder line with blue background. The circle represents a potential cutoff.

molecule and the closest periodic image of its neighbors are considered.

Short ranged forces are often truncated to increase computational efficiency. For consistency with the minimum image convention, this cut-off distance must be less than or equal to half the box length. Boundary conditions can have an effect on the system. This is especially pronounced for small system sizes and for properties with a large long-range contributions, such as light scattering factors. They also inhibit long wavelength fluctuations that are important near phase transitions [35, 4].

2.4.5   Thermodynamic properties

In Gibbs ensemble simulation, the thermodynamic properties of a system resulting from the simulation results are the enthalpy, the internal energy, the boiling temperature and the critical point. The enthalpy is calculated by equation $H = U + pV$ or $H = E + pV$ from the configurational energy U or internal energy E, pressure p and volume V. The enthalpy of vaporization $\Delta_{\text{vap}}H$ and the internal energy $\Delta_{\text{vap}}U$ are estimated readily as the difference in heat content between coexisting liquid and vapor ($\Delta_{\text{vap}}H = H_{\text{v}} - H_{\text{l}}$) and ($\Delta_{\text{vap}}U = U_{\text{v}} - U_{\text{l}}$). The entropy of vaporization is then $\Delta_{\text{vap}}S = \Delta_{\text{vap}}H/T$. The chemical potential of each species can be calculated

using the Widom equation Eq. 2.88 [133].

The form of the coexistence curve obtained from Gibbs ensemble simulations has been examined by Mon and Binder [80] for the two-dimensional Ising model, by Recht and Panagiotopoulos (1993) [100] and Smit (1993) [107] for a continuous-space binary mixture in two and three dimensions and by Panagiotopoulos [101] for truncated Lennard-Jones potentials in two and three dimensions. Smit et al. (1995) [110] showed that the Ising scaling exponent can also fit the experimental data. Smit and Williams (1990) [111] also showed that the critical point can be calculated by fitting the coexistence densities to the density scaling law equation 2.93 along with the law of rectilinear diameters [104]:

$$
\begin{aligned}
\frac{\rho_l - \rho_v}{2} &= \rho_c + A(T_c - T) \\
\rho_l - \rho_v &= B(T - T_c)^\beta
\end{aligned}
\tag{2.93}
$$

where ρ_l is the coexistence liquid density, ρ_v is the coexistence vapor density, ρ_c is the critical density. T_c is the critical temperature, β is the critical exponent here a non-classical value ($\beta \approx 0.325$) is used. A and B are constants. Eq. 2.93 is solved using a least-squares fit to the vapor-liquid coexistence data.

The Antoine equation is a simple empirical 3-parameter equation that for vapor pressures. It is used here to correlate the vapor pressures obtained from GEMC simulations [136, 102]:

$$
\ln P = A - \frac{B}{T + C}
\tag{2.94}
$$

where A, B, and C are Antoine constants. P is vapor pressure and T is temperature. The parameters A, B, C were compared with the experimental parameters.

The enthalpy of vaporization is a characteristic parameter that reflects the amount of heat energy required to vaporize one mole of the substance. The relation between

vapor pressure, heat of vaporization, and temperature is given by the Clausius-Clapeyron equation [136, 102].

$$\ln\left(\frac{P_1}{P_2}\right) = -\frac{\Delta_{\text{vap}}H}{R}\left(\frac{1}{T_1} - \frac{1}{T_2}\right) \tag{2.95}$$

For the standard state $P^0 = 0.1$ MPa this relation is rewritten as

$$\ln\left(\frac{P}{P^0}\right) = \left(-\frac{\Delta_{\text{vap}}H}{R}\right)\left(\frac{1}{T}\right) + \frac{\Delta_{\text{vap}}S}{R} \tag{2.96}$$

Here T_1 and T_2 are the temperatures at the pressure P_1 and P_2, $\Delta_{\text{vap}}S$ is the entropy of vaporization (J/K.mol) at P^0. The slope of $\ln P$ with respect to $1/T$ is proportional to the enthalpy of vaporization, and it is found to be nearly constant except in the critical area. From the slop of a plot of $\ln P_{\text{v}}$ vs. $1/T$ therefore $\Delta_{\text{vap}}H$ can be obtained and from the intercept $\Delta_{\text{vap}}S$ can be calculated too.

Chapter 3

Calculation Methods

This chapter describes the calculation techniques for *ab initio* intermolecular interaction pair potentials, the virial coefficients of the dimers H_2-H_2, H_2-O_2, F_2-F_2 and H_2-F_2 as well as the GEMC-NVT and NPT simulation and the calculations of the thermodynamic properties for the vapor-liquid equilibria of the pure fluids hydrogen and fluorine.

3.1 Program and Resources

3.1.1 Calculation program

Program packages

- *Gaussian03*^{TM} [36] was used to calculate the molecular properties of the single molecules hydrogen, oxygen and fluorine, and the *ab initio* intermolecular energies of the dimers H_2-H_2, H_2-O_2, F_2-F_2 and H_2-F_2 at the levels of theory MPn (n = 2, 3, 4) and CCSD(T) with basis sets 6-31G, 6-311G and aug-cc-pVmZ (m = 2, 3, 4).

- *Auto2Fit* v3.0 [12] estimates the adjustable parameters of the analytical potential functions by fitting them to the *ab initio* intermolecular energies with the Genetic Algorithm (GA).

- *ThermoC* program [18, 22] calculates the second virial coefficients, vapor pressure, vapor-liquid equilibria and the thermodynamic properties of the pure fluids with several equations of state.

Programs and utilities in Code C and Fortran

The programs below have been coded in C and Fortran 77.

- Fitting program with the Levenberg-Marquardt algorithm

- BSSE (Basis Set Superposition Error) program

- Virial program for multi-dimensional integrals

- First-order quantum correction program (Fortran)

- Extrapolation program to complete basis set limit

- Start configuration program

- GEMC-NVT program

- GEMC-NPT program

3.1.2   Data and Resources

Computations were carried out on computers of the group of Prof. Deiters at the Institute of Physical Chemistry as well as in the computer center of the University of Cologne. Experimental data used for this work were taken mostly from the compilations [17, 124, 119, 66, 28, 75, 47] as well as from other sources listed in the bibliography.

3.2   *Ab initio* quantum chemical calculations

3.2.1   Molecular orientation

In this work the linear molecules hydrogen, oxygen and fluorine are represented as 5-site models, with two sites placed on the atoms (H, O or F), one site in the center of gravity (M), and two sites half-ways between the atoms and the center (N). The molecules are treated as rigid; the interatomic distances are set to 0.74130 Å for hydrogen, 1.20741 Å for oxygen and 1.418 Å for fluorine [119, 66].

As these molecules are linear, the intermolecular pair potential is a function of
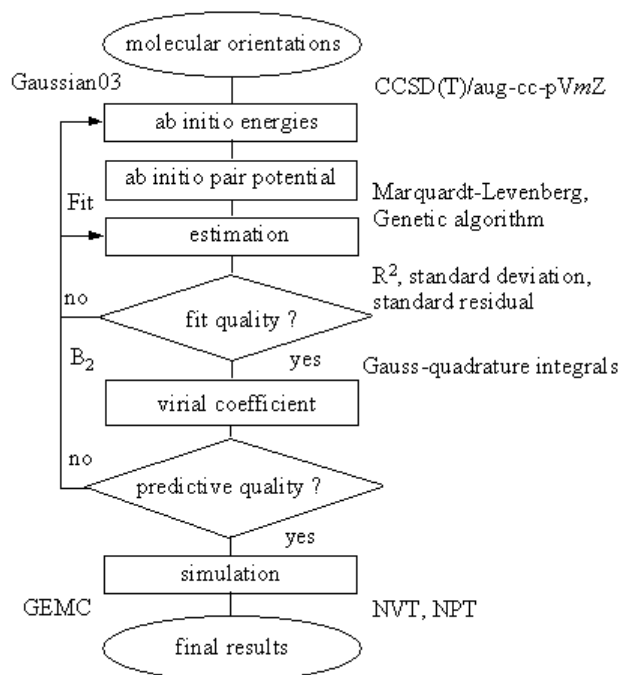
Figure 3.1: The block diagram of research process.

the distance r between the centers of gravity and the three angular coordinates, α, β, and ϕ, which are explained in Fig. 3.2.

Intermolecular energies were calculated for all values of r from 2.6 Å to 15.0 Å with an increment of 0.2 Å; the angles α, β, and ϕ were varied from 0 to 180° with an increment of 45°. Care was taken to recognize identical configurations in order to reduce the computational workload. Fig. 3.2 describes also four special orientations, which were used to check the performance of the interaction potential functions created in this work.

3.2.2 *Ab initio* calculations

Predicting single-molecule properties

The accuracy of computations depends on the theoretical method and the basis set. Consequently they need to be reexamined before carrying out any calculation. The basic molecular quantities which were considered are the dissociation energies, the vibrational frequencies and the bond lengths.

L: = 0,   = 0,   = 0   T: = 90,   = 0,   = 0

H: = 90,   = 90,   = 0   X: = 90,   = 90,   = 90
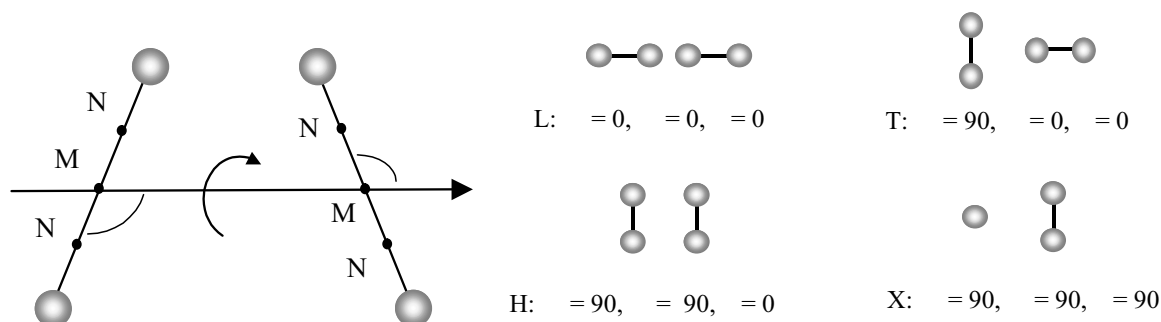
Figure 3.2: A 5-site model of a diatomic molecule and selected orientations for quantum chemical approaches.

The dissociation energy is defined as the energy difference between a molecule and its component atoms [36, 34, 10]. For the molecules hydrogen, oxygen and fluorine, because of molecular symmetry, it can be calculated as

$$\Delta E = 2E_{\mathrm{a}} - E_{\mathrm{m}} \tag{3.1}$$

Here E_a and E_m are the energies of an atom and a molecule, respectively. The molecular energy is corrected for zero-point energy (ZPE). The molecular energy is calculated from carrying out molecular optimization. The vibrational frequency and the bond lengths of the molecules hydrogen, oxygen and fluorine are derived from such an optimization. Two single point energy calculations for the atoms and the molecule itself are carried out, too [34].

Calculating *ab initio* interaction energies

The Hartree–Fock SCF method is a widely used method in quantum chemistry; it had proven to be useful for the calculation of chemical bond energies and even of hydrogen bonding energies. Dispersion forces, however, are caused by electron correlations, and these effects are excluded in pure SCF calculations [34].

A full configuration interaction treatment (CI) for electron correlations requires enormous computational resources and is usually not practical, as shown in Section 2.1.1. The post-SCF methods based on Møller–Plesset perturbation theory

MPn (n = 2, 3, 4) and coupled-cluster method CCSD(T) are useful to capture at least a part of the electron correlation effects. Due to the diffuse, wide-range nature of dispersion force fields, it is necessary to adopt appropriate basis sets as presented in Section 2.1.2. The basis sets used here for calculating the *ab initio* intermolecular energies are aug-cc-pVDZ (for oxygen: 10s5p2d/4s3p2d, for hydrogen: 5s2p/3s2p, for fluorine: 10s5p2d/4s3p2d), aug-cc-pVTZ (for oxygen: 12s6p3d2f/5s4p3d2f, for hydrogen: 6s3p2d/4s3p2d, for fluorine: 11s6p3d2f/5s4p3d2f) and aug-cc-pVQZ(for oxygen: 12s6p3d2f1g/5s4p3d2f1g, for hydrogen: 6s3p2d1f/4s3p2d1f, for fluorine: 12s6p3d2f1g/5s4p3d2f1g) proposed by Dunning et al. [54, 13] and the small polar basis sets: 6-31G (for oxygen: 10s4p/ 6s4p, for hydrogen: 4s/3s, for fluorine: 10s4p/6s4p) and 6-311G (for oxygen: 11s5p/ 6s5p, for hydrogen: 5s/3s, for fluorine: 11s5p/ 6s5p) [13, 48].

The *ab initio* energy results were corrected for the basis set superposition error with the counterpoise correction method proposed by Boys and Bernardi [6, 10] in Section 2.1.3.

Extrapolating to the basis set limit

The electronic energies are extrapolated to the basis set limit with the extrapolation scheme described in Section 2.1.5,

$$\Delta E(m) = \Delta E(\infty) + cm^{-3} \tag{3.2}$$

with $m = 2$ (for aug-cc-pVDZ basis set) or 3 (for aug-cc-pVTZ). If results for two different basis sets are available, it is possible to calculate the energy value for an infinite basis set from Eq. 3.2; this result is referred to as aug-cc-pV23Z. The extrapolation scheme is adequate for our *ab initio* energy calculations here.

3.2.3 Building the pair potential functions

The analytical potential functions consist of terms for the repulsive and the dispersive interaction forces and the charge interaction. These are very universal. Modelling the molecular anisotropy by spherical harmonics is possible in principle, too. But it was not attempted here for reasons explained in Chapter 1 and Section 2.2. Instead, multi-center potential functions as proposed in Section 2.2.3 and

Section 2.2.4 were better suited for modelling a molecular system. 2-site or even 3-site molecular models did not represent the *ab initio* data well, but 5-site models were sufficient [5, 65].

For the dimer hydrogen and the mixture hydrogen-oxygen two pair potential functions were constructed by incorporating the repulsive and the dispersive part, which were combined from parts of the site-site pair potential functions Eq. 2.29, Eq. 2.28 and Eq. 2.30 as shown in Section 2.2.4. The other two were also built up similarly for the dimer fluorine and the mixture hydrogen-fluorine. The damping functions were used for these analytical potential functions demonstrated with Eq. 2.29, Eq. 2.30, and Eq. 2.27.

In principle such a 5-site model leads to an *ab initio* pair potential function consisting of 25 spherical site-site interactions. But because of molecular symmetry only six different site-site potentials have to be fitted for the dimers hydrogen and fluorine, and eight for the dimers hydrogen–oxygen and hydrogen-fluorine. The new *ab initio* intermolecular interaction potential functions developed within this thesis are set up according to Eq. 3.3, Eq. 3.4, Eq. 3.5 and Eq. 3.6.

The first two of them are used for the dimers H_2-H_2, and H_2-O_2.

$$u = \sum_{i=1}^{5} \sum_{i=1}^{5} \left[D_e^{ij} e^{-\alpha_{ij} r_{ij}} + f_1(r_{ij}) \sum_{n=6,8,10} \frac{C_n^{ij}}{r_{ij}^n} + f_2(r_{ij}) \frac{q_i q_j}{4\pi\epsilon_0 r_{ij}} \right]$$
(3.3)

with $f_1(r_{ij}) = (1 + e^{-2(\delta_{ij} r_{ij} - 2)})^{-15}$ and $f_2(r_{ij}) = 1 - e^{-\beta_{ij} r_{ij}}$

$$u = \sum_{i=1}^{5} \sum_{i=1}^{5} \left[D_e^{ij} e^{-\alpha_{ij} r_{ij}} + f_1(r_{ij}) \sum_{n=6,8,10,12} \frac{C_n^{ij}}{r_{ij}^n} + f_2(r_{ij}) \frac{q_i q_j}{4\pi\epsilon_0 r_{ij}} \right]$$
(3.4)

with $f_1(r_{ij}) = 1 - e^{-\delta_{ij} r_{ij}} \sum_{k=0}^{10} \frac{(\delta_{ij} r_{ij})^k}{k!}$ and $f_2(r_{ij}) = 1 - e^{-\beta_{ij} r_{ij}}$

The other two are used for the dimers F_2-F_2 and H_2-F_2

$$u = \sum_{i=1}^{5} \sum_{j=1}^{5} \left[D_e^{ij} \left((1 - e^{-\alpha_{ij}(r_{ij} - \beta_{ij})})^2 - 1 \right) + f(r_{ij}) \left(\sum_{n=6,8,10} \frac{C_{ij,n}}{r_{ij}^n} + \frac{q_i q_j}{4\pi\epsilon_0 r_{ij}} \right) \right]$$
(3.5)

with $\quad f(r_{ij}) = (1 + e^{-2(\delta_{ij} r_{ij} - 2)})^{-15}$

$$u = \sum_{i=1}^{5} \sum_{i=1}^{5} \left[D_e^{ij} \left((1 - e^{-\alpha_{ij}(r_{ij} - \beta_{ij})})^2 - 1 \right) + f(r_{ij}) \left(\sum_{n=6,8,10,12} \frac{C_{ij,n}}{r_{ij}^n} + \frac{q_i q_j}{4\pi\epsilon_0 r_{ij}} \right) \right]$$
(3.6)

with $\quad f(r_{ij}) = 1 - e^{-\delta_{ij} r_{ij}} \sum_{k=0}^{10} \frac{(\delta_{ij} r_{ij})^k}{k!}$

Here the r_{ij} denote site-site distances, q_i and q_j are electric charges of sites, and $C_{ij,n}$ are dispersion coefficients; the leading dispersion term is always proportional to r_{ij}^{-n}. The site charges q_i and q_j are evaluated by fitting to the electrostatic potential of the molecule shown in Section 2.1.6. In the 5-site model (Fig. 3.2) the auxiliary sites N, placed on the molecular axis half-ways between the outer sites (H, O or F) and the center M, bear each a charge of $+q$, and the central site M a charge of -2q. The outer sites have no electric charge.

3.3 Analytical potential fit

The adjustable parameters of the *ab initio* intermolecular pair potential functions can be estimated by nonlinear least-square fitting to the *ab initio* interaction energy values resulting from the *ab initio* calculations. But this fit proved to be very difficult, because of the object potential functions of the fitting problem have many local minima. Consequently the fit process has to be carried out by two steps. For the first step the global minima are coarsely located by means of the genetic algorithm. Then these initial parameters are optimized with the Marquardt-Levenberg algorithm (Section 2.2.6). The fit programs were described in Section 3.1.1.

3.4   Calculating the virial coefficients

3.4.1   Integral calculations

Virial coefficients are related to intermolecular potentials by rigorous statistical thermodynamic theory; the second virial coefficient depends on the pair potential only. On the other hand, at least second virial coefficients have been determined experimentally for many gases. The calculation of the second virial coefficients from *ab initio* potential functions is a stringent and necessary test for the usefulness of such *ab initio* potentials. Computer simulations of some of the properties of the liquid state might fail to give satisfactory results because multi-body potentials could not be accounted for, or because these properties are difficult to sample by simulations. But a failure to reproduce second virial coefficients points to an inadequacy of the pair potential used.
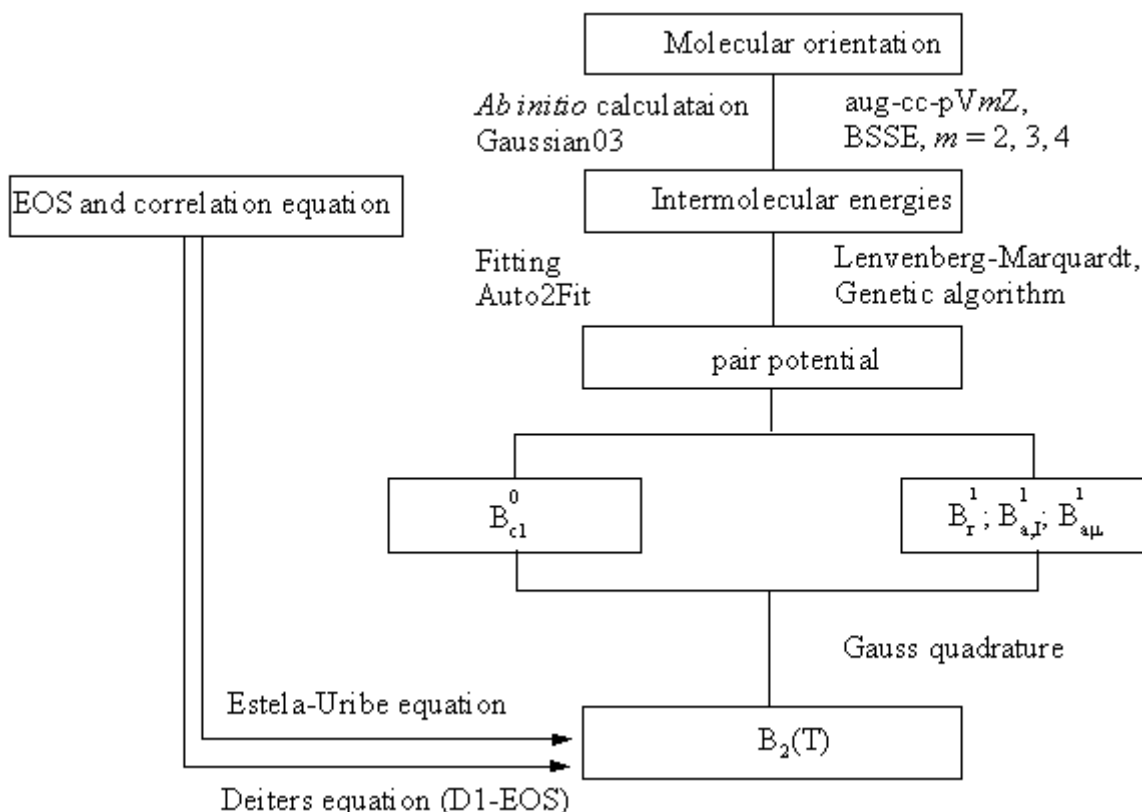
Figure 3.3: The block diagram for calculating the virial coefficients B_2.

The prediction of the second virial coefficients for the dimers H_2-H_2, H_2-O_2, F_2-F_2 and H_2-F_2 was done as outlined in the block diagram Fig. 3.3. The case of these gases is more complicated because of quantum effects, in which the interaction consists of atoms or molecules with small masses or small moments of inertia. These can in principle be obtained from a perturbation expansion of Planck's constant as given in Section 2.3.3. The first order quantum corrections to the second virial coefficients of linear molecules can be calculated with Eq. 2.57, Eq. 2.62, Eq. 2.63, and Eq. 2.64 shown in Section 2.3.3.

In this work Eq. 2.64 is used for calculating the quantum corrections to the virial coefficients of the dimers H_2-H_2, H_2-O_2, F_2-F_2 and H_2-F_2. It is broken down into Eq. 2.65. The virial coefficients can be computed by the two following steps: first the classical second virial coefficients B_{cl}^0 are calculated from equation Eq. 2.66. Second the first-order correction terms $B_r^{(1)}$, $B_{a,I}^{(1)}$ and $B_{a,\mu}^{(1)}$ are calculated using the equations Eq. 2.67, Eq. 2.68 and Eq. 2.69. The total quantum-corrected second virial coefficient $B_2(T)$ is defined as the sum of the contributions from the expressions Eq. 2.66, Eq. 2.67, Eq. 2.68 and Eq. 2.69.

All integrals of the virial expressions as mentioned above were estimated numerically with a 4-dimensional Gauss–Legendre quadrature method described in section 2.3.4. The second virial coefficients were calculated using the programs listed Section 3.1.1.

3.4.2 Correlation equation calculations

In this thesis the empirical correlation equations Eq.2.46 and Eq. 2.47 of Estela-Uribe and Jaramillo (Section 2.3.1) were used to calculate the second virial coefficients of the dimers hydrogen and fluorine and especially the cross second virial coefficents of the binary mixtures hydrogen-oxygen and hydrogen-fluorine. The obtained results with these correlation equations are compared with the virial coefficients resulting from the *ab initio* potential functions. The experimental critical parameters of the hydrogen, oxygen and fluorine were used as input for these correlation equations. The two correlation parameters included in Eq. 2.47 were set to zero for the binary interactions hydrogen–oxygen and hydrogen-fluorine.

3.4.3   Calculation from equations of state

The Deiters equation of state (denoted D1) Eq. 2.49 described in Section 2.3.2 was used here to calculate the virial coefficients of the dimer F_2-F_2. The thermodynamic properties of vapor-liquid equilibria for the pure fluid fluorine were also calculated by this equation. The results from this equation were compared with those calculated from *ab initio* pair potentials Eq. 3.5 and Eq. 3.6, as well as those resulting from GEMC-NVT simulation. This task is also to test the accuracy of the potentials Eq. 3.5 and Eq. 3.6. The Deiters equation of state (D1) is contained in program *ThermoC*, described in Section 3.1.1.

3.5   Gibbs ensemble Monte Carlo Simulation

3.5.1   Simulation details

The thermodynamic properties of the pure fluids hydrogen and fluorine studied here are the orthobaric densities, the vapor pressures, the enthalpy of vaporization, the entropy of vaporization, the boiling temperature, and the critical parameters, which can be calculated with the Gibbs ensemble Monte Carlo simulation techniques explained in Section 2.4.2.

The NPT-GEMC simulation was used to calculate the density, and the internal energy of fluid hydrogen and fluorine to examine the accuracy of the pair potentials. For hydrogen this simulation was investigated on isobars at 1.0 MPa and 5.0 MPa and for temperatures from 26.0 K to 250 K, respectively. Similarly for fluorine it was performed also on isobars at the pressures 1.0 MPa and 10.0 MPa for temperatures range from 90.0 K to 270 K; NVT-GEMC simulations were performed to obtained coexisting liquid and vapor densities, and vapor pressures. They were in the temperature range 18.0 K to 32.0 K with an increment 2.0 K for hydrogen, and from 60.0 K to 140.0 K with an increment 10.0 K for fluorine.

The pair potential functions Eq. 3.3 and Eq. 3.4 for hydrogen, and Eq. 3.5 and Eq. 3.6 for fluorine were used for both simulation cases. Total number of particles N = 512 were used in both GEMC-simulations with the standard periodic boundary conditions and the minimum image convention. For NVT-GEMC simulation runs
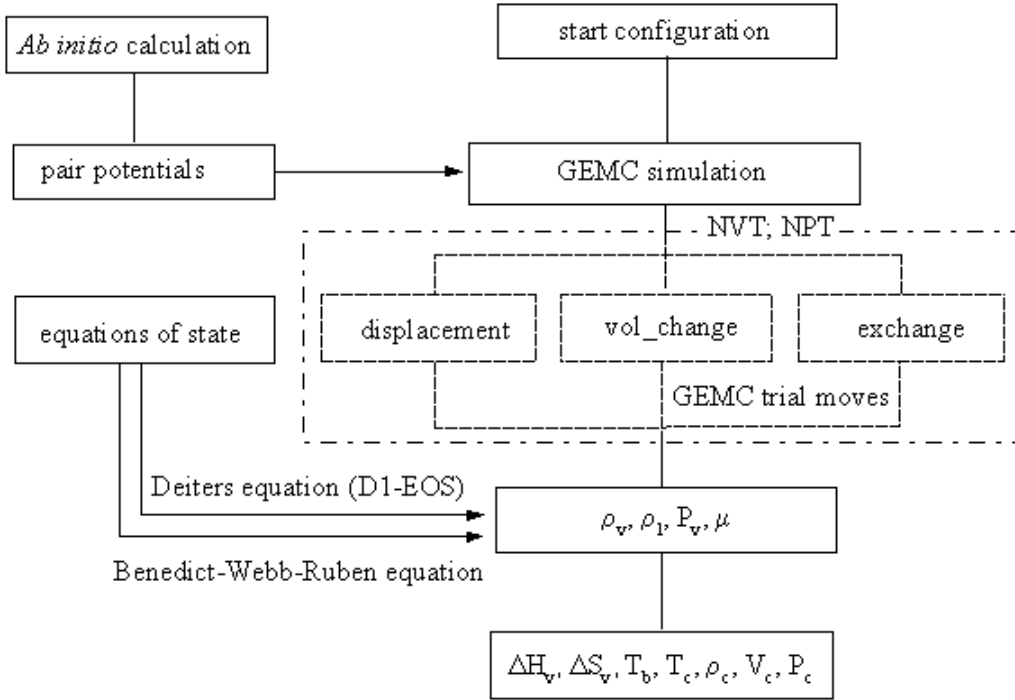
Figure 3.4: The block diagram for predicting the phase behavior.

the equilibration between two phase required $1 - 2 \times 10^6$ cycles. The simulation parameters were set for 50% acceptance ratios for translations and volume fluctuations. All movements were performed randomly with defined probabilities. The accumulative averages of desired quantities were established within 1.0×10^3 cycles, after initial equilibration had been reached within 5.0×10^4 cycles. The simulation data were exported using block averages with 1000 cycles per block. The statistical errors in the simulation runs were estimated by dividing each run into 100 blocks and taking the largest deviation of a block mean from the total mean as error. The simulations were started with equal densities in two phases. The simulation systems were equilibrated for about 1.0×10^6 cycles. The cut-off radius r_c was set to 7.5 Å for hydrogen and 8.5 Å for fluorine. Corrections for long-range interactions for the internal energy were computed by the standard relations [4].

3.5.2 Structural properties

The structural properties of the fluids hydrogen and fluorine were studied for the liquid phase at different temperatures with the NVT- and NPT-GEMC simulations,

respectively; in both cases the temperature dependence is shown by site-site pair distribution functions g(r) (Section 2.4.3). The site-site pair correlation functions for the interactions H-H, F-F, N-N, M-M, H-M and F-M for the fluids hydrogen and fluorine were achieved by simulations shown in Section 9.2 and 10.2. The structural properties of each fluid were compared with experimental data and with data from literature, if available.

3.5.3   Calculating the phase coexistence properties

The critical temperatures T_c/K, densities ρ_c/gcm^{-3} and volumes V_c/cm^{3}mol^{-1} of the pure fluids hydrogen and fluorine were derived from a least-squares fits to the densities of coexisting phases using the relations Eq. 2.93 of the rectilinear diameter law shown in Section 2.4.5.

The critical pressures P_c/MPa of hydrogen and fluorine were calculated with the Antoine equation Eq. 2.94, which had been fitted to the vapor pressure curves. The enthalpy of vaporization $\Delta_{vap}H$, entropy of vaporization $\Delta_{vap}S$ and the boiling temperature T_b of these fluids at the standard state $P = 0.101$ MPa were estimated by the Clausius-Clapeyron equation Eq. 2.95 and Eq. 2.95, which was also fitted to the simulation vapor pressure values of hydrogen and fluorine. In all cases the comparisons with literature data are also included [18, 90, 76, 74, 66, 17].

Chapter 4

Results and Discussion

This chapter describes the results of the methods as mentioned in (Chapter 3), which are the *ab initio* intermolecular pair potentials, the second virial coefficients of the dimers H_2-H_2, F_2-F_2, H_2-O_2 and H_2-F_2, and the vapor-liquid equilibria for the pure fluids hydrogen and fluorine.

4.1   *Ab initio* quantum chemical calculations

4.1.1   Predicting single-molecule properties

The dissociation energies, the vibrational frequencies and the bond lengths of the molecules hydrogen, oxygen and fluorine were chosen for assessing to the accuracy of the *ab initio* quantum chemical methods MPn (at levels 2 to 4) and CCSD(T) with the basis sets, discussed in (Section 3.2.2), because these properties are close, related to the intermolecular pair potential. The comparison of the dissociation energies of these molecules is shown in Table 6.2 as well as Figures 4.1, 4.2 and 4.3. The vibrational frequencies and bond lengths are given in Tables 6.1 and 6.3 (Chapter 6). These turned out to depend very much on the various levels of theory and the basis sets. The Møller-Plesset perturbation method MPn (n = 2, 3, 4) was not appropriate for the dimer interaction calculations of this work. The results shows that especially the methods MP2, MP3 usually underestimated the interaction energies. This was also shown in the recent publications of Diep et al. [25] and Deiters [65, 85].

On the other hand the single-molecule properties resulting from the method CCSD(T)

using the extrapolated basis set limit aug-cc-pV23Z were rather close to experimental data. With a much larger basis set it might be possible to obtain more accurate results, but the computational cost would be too high. Even the use of a larger basis sets aug-cc-pVQZ or aug-cc-pV5Z in calculations for the molecules oxygen and fluorine proved to be difficult. Nevertheless, the extrapolation scheme could be shown to work quite well (Section 2.1.5 and 3.2.2). Patton et al (1999) investigated the use of infinite basis set limits in electronic structure theory [33]; they obtained the dissociation energies of 457.741 kJ/mol for H_2 and 500.0 kJ/mol for O_2, which is not far different from the experimental data and the calculated results in Table 6.2. Tables 6.2, 6.1 and 6.3 show that the CCSD(T) calculations with the extrapolated basis sets gave the results within 0.5-1.0% of the experimental values. This was also proven by a series of further studies using the extrapolation scheme [84, 85, 65, 64] for the rare gases and nitrogen. The monomer properties of nitrogen quadruple moment, mean polarizability, anisotropic part of the polarizability and bond length were estimated with this extrapolation scheme, and were found to be satisfyingly close to experimental data [65]. The CCSD(T) method appeared to account for the most significant electron correlation effects. It was used for this computational work.
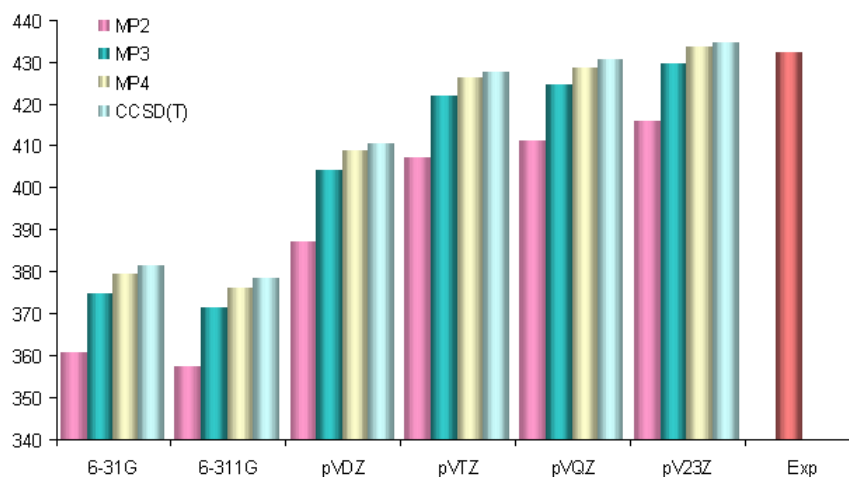
Figure 4.1: Comparison of dissociation energies in kJ/mol of the molecule H_2.
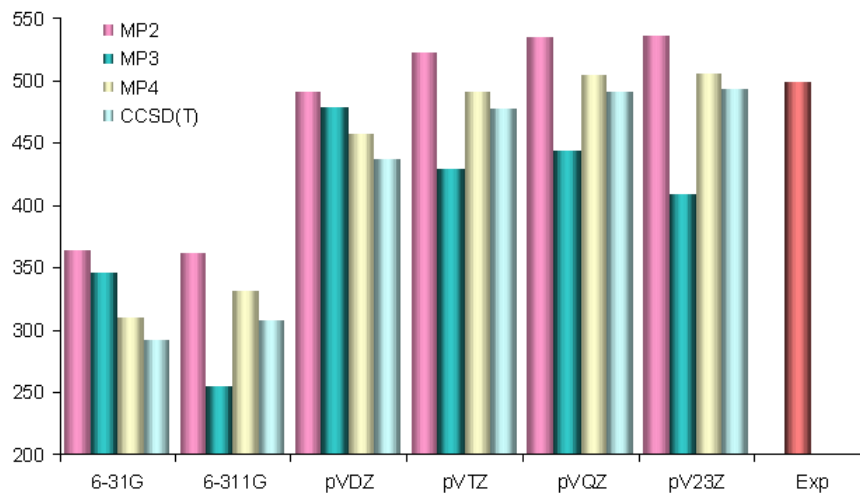
Figure 4.2: Comparison of dissociation energies in kJ/mol of the molecule O_2.
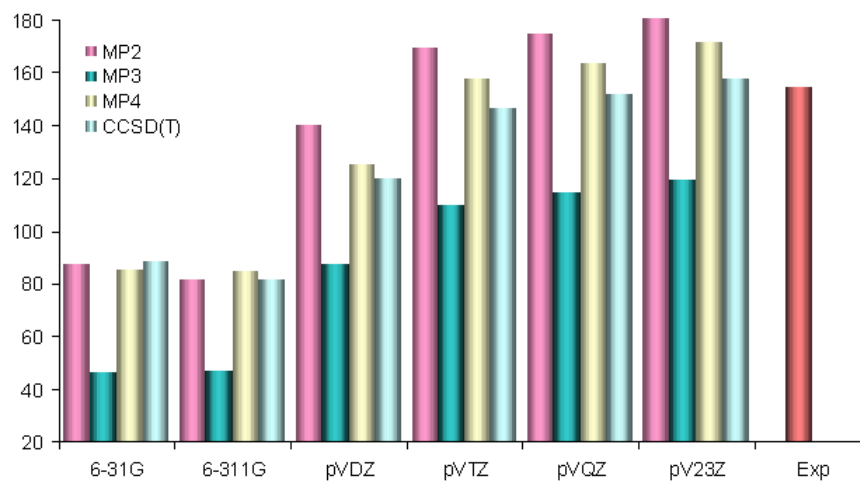
Figure 4.3: Comparison of dissociation energies in kJ/mol of the molecule F_2.

4.1.2 *Ab initio* calculations for dimers

To compare the new potential energy surfaces with existing ones, the interaction energy versus the distance of the centers of gravity was plotted for the four special orientations (Fig. 3.2) illustrated in Sections 6.2 and 6.3. In *ab initio* calculations the experimental bond lengths were taken from the experimental sources [66, 119]. Table 4.1 shows the comparison of intermolecular energies for the two special orientations T and H of the dimer hydrogen between the results of Diep et al. [25] and those of this work. It is found that the interaction energies of both orientations at a

Table 4.1: Convergence of interaction energy for the two represented configurations T and H (Fig. 3.2) of the dimer hydrogen at 3.4 Å center of gravity distance using the theoretical level CCSD(T) with complete basis set limit.

Configuration	Interaction energy/μE_H	basis set	ref.
$\alpha = 90$, $\beta = 0$, $\phi = 0$	-160.58920	CBS limit	[25]
	-171.82481	aug-cc-pV23Z	this work
$\alpha = 90$, $\beta = 90$, $\phi = 0$	-46.17217	CBS limit	[25]
	-48.83019	aug-cc-pV23Z	this work

3.4 Å center of gravity separation resulting from the level of theory CCSD(T) with basis set limit aug-cc-pV23Z were lower. This difference might be caused by the experimental bond length used. But these effects are insignificant. This is illustrated in Fig. 4.4 for T orientation of the dimer H_2-H_2. Post-SCF calculations of electron correlation effects at the levels MPn (n = 2, 3, 4) and CCSD(T) are depicted in Figures 6.1, 6.2, 6.3 and 6.4. The *ab initio* intermolecular energies of the four special configurations (Fig. 3.2) of hydrogen are also compared with the results of Diep and Johnson [25] see in Fig. 6.1. One can see that the interaction energies converged rapidly with the level of theory. Going from the methods MPn (n = 2, 3, 4) to CCSD(T), the energy changes are significant, although the MP3 and MP4 are very close to CCSD(T). The potential energy surface of hydrogen is shown in Figure 4.5.

Recently a new four-dimensional potential energy surface for the dimer CO-CO has
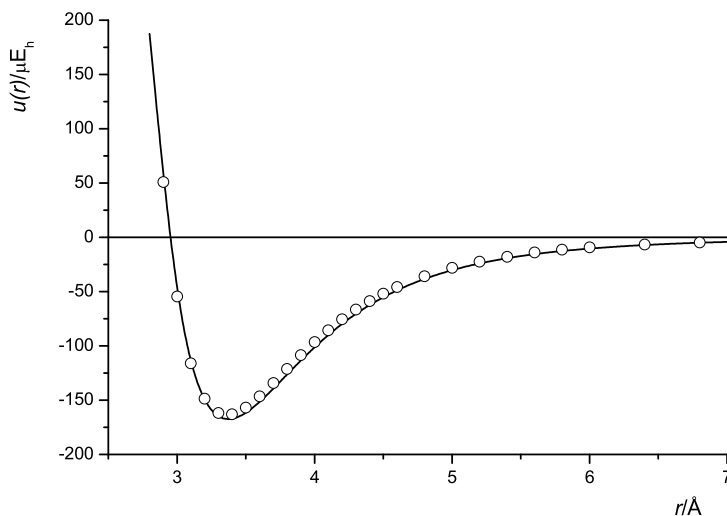
Figure 4.4: Comparison of interaction energies in μE_H for T orientation of the dimer H_2-H_2 at CCSD(T) level of theory. —, with basis set aug-cc-pV23Z (this work); ○, results using basis set limit CBS of Diep and Johnson [25].

been obtained from symmetry adapted perturbation theory (SAPT) calculations by Vissers et al. (2005) [130]. They show that two possible reasons for the inaccuracies of the potentials are the use of the multipole approximation and the neglect of electronic correlation effects on the exchange repulsion energy. The high-order electronic correlation effects are very important. Furthermore, larger basis sets are needed for an accurate description of the potential energy surface. All these results show that the performance of MP2 is rather system dependent, and that it might be appropriate to use CCSD(T), if possible, perhaps even with a smaller basis set. So the method CCSD(T) is adequately accurate for describing the electron correlation.

In a recent publication Noorbala and Sabzyan [105, 88] calculated the intermolecular potential energy surface for the system F_2-F_2 using the MP2/6-31G* level of theory. Their results also included the BSSE corrections. But there was a large difference between their calculated results and these obtained with CCSD(T)/aug-cc-pVmZ (m= 2, 3, 23). The accuracy of the levels of theory with the small polar basis sets was also proven in Section 6.2 and Section 6.3, and also appeared at the calculation
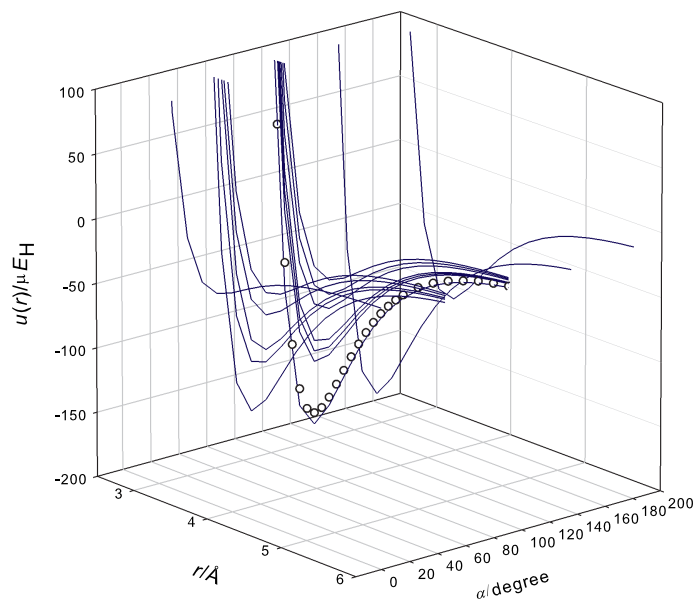
Figure 4.5: Intermolecular potential energy surface for the dimer H_2-H_2 built from the intermolecular energies using CCSD(T)/aug-cc-pV23Z as shown in Table 6.5; ∘, results for T orientation using basis set limit CBS of Diep and Johnson [25].

of the single-molecule properties in Section 4.1.1.

In 1994 Domanski et al. published *ab initio* quantum chemical calculations for the carbon dioxide dimer and from them established a pair potential function usable in molecular simulations [27]. In their study the 6-31G* basis set was used and the electron correlations were taken into account by the 2nd order Møller-Plesset theory. However, the small basis 6-31G* cannot yield accurate results as shown by Bock [5]. Therefore the level of theory MP2/6-31G* proved insufficient for *ab initio* calculations.

A comparison of the influence of the size of basis sets is also given in Figures 6.5, 6.6, 6.7 and 6.8. These figures show that the interaction energy significantly depends on the size of basis set. An increase of the size of the basis set also shifts the repulsive wall to the left. A comparison of minimal interaction energies for the four orientations of Fig. 3.2 of the four dimers are shown in Table 6.4. Figure 4.4 confirms that the pair potentials aug-cc-pV23Z are indeed of high quality, and that

the $1/m^3$ extrapolation method is a reliable way to evaluate the basis set limit. In contrast to the new pair potential energy surfaces the methods MPn ($n = 2, 3, 4$) resulted in interaction energies having larger deviations of the well depths and well positions. This was also shown by Diep and Johnson [25]. The interaction energy points were generated to represent the 4-dimensional potential energy surfaces of the dimers H_2-H_2, F_2-F_2, H_2-O_2 and H_2-F_2 also shown in Tables 6.5 and 6.8.

4.1.3 Fitting the potential energy surface

For computer simulations it is necessary to have analytical pair potential functions. Their adjustable parameters were estimated by combining the Genetic algorithm and the Marquardt-Levenberg algorithm. For simplification a few of the damping parameters (δ_{ij}), exponents (β_{ij}) were set to fixed values as shown in Tables 7.1, 7.2, 7.3 and 7.4.

Each of the new pair potential functions of this work (Section 3.2.3) were fitted to a set of 930 interaction energy points calculated for the dimers H_2-H_2, F_2-F_2, H_2-O_2 and H_2-F_2. There were from 36 to 64 adjustable parameters in total for each pair potential. The correlation between the fitted versus *ab initio* energies is depicted in Figures 4.6, 7.1 for hydrogen, Figures 7.2, 7.3 for hydrogen-oxygen, Figures 4.7, 7.4 for fluorine, and Figures 7.5, 7.6 for hydrogen-fluorine.

The values of root mean-square deviations (rms), multiple correlation coefficients (R^2), and average residuals of the fitted analytical potential functions are given in Tables 4.2 and 4.3, These are used to test the correlation between the *ab initio* energies and the predicted energies from the potential models. The estimates of the errors here are important for assessing the quality of the fit. These values determine the range where the actual responses can be found with a given probability. The statistical values in Tables 4.2 and 4.3 are calculated with the following formulae: The root mean square deviation (rms) for a set of N residuals ($\widehat{Y}_i - Y_i$) is

$$\text{rms} = \sqrt{\frac{\sum_{i=1}^{N}(\widehat{Y}_i - Y_i)^2}{N}} \tag{4.1}$$

Table 4.2: The statistical results for fitting the intermolecular potentials Eq. 3.3 and Eq. 3.4 for the dimers hydrogen and hydrogen-oxygen. The values are in μE_H.

potential	H_2-H_2			
			residual	
	R^2	rms	min	max
Eq. 3.3	0.9999	0.2329	-6.311	6.284
Eq. 3.4	0.9999	0.4258	-7.449	7.911
potential	H_2-O_2			
			residual	
	R^2	rms	min	max
Eq. 3.3	0.9981	6.3268	-7.903	7.347
Eq. 3.4	0.9978	6.5214	-8.742	5.106

Table 4.3: The statistical results for fitting the intermolecular potentials Eq. 3.5 and Eq. 3.6 for the dimers fluorine and hydrogen-fluorine. The values are in μE_H.

potential	F_2-F_2			
			residual	
	R^2	rms	min	max
Eq. 3.5	0.9997	27.042	-8.836	7.713
Eq. 3.6	0.9998	20.294	-9.386	6.454
potential	H_2-F_2			
			residual	
	R^2	rms	min	max
Eq. 3.5	0.9999	4.564	-5.854	5.577
Eq. 3.6	0.9999	3.992	-8.579	8.732
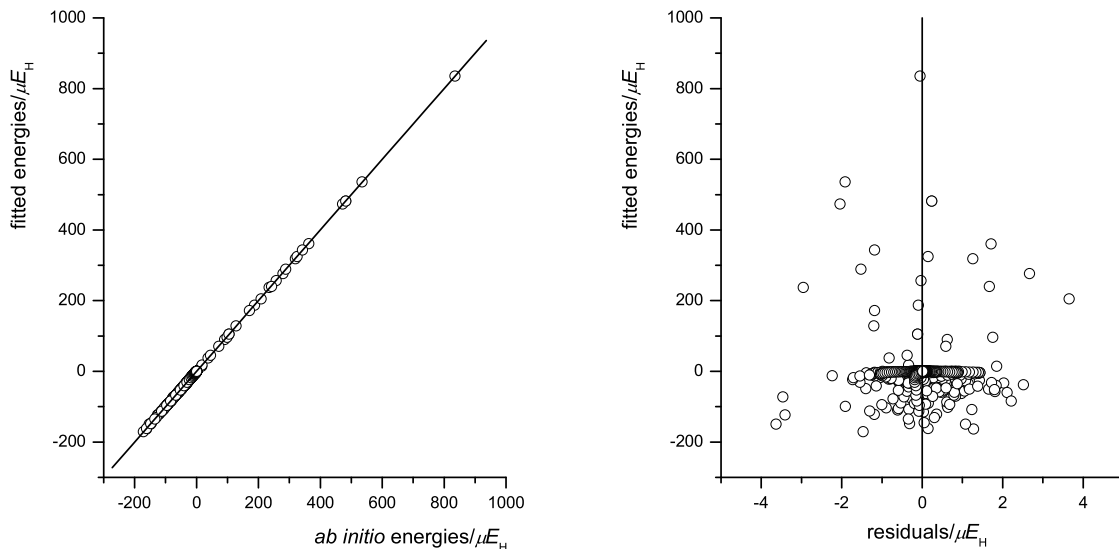
Figure 4.6: Quality of the 5-site *ab initio* analytical potential fit Eq. 3.3 for hydrogen at the theoretical level CCSD(T)/aug-cc-pV23Z.

The multiple correlation coefficient (R^2) shows the correlation quality between the *ab initio* energies and the predicted energies. It can only lie between 0 and 1.

$$R^2 = \frac{\sum_{i=1}^{N}(\widehat{Y_i} - \overline{Y})^2}{\sum_{i=1}^{N}(Y_i - \overline{Y})^2}; \text{ with } \overline{Y} = \frac{Y_1 + Y_2 + ... + Y_N}{N} \tag{4.2}$$

Y_i and $\widehat{Y_i}$ are the *ab initio* energies and the predicted energies.

In this work residual analysis is also accomplished with plots of the residuals vs. the predicted energies as shown in Figures 4.6, and 4.7. The plots of the residuals in Figures 4.6, and 4.7 show a proportion of the predicted energies on both sides of the expected average for the residuals between -4.0 and 4.0 for hydrogen, and -8.0 and 8.5 for fluorine. These show that the residual area of the potential Eq. 3.3 for hydrogen resulting from the least-square fit is narrower than the residual area of the potential Eq. 3.3 for fluorine. So the quality of the fit for Eq. 3.3 is better, but this difference is insignificant for the 930 interaction energy points over energy potential surface too. The correlation plots between the *ab initio* energies vs. the predicted
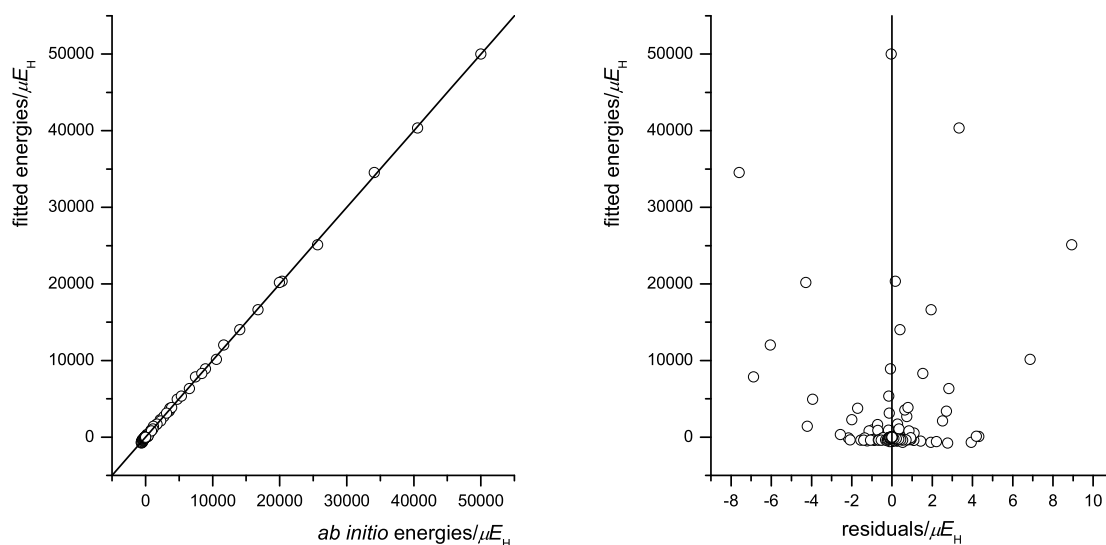
Figure 4.7: Quality of the 5-site *ab initio* analytical potential fit Eq. 3.5 for fluorine at the theoretical level CCSD(T)/aug-cc-pV23Z.

energies and the plots of the residuals in Figures 4.6, 7.1, and 7.2, 7.3, and 4.7, 7.4, and 7.5, 7.6 are another way of assessing the quality of the fit.

All optimized parameters of these models are given in Tables 7.1, 7.2, 7.3, and 7.4. These pair potential functions turned out to be difficult to achieve, because of many local minima that could snare easily the Marquardt-Levenberg algorithm. However, the Genetic algorithm proved good for overcoming this problem. It was used to locate the global minima for potential energy surfaces coarsely, then the parameters were tuned accurately with the Marquardt-Levenberg algorithm. The quality of the fits turned out to be quite and satisfactory, as shown in Section 7. The new 5-site intermolecular potential functions *ab initio* of this work are able to surpass the accuracy of the 2- and 3-site potential functions.
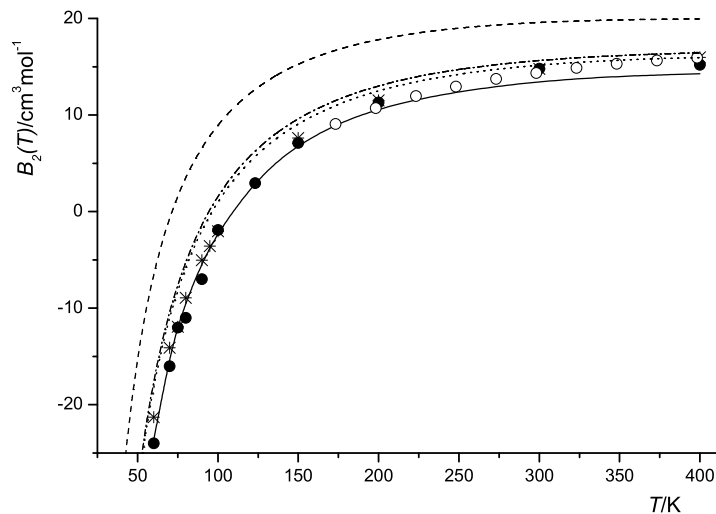
Figure 4.8: Second virial coefficients B_{cl}^0 of hydrogen using the pair potential Eq. 3.3 resulting from CCSD(T) level of theory; - - -: aug-cc-pVDZ; $- \cdot - \cdot -$: aug-cc-pVTZ; $\cdots$: aug-cc-pVQZ; —: aug-cc-pV23Z; •: experimental data [28, 66]; ○: Lennard-Jones potential by Wang [132]; ∗: spherical harmonic potential by Etters and Diep [32, 25, 26].

4.2 Prediction of virial coefficients

4.2.1 Comparison with the pair potentials

The classical virial coefficients B_{cl}^0 of hydrogen and fluorine computed from the equation Eq. 2.66 using the *ab initio* 5-site pair potentials Eq.(3.3-3.6), are listed in Tables 8.1 and 8.4, and plotted in Figures 4.8, 4.9, 4.10 and 4.11, respectively. Figures show the experimental 2nd virial coefficients [28, 66, 17] of hydrogen and fluorine and those calculated for the 3 different basis sets aug-cc-pVmZ ($m = 2, 3, 4$) and for the extrapolated *ab initio* results (denoted aug-cc-pV23Z), respectively. Of course, these *ab initio* calculations were performed at the level of theory CCSD(T).

Furthermore, for the hydrogen dimer the 2nd virial coefficients were also calculated from the spherical harmonic potentials worked out by Etters et al [32], and Diep and Johnson [25, 26]. Diep and Johnson computed the second virial coefficients
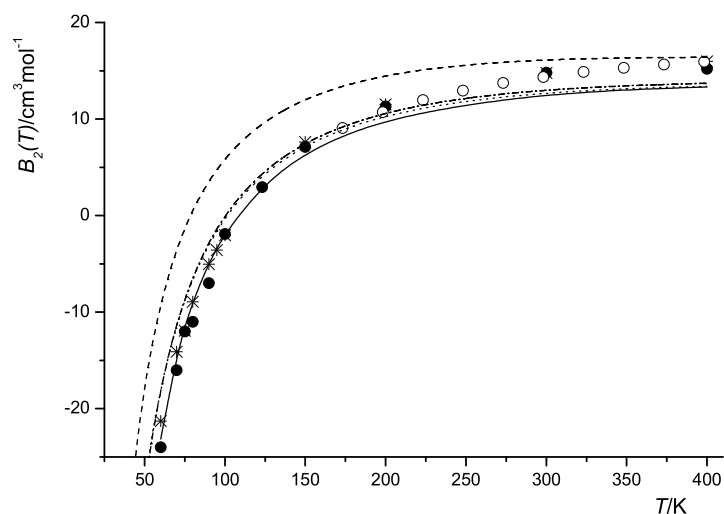
Figure 4.9: Second virial coefficients B_{cl}^0 of hydrogen using the pair potential Eq. 3.4 resulting from CCSD(T) level of theory; for an explanation of the symbols see Fig. 4.8 and text.

at level of theory CCSD(T) with complete basis set limit (CBS), using the path integral and semiclassical method in the temperature ranges from 15-100 K [25] and from 100-500 K [26], respectively. They obtained that the interaction between two H_2 molecules can be very different, depending on their relative orientation; hence a description of the relative molecular orientations during collision period is essential. In recent publication the second virial coefficients of hydrogen were predicted by Wang [132] using the site-site Lennard-Jones 6-12 interaction potential function form, depicted also in Figures 4.8 and 4.9. All their results included the quantum corrections, too.

The virial coefficients B_{cl}^0 of hydrogen estimated directly from the new pair potentials Eq. 3.3 and Eq. 3.4, did not involve the quantum corrections. But the agreement between the calculated virial coefficients and experimental data is very good, as can be seen from Table 8.1 and Figures 4.8 and 4.9. Figures 4.10 and 4.11 show similar calculation results for the 2nd virial coefficients of fluorine. They also show predictions with the Deiters equation of state (D1 EOS). This equation was chosen, because it is able to fit the critical parameters for fluorine. It has also been
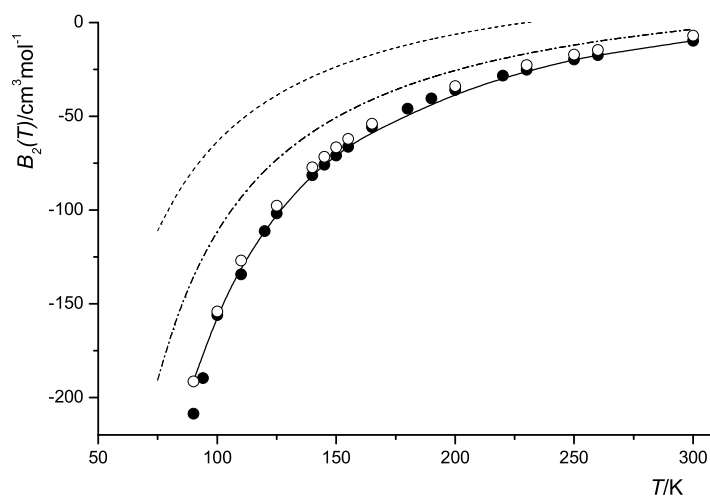
Figure 4.10: Second virial coefficients B_{cl}^0 of fluorine using the pair potential Eq. 3.5 resulting from CCSD(T) level of theory; - - -: aug-cc-pVDZ; $- \cdot - \cdot -$: aug-cc-pVTZ; —: aug-cc-pV23Z; $\bullet$: experimental data [17, 28]; $\circ$: calculated with Deiters equation of state (D1) [18].

used to calculate the virial coefficients, the vapor-liquid equilibrium and thermodynamic properties of heavy molecules [18, 22, 85] as mentioned in Section 2.3.2. In this case it is also a suitable way for testing the accuracy of the 5-site pair potentials Eq. 3.5 and Eq. 3.6 resulting from the *ab initio* calculations.

The 2nd virial coefficients resulting from the level of theory CCSD(T)/aug-cc-pV23Z using the pair potentials Eq. 3.5 and Eq. 3.6 were found to be very close to experimental data and with those calculated by Deiters equation of state (D1). With basis sets aug-cc-pVDZ or aug-cc-pVTZ (without extrapolation) the results were not as good. Significant improvements are obtained if the cardinal number m of aug-cc-pVmZ is increased. The double-zeta basis sets are inadequate, as the quality of the prediction charges very much when going from aug-cc-pVDZ to aug-cc-pVTZ. In contrast to this, the changes observed when going to aug-cc-pVQZ are small. The change of the second virial coefficients is also very obvious in Figures 4.10 and 4.11 for fluorine. Still the classical virial coefficients resulting from the pair potentials differ slightly from experimental data. The quantum effects need to be considered.
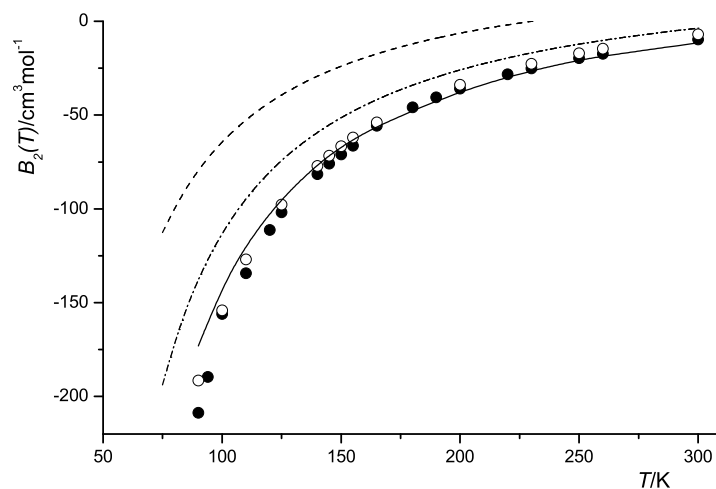
Figure 4.11: Second virial coefficients B_{cl}^0 of fluorine using the pair potential Eq. 3.6 resulting from CCSD(T) level of theory; for an explanation of the symbols see Fig. 4.10 and text.

4.2.2 Virial coefficients of dimers H_2-H_2 and H_2-O_2

The resulting second virial coefficients of hydrogen from the *ab initio* 5-site pair potentials shown in Tables 8.1 without the quantum effects, seem to be in reasonably good agreement with the experimental data and with those calculated by different methods. However for light molecules such hydrogen the de Broglie wavelengths of particles are the order of magnitude of the interacting distance. Hence quantum effects can be important over a wide range of temperature. In this Section the *ab initio* pair potential functions Eq. 3.3 and Eq. 3.4 resulting from the level of theory CCSD(T) with complete basis set limit aug-cc-pV23Z for hydrogen are used for computing the first-order quantum corrections. The cross second virial coefficients of the dimer hydrogen-oxygen are also considered here over the temperature range from 49.8 K to 400 K for the quantum effects. The total first-order quantum-corrected second virial coefficient of these systems $B_2(T)$ is defined as the sum of the contributions from Eqs. 2.66, 2.67, 2.68 and 2.69 (Section 2.3.3).

The second virial coefficients of the dimer H_2-H_2 including the first-order quantum corrections at the temperature range from 60 K to 400 K are shown in Table 8.2.
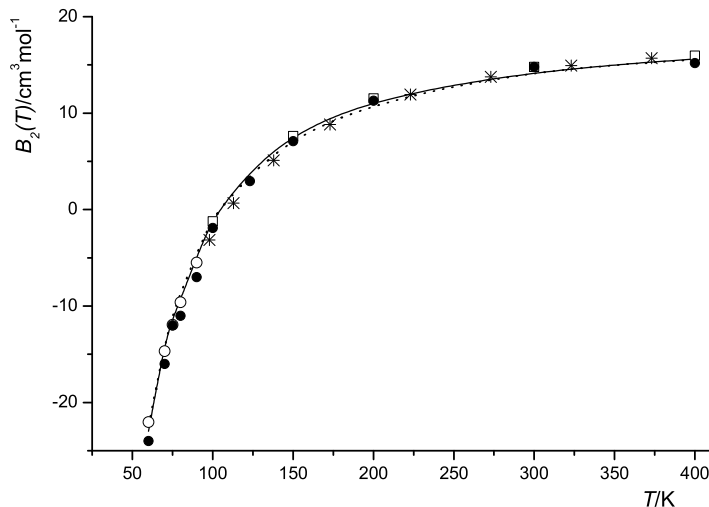
Figure 4.12: Second virial coefficients of hydrogen are calculated using the pair potentials (this work): —: pair potential Eq. 3.3; ⋯: pair potential Eq. 3.4; •: experimental data [28, 66]; ○: path integral, and □: semi-classical method (Diep [25, 26]); ∗: Lennard-Jones 6-12 potential [79].

It appears that the results obtained with the pair potential functions Eq. 3.3 are marginally better than those obtained with Eq. 3.4, although the latter function has more adjustable parameters. But the differences are insignificant. More important here is the fact that an accurate prediction of second virial coefficients from an *ab initio* pair potential without recourse to experimental data is possible, and that the CCSD(T) method, applied to basis sets aug-cc-pVDZ and aug-cc-pVTZ, and followed by an extrapolation to the basis set limit aug-cc-pV23Z, is evidently able to generate virial coefficients almost within the uncertainties of the experiments as one can see in Fig. 4.12. The results of this work also agree well with the results of the spherical harmonic potential [25, 26] and Lennard-Jones 6-12 potential [79]; although the deviations from the latter are larger.

From Table 8.2 it is worth noting that quantum corrections contribute significantly to the second virial coefficient of hydrogen even at high temperatures. Of these corrections, only the radial term is important; the angular terms are usually much
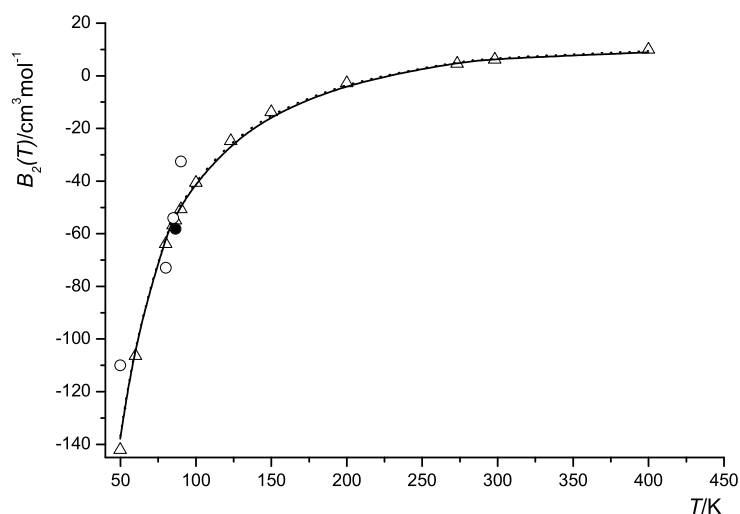
Figure 4.13: Cross second virial coefficient of the hydrogen-oxygen system. ——: *ab initio* prediction (this work) based on Eq. (3.3), $\cdots$: prediction based on Eq. (3.4), $\triangle$: calculated from empirical correlation [31, 30], $\bullet$: interpolation from neon mixtures (see section 4.2.2); other symbols: experimental data (see Table 8.3).

smaller in size. The calculated values of cross second virial coefficients of hydrogen-oxygen are given in Table 8.3.

Experimental values of the hydrogen–oxygen interaction are difficult to find in the literature. There are some experiments, however, from which these virial coefficients can be calculated:

- Van Itterbeek and van Doninck measured the speed of sound in (hydrogen + oxygen) mixtures at low temperatures and pressures [124]. The pressure dependence of this property is related to the virial coefficients. The values of the cross virial coefficient obtained by these authors lie reasonably close to our predictions (see Table 8.3); it should be noted, however, that their evaluation method involved several simplifications (linearizations, neglect of temperature derivatives of the virial coefficient), and that their results exhibit an uncertainty of about 20%.

- McKinley et al. measured solid–fluid equilibria of the (hydrogen + oxygen)

system [77]. With the usual assumptions and simplifications (no hydrogen dissolved in the solid oxygen, neglect of higher virial coefficients) it is possible to estimate cross second virial coefficients from these data. The result agrees reasonably well with the *ab initio* prediction. The sublimation pressure of γ-oxygen, which is required for the equilibrium calculation, was taken from the work of Roder [103].

In an earlier publication on high-pressure phase equilibria of the (hydrogen + oxygen) system it had been suggested that the parameters of the hydrogen–oxygen interaction could be interpolated from those of the the systems (hydrogen + nitrogen), (neon + nitrogen), and (neon + oxygen) (Deiters et al. (1993) [24]). This idea can be extended to second virial coefficients as follows: Eq. 2.66 can be simplified—although with some loss of accuracy—by performing the integrations over the orientation variables:

$$B^{(0)}(T) = -2\pi N_A \int_0^\infty \left[\exp\left(-\frac{\overline{u}(r,T)}{k_{\mathrm{B}}T} \right) - 1 \right] r^2 dr \tag{4.3}$$

Here $\overline{u}(r;T)$ denotes an angle-averaged pair potential. For small molecules like the ones studied here the assumption of conformal pair potentials is usually acceptable, i.e., pair potentials can be written as

$$\overline{u}(r,T) = \epsilon \widetilde{u}(\widetilde{r}, \widetilde{T}) \ \text{ with } \ \widetilde{r} = \frac{r}{\sigma} \ \text{ and } \ \widetilde{T} = \frac{k_{\mathrm{B}}T}{\epsilon} \tag{4.4}$$

where $\widetilde{u}(\widetilde{r}, \widetilde{T})$ is a universal (reduced) pair potential function. Then Eq. 4.3 becomes

$$B^{(0)}(T) = -2\pi N_A \sigma^3 \int_0^\infty \left[\exp\left(-\frac{\widetilde{u}(\widetilde{r}, \widetilde{T})}{\widetilde{T}} \right) - 1 \right] \widetilde{r}^2 d\widetilde{r} \tag{4.5}$$

This equation is used for the cross virial coefficient of the hydrogen–oxygen system, assuming $\epsilon_{\mathrm{H_2;O_2}} = \epsilon_{\mathrm{H_2;N_2}} + \Delta\epsilon_{\mathrm{O_2;N_2}}$, where the last term is supposed to be small. Taylor expansion of the Boltzmann factor of this term, truncation after the linear term, and rearrangement yield

$$\frac{B^{(0)}_{\mathrm{H_2,O_2}}(T)}{N_A \sigma_{\mathrm{H_2,O_2}}} \approx \frac{B^{(0)}_{\mathrm{H_2,N_2}}(T)}{N_A \sigma_{\mathrm{H_2,O_2}}} - 2\pi \frac{\Delta\epsilon_{\mathrm{O_2,N_2}}}{\widetilde{T}_{\mathrm{H_2,N_2}}} \int_0^\infty \widetilde{u}(\widetilde{r}, \widetilde{T}_{\mathrm{H_2,N_2}}) \left[\exp\left(-\frac{\widetilde{u}(\widetilde{r}, \widetilde{T}_{\mathrm{H_2,N_2}})}{\widetilde{T}_{\mathrm{H_2,N_2}}} \right) - 1 \right] \widetilde{r}^2 d\widetilde{r} \tag{4.6}$$

where the integral is a function of the reduced temperature T only. A similar equation holds for the cross virial coefficients of the (neon + oxygen) and (neon + nitrogen) systems, for which experimental data are available [28]. Therefore $\Delta\epsilon_{O_2;N_2}$ can be determined from the neon data and then substituted into Eq. 4.6 to give the second virial coefficient of (hydrogen + oxygen) at the same reduced temperature as the (neon + oxygen) system (tacitly assuming that this value also holds for the hydrogen systems). For the parameters ϵ and σ usual Lennard-Jones parameters [45] and Berthelot–Lorentz combining rules were used. It turns out that the hydrogen–oxygen cross virial coefficient obtained from this interpolation (-58.1 cm^3/mol) agrees reasonably well with the *ab initio* predictions as well as with the experimental values (see Fig. 4.13).

Recently Estela-Uribe and Jaramillo (2005) [30] published empirical correlation equations for second virial coefficients which are based on the corresponding-states approach of Lee and Kesler [61]. In their work, binary interactions are characterized by so-called pseudocritical parameters, which are interpolations of the pure-fluid critical temperatures and densities as shown in Section 2.3.1. These two correlation parameters were set to zero for the hydrogen–oxygen interaction, and the correlations of Estela-Uribe and Jaramillo used to predict cross second virial coefficients. The results, presented in Table 8.3, show a remarkably good agreement with the predictions from quantum mechanics.

4.2.3   Virial coefficients of dimers F_2-F_2 and H_2-F_2

For the dimer F_2-F_2 the second virial coefficients $B_2(T)$ were also calculated in the temperature range from 90 K to 300 K using the level of theory CCSD(T) with the basis set limit aug-cc-pV23Z. The results without quantum effects are shown in Table 8.4, and Figures 4.10 and 4.11. It turned out that the results derived from Eq. 3.5 and Eq. 3.6, were close to the experimental data as mentioned in Section 4.2.1.

The 2nd virial coefficients $B_2(T)$ resulting from such pair potential functions are also close to those obtained with Deiters equation of state (D1), as can be seen in Figures 4.10 and 4.11. But there are still some differences. Consequently, quantum effects are also considered here for the dimers F_2-F_2 and H_2-F_2. Especially the cross second virial coefficients of the hydrogen-fluorine interaction are not found in the
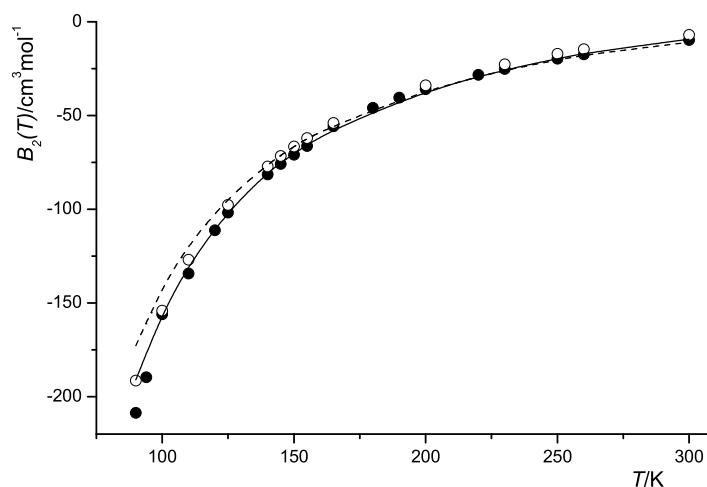
Figure 4.14: Second virial coefficient of fluorine. ——: calculated by Eq. 3.5 and - - -: calculated by Eq. 3.6 (this work), ∘: calculated with Deiters equation of state (D1) [18], ●: experimental data [17, 28].

literature. Those are calculated here in the temperature range 49.8-400 K including the quantum effects.

The accurate prediction of cross second virial coefficients from an *ab initio* pair potential function also without recourse to experimental data is important, and the method CCSD(T), applied to basis set limit, is positively able to calculate the second virial coefficients of fluorine almost within uncertainties of the experiments as can see in Figure 4.14. The resulting virial coefficients of fluorine also included the first-order quantum corrections, due to the effects of relative translational motions, and the molecular rotations.

The formulae Eq. 2.66-Eq. 2.69 were used directly for the linear molecules fluorine and hydrogen as proposed by Pack [89]. The values of second virial coefficients for fluorine with the quantum effects shown in Table 8.5 too. It turns out that quantum corrections contribute significantly to the second virial coefficients of fluorine over a wide temperature range. Table 8.5 shows that the contribution of translational motions in the corrections is more important; the molecular rotations (i.e the angular
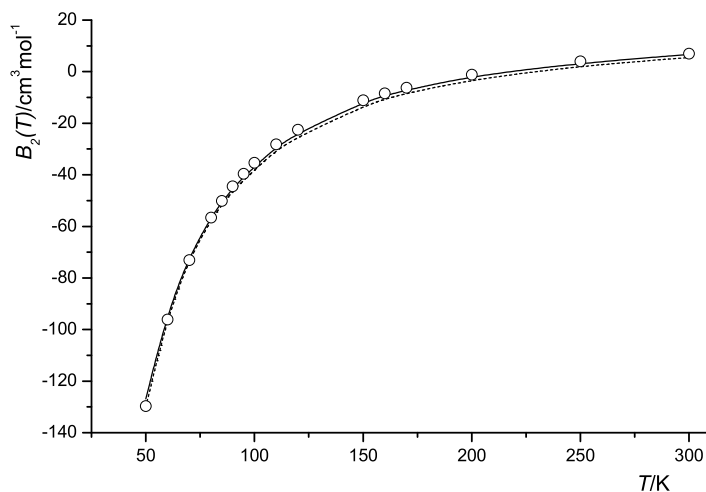
Figure 4.15: Cross second virial coefficient of the hydrogen-fluorine system. —: calculated from Eq. 3.5 and - - -: calculated from Eq. 3.6 (this work); ○: calculated from empirical correlation [30, 31].

terms) are usually much smaller in size. The calculated virial coefficients resulting from the *ab initio* pair potentials were also compared with those predicted with Deiters equation of state (D1 EOS) [18] and with the experimental data [17, 28]. It appeared that the differences are very small. The results derived from Deiters equation of state [18], are in excellent agreement with the experimental data. This is also a suitable way for testing the accuracy of the results resulting from the pair potentials, respectively.

The empirical correlation equations of Estela-Uribe and Jaramillo [30] were also applied to system hydrogen-fluorine too. The results, presented in Table 8.6, show a remarkably good agreement with the predictions from quantum mechanics.

We conclude that our newly developed *ab initio* intermolecular pair potential functions for the dimers H_2-H_2, H_2-O_2, F_2-F_2 and H_2-F_2, derived from four very accurate potential energy surfaces at the high level of theory CCSD(T) with basis set limit aug-cc-pV23Z, are reliable and usable for the prediction of virial coefficients.

4.3 Gibbs ensemble Monte Carlo simulation

4.3.1 Comparison of thermodynamic properties

This section describes the comparison of the liquid phase densities which resulted from NPT simulations using the *ab initio* pair potentials Eq. 3.3 and Eq. 3.4 for hydrogen, and Eq. 3.5 and Eq. 3.6 for fluorine at two different constant pressures. The results are given in Table 9.1 and Figures 9.1, 10.1. The comparisons between these results and those derived from the equations of state were also included.

For the pure fluid hydrogen the liquid phase densities were predicted at two constant pressures of 1.0 MPa and 5.0 MPa, in the temperature range 26–250 K. The experimental values [76] and those derived from the modified Benedict-Webb-Rubin equation of state for hydrogen [139] were used for comparison with these simulation results. In general the liquid phase densities of hydrogen resulting from both *ab initio* pair potentials Eq. 3.3 and Eq. 3.4, are very close to the experimental data and those obtained from the empirical equation of state [139]. The *ab initio* pair potential Eq. 3.3 gave very similar results with experimental data, although the potential Eq. 3.3 has gotten fewer adjustable parameters. The absolute average deviations in liquid phase density are 1.538, 3.548 and 3.277 kg/m^3 at 1.0 MPa, and 1.005, 0.575 and 3.162 kg/m^3 at 5.0 MPa, computed with the *ab initio* pair potentials Eq. 3.3, Eq. 3.4, and Benedict-Webb-Rubin equation of state [139], respectively. This proves that *ab initio* pair potentials developed for hydrogen are accurate and reliable.

In recent publications the thermodynamic properties and phase equilibria of the pure fluid normal and para-hydrogen were predicted with path integral hybrid Monte Carlo simulation technique developed by Wang and Johnson (1996) [131]. The pair potentials used in their work were Lennard-Jones 6-12 potentials with parameters obtained from Silvera-Goldman, Buck, Buch and Dondi. The different potentials were compared with each other by Wang and Johnson and then used in NVT canonical and NPT Monte Carlo simulations. In the isobar diagram Figure 9.1, there is no visible the difference between the results of this work and those of Wang and Johnson [131].

For fluorine the liquid phase densities were estimated similarly at two constant

pressures of 1.0 MPa and 10.0 MPa, over the temperature range from 90 K to 270 K with NPT simulation using *ab initio* pair potentials Eq. 3.5 and Eq. 3.6. The results derived from these *ab initio* pair potentials, were compared with experimental values [17]. Furthermore NPT simulations were also performed at different temperatures and pressures. The results are shown in Table 9.1 and Figure 10.1. It turned out that the densities obtained from the simulations are in good agreement with experimental data and those resulting from the Deiters equation of state (D1) [18]. This equation of state may be an appropriate way to assess the accuracy of the obtained results from the GEMC simulation. The absolute average deviations in liquid phase density resulted in 4.70, 5.01 and 4.61 kg/m^3 at 1.0 MPa, and 13.73, 38.85 and 13.38 kg/m^3 at 10.0 MPa, calculated using the pair potentials Eq. 3.3, Eq. 3.4, and Deiters equation of state [18], respectively. These results show that the results obtained from the *ab initio* pair potentials are almost within the uncertainties of experimental values.

4.3.2   Structural properties

This section describes the features of the site-site pair distribution functions resulting from two GEMC-NVT and NPT simulation techniques for the pure fluids hydrogen and fluorine. The *ab initio* pair potentials Eq. 3.3, Eq. 3.4 of hydrogen, and Eq. 3.5, Eq. 3.6 of fluorine, respectively, were used for those simulations.

The temperature dependence of the radial distribution functions at two different pressures is depicted in Figures 9.2-9.17 for hydrogen and Figures 9.2-9.17 for fluorine. As 5-site potential models were used, the interactions of ghost sites N, M on the molecules were also represented here by site-site correlation functions. The height of site-site pair correlation functions decreased with increasing temperature from 26.0 K to 250.0 K at 1.0 MPa and 5.0 MPa for hydrogen and from 90.0 K to 270.0 K at 1.0 MPa and 10.0 MPa for fluorine. In general the peaks for the interaction of sites including an atomic nucleus were higher than those without a nucleus.

For the pure fluids hydrogen and fluorine the peaks of g_{H-H} and g_{F-F} were highest. The g_{H-M} and g_{F-M} were lower. But the peaks of g_{N-N} were smallest. The height of peaks decreases distinctively when the temperature increases. All first peaks of the site-site correlation functions for hydrogen are located between 2.893 Å and 3.205

Table 4.4: The height of first peaks of the site-site distribution functions of pure fluid hydrogen calculated with NPT simulation using the *ab initio* pair potential Eq. 3.3 at different temperatures and constant pressures of 1.0 MPa and 5.0 MPa.

	at 1.0 MPa				at 5.0 MPa			
T/K	$g_{\text{H}-\text{H}}$	$g_{\text{N}-\text{N}}$	$g_{\text{M}-\text{M}}$	$g_{\text{H}-\text{M}}$	$g_{\text{H}-\text{H}}$	$g_{\text{N}-\text{N}}$	$g_{\text{M}-\text{M}}$	$g_{\text{H}-\text{M}}$
26.0	2.92	1.97	2.53	2.69	2.79	1.85	2.40	2.56
30.0	2.69	1.87	2.37	2.51	2.55	1.76	2.24	2.39
60.0	1.75	1.51	1.67	1.71	1.67	1.44	1.59	1.62
90.0	1.49	1.35	1.44	1.47	1.42	1.28	1.37	1.40
120.0	1.35	1.25	1.33	1.33	1.28	1.21	1.26	1.29
250.0	1.16	1.13	1.14	1.15	1.12	1.07	1.09	1.11

Table 4.5: The height of first peaks of the site-site distribution functions of pure fluid hydrogen derived with NPT simulation using the *ab initio* pair potential Eq. 3.4 at different temperatures and constant pressures of 1.0 MPa and 5.0 MPa.

	at 1.0 MPa				at 5.0 MPa			
T/K	$g_{\text{H}-\text{H}}$	$g_{\text{N}-\text{N}}$	$g_{\text{M}-\text{M}}$	$g_{\text{H}-\text{M}}$	$g_{\text{H}-\text{H}}$	$g_{\text{N}-\text{N}}$	$g_{\text{M}-\text{M}}$	$g_{\text{H}-\text{M}}$
26.0	2.88	1.94	2.51	2.67	2.74	1.84	2.37	2.53
30.0	2.79	1.90	2.44	2.59	2.67	1.80	2.32	2.46
60.0	2.41	1.74	2.15	2.27	2.27	1.65	2.04	2.14
90.0	2.20	1.66	2.01	2.09	2.11	1.57	1.91	1.99
120.0	2.07	1.61	1.92	1.99	1.98	1.54	1.82	1.89
250.0	1.83	1.49	1.73	1.77	1.75	1.42	1.64	1.69

Å. The second peaks are located between 6.081 Å and 6.234 Å. For the pure fluid fluorine the first peaks of site-site correlation functions are located between 4.01 Å and 4.861 Å. The second peaks are located between 5.256 Å and 5.717 Å. The results are shown in Tables 4.4-4.6.

The structural properties of the liquid phases hydrogen and fluorine were also obtained from GEMC-NVT simulation. The heights of peaks of the site-site radial distribution functions obtained from the GEMC-NVT simulation are approximately, the same as those resulting from NPT simulation. The first strongly peaks are also located in the range 3.21 Å to 3.29 Å using pair potential Eq. 3.3 and in the range

Table 4.6: The height of first peaks of the site-site distribution functions of pure fluid fluorine derived with NPT simulation using the *ab initio* pair potential Eq. 3.5 at different temperatures and constant pressures of 1.0 MPa and 10.0 MPa.

T/K	at 1.0 MPa				at 10.0 MPa			
	$g_{\mathrm{F-F}}$	$g_{\mathrm{N-N}}$	$g_{\mathrm{M-M}}$	$g_{\mathrm{F-M}}$	$g_{\mathrm{F-F}}$	$g_{\mathrm{N-N}}$	$g_{\mathrm{M-M}}$	$g_{\mathrm{F-M}}$
90.0	4.28	3.41	3.75	4.01	4.07	3.23	3.55	3.80
120.0	4.12	3.22	3.62	3.69	3.92	3.07	3.44	3.52
150.0	3.89	3.05	3.41	3.58	3.69	2.88	3.21	3.40
180.0	3.68	2.88	3.22	3.41	3.50	2.73	3.04	3.23
210.0	3.51	2.67	3.06	3.27	3.34	2.50	2.90	3.10
270.0	3.24	2.48	2.81	2.91	3.05	2.33	2.65	2.79

Table 4.7: The height of first peaks of the site-site distribution functions of pure fluid fluorine derived with NPT simulation using the *ab initio* pair potential Eq. 3.6 at different temperatures and constant pressures of 1.0 MPa and 10.0 MPa.

T/K	at 1.0 MPa				at 10.0 MPa			
	$g_{\mathrm{F-F}}$	$g_{\mathrm{N-N}}$	$g_{\mathrm{M-M}}$	$g_{\mathrm{F-M}}$	$g_{\mathrm{F-F}}$	$g_{\mathrm{N-N}}$	$g_{\mathrm{M-M}}$	$g_{\mathrm{F-M}}$
90.0	4.09	3.22	3.56	3.69	3.79	2.89	3.20	3.60
120.0	3.89	3.04	3.41	3.56	3.66	2.74	3.06	3.48
150.0	3.69	2.87	3.22	3.43	3.43	2.58	2.89	3.35
180.0	3.49	2.74	3.03	3.28	3.24	2.43	2.72	3.19
210.0	3.33	2.51	2.91	3.14	3.10	2.24	2.60	3.06
270.0	3.04	2.31	2.66	2.97	2.81	2.08	2.37	2.91

3.18 Å to 3.39 Å using pair potential Eq. 3.4 for hydrogen. For fluorine they are located in the range 3.98 Å to 4.87 Å and 3.87 Å to 4.86 Å using pair potentials Eq. 3.5 and Eq. 3.6. The radial correlation functions resulting from NVT simulation are depicted in Figures 9.18-9.25 for hydrogen, and 10.18-10.25 for fluorine.

In a recent publication (1998) [82] Nagel et al. calculated the proton-proton pair distribution function $g_{\mathrm{HH}}(r)$ in dense fluid hydrogen by an efficient quantum mechanical simulation scheme, wave-packet molecular dynamics (WPMD), and found a strong first peak with an estimated height of 3.0. This is in good agreement with the results derived from *ab initio* pair potentials Eq. 3.3 and 3.4.

In 1995 Santis et al. [106] also calculated the thermodynamic and structural properties of the pure liquid fluorine analysing the experimental atom-atom pair distribution functions and using molecular dynamics calculations. Their results were different from experimental $g(r)$ of fluorine around 5.0 Å. However there were some oscillations below 2.0 Å, indicating that significant experimental uncertainties might have affected the experimental data. The first peaks of the site-site pair correlation functions for pure liquid fluorine resulting from the GEMC-NVT and NPT simulations are located between 3.86 Å and 4.88 Å. Thus our results, exhibited in Figures 10.2-10.25, agree well with literature results within the uncertainties of the experimental data.

4.3.3 The thermodynamic properties of hydrogen

The simulation results are shown in Tables 9.2 and 9.3 together with their estimated statistical uncertainties. The vapor-liquid coexisting phase and the vapor pressure curves of hydrogen are displayed in Figure 4.16 and Figure 4.17. Experimental data [76, 66], values from the modified empirical equation of state [139] as well as from Wang and Johnson using the Silvera and Goldman (SG) potential [131] are also included.

The vapor pressures and enthalpies of vaporization derived from the same simulations are depicted in Figures 4.17 and 4.18. These vapor pressures differ on absolute average from the experimental data typically by about 3.49% and 9.14%. These differences is small within statistical uncertainties of experimental resources and a few previous publications [139, 131].

The critical temperature, density and volume of the pure fluid hydrogen could not be calculated directly from the simulations, but they could be obtained from the densities of vapor-liquid equilibria by the least-square fit to the formulas Eq. 2.93, as shown in Table 4.8 and Figure 4.16. The critical pressure of hydrogen was calculated from the Antoine equation Eq. 2.94. The results agreed reasonable well with experimental data.
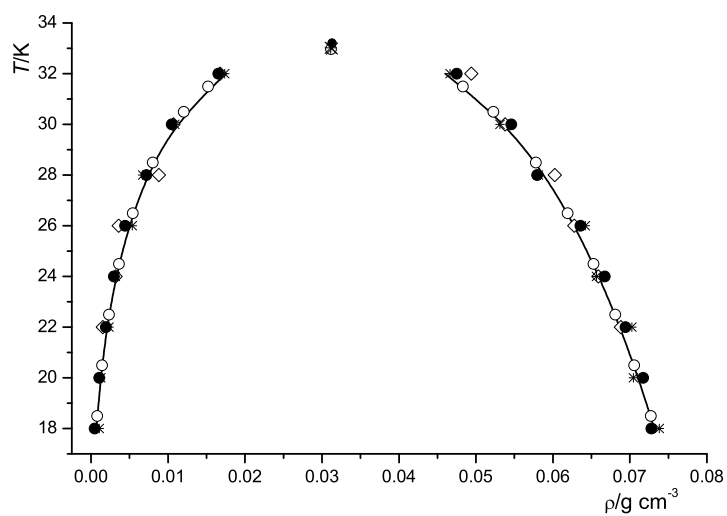
Figure 4.16: Vapor-liquid coexistence diagram of hydrogen. Symbols: —, experimental data [76, 75]; ○, modified Benedict-Webb-Rubin equation of state [139]; ◇, simulated by Wang and Johnson using Silvera and Goldman (SG) potential [131]; ●, ∗: *ab initio* pair potentials Eq. 3.3 and Eq. 3.4.
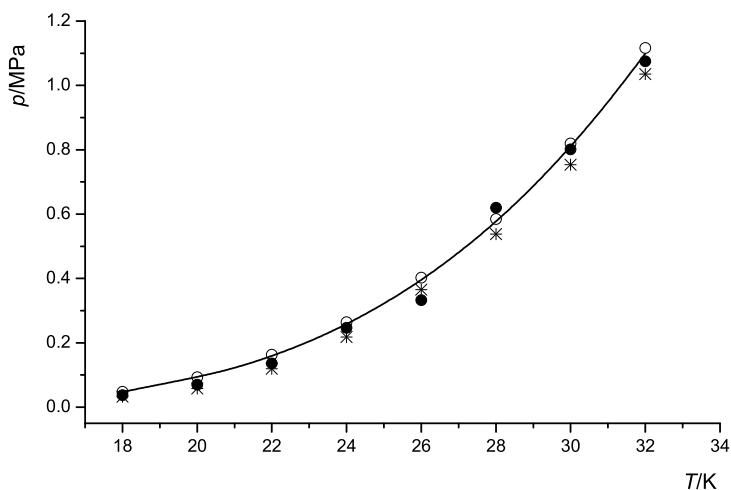
Figure 4.17: Vapor pressure of hydrogen. Symbols: —, experimental data [76, 66]; ○, modified Benedict-Webb-Rubin equation of state [139]; ●, and ∗ : *ab initio* pair potentials Eq. 3.3 and Eq. 3.4.
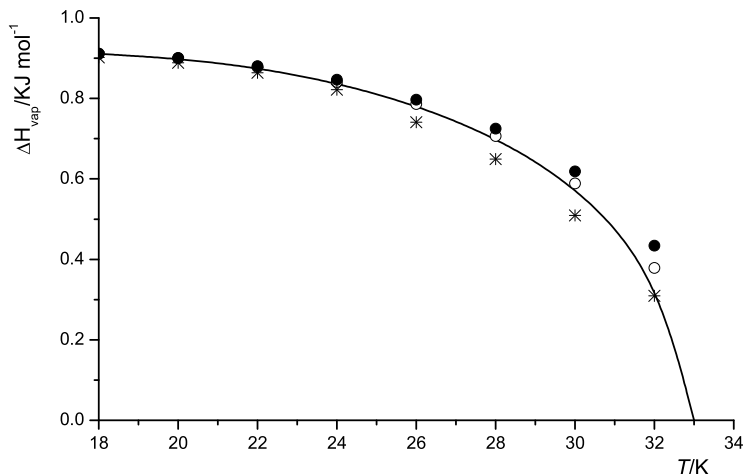
Figure 4.18: Vaporization enthalpy of hydrogen. Symbols: —, experimental data [76, 66]; ∘, modified Benedict-Webb-Rubin equation of state [139]; •, ∗: *ab initio* pair potentials Eq. 3.3 and Eq. 3.4.

However there are still some discrepancies between the simulation results and either experimental data or the values obtained from Benedict-Webb-Rubin equation of state [139]. This can be caused by either neglecting 3-body interactions or by using a too small number of particles used for simulations. Even so, the simulation results obtained with the GEMC-NVT simulation are within statistical uncertainties of different experimental sources. However, the simulation results that were predicted from pair potential Eq. 3.3 are usually different from the results of pair potential Eq. 3.4 by about 2.5%. The critical parameters and the thermodynamic properties differed by about 1.0% from the experimental values, respectively.

The accuracy of the simulation results for pure fluid hydrogen can be appreciated more by using the Clausius-Clapeyron equations Eq. 2.95 and 2.96 (Section 2.4.5) to calculate the enthalpy of vaporization $\Delta_{\text{vap}}H$, entropy of vaporization $\Delta_{\text{vap}}S$ and boiling temperature T_{b} Table 4.9. These thermodynamic properties are in good agreement with the published experimental data [76, 66], as exhibited in Table 4.9.

The adjustable constants A, B, C of the Antoine equation Eq. 2.94 are used to

Table 4.8: Critical properties of pure fluid hydrogen resulting from the GEMC-NVT simulation using *ab initio* pair potentials Eq. 3.3 and Eq. 3.4; EOS : empirical equation of state [139]; Exp.: experimental values.

method	T_c/K	ρ_c/g cm^{-3}	P_c/MPa	V_c/cm^{3}mol^{-1}	ref.
Eq. 3.3	33.2162	0.0313	1.1258	64.3806	this work
Eq. 3.4	33.0236	0.0311	1.0990	64.7907	this work
EOS	32.9718	0.0312	1.2837	64.1539	[139]
Exp.	33.1900	0.0312	1.2928	64.1026	[76]
Exp.	33.0	0.0310	1.2930	64.5677	[66]

Table 4.9: Enthalpy of vaporization $\Delta_{vap}H$, entropy of vaporization $\Delta_{vap}S$ and boiling temperature T_b of pure fluid hydrogen at the standard state $P = 0.1013$ MPa predicted from simulation vapor pressures.

method	$\Delta_{vap}H$/kJmol^{-1}	$\Delta_{vap}S$/kJ/mol.K	T_b/K	ref.
Eq. 3.3	1.17148	0.05608	20.8911	this work
Eq. 3.4	1.21621	0.05717	21.2740	this work
EOS	1.07399	0.05305	20.2457	[139]
Exp.	1.07786	0.05299	20.3900	[76]
Exp.	1.07752	0.05314	20.2754	[66]

Table 4.10: The parameters A, B, β of Ising relations Eq. 2.93, and constants A, B, C of Antoine equation Eq. 2.94 for pure fluid hydrogen obtained from fits to the simulation results.

method	Ising parameter				Antoine constant			
	A	B	β	ref.	A	B	C	ref.
Eq. 3.3	-0.000400994	0.292517	0.325		3.63014	99.118	6.363	
Eq. 3.4	-0.000460265	0.390985	0.325		3.65736	99.484	5.862	
EOS.	-0.000395786	0.386943	0.320	[139]	3.40068	90.054	6.229	[139]
Exp.	-0.000426230	0.397981	0.320	[76]	3.54314	99.395	7.726	[125]

assess the accuracy of the simulation results resulting in the temperature range 18.0-32.0 K too. Those were compared to the experimental constants of the Antoine equation [125] in temperature range 21.01-32.27 K for hydrogen, as presented in Table 4.10. The discrepancies are insignificant. It turns out that the thermodynamic properties of vapor-liquid coexisting phase for pure fluid hydrogen resulting from the GEMC-NVT simulation are in good agreement with experimental data.

4.3.4 The thermodynamic properties of fluorine

For the pure fluid fluorine the GEMC-NVT simulation was also used here to determine the thermodynamic properties of vapor-liquid equilibria. The simulation runs were carried out over the temperature range 60–140 K, which is near to the critical point of fluorine. At each temperature the system was equilibrated for 10^5 cycles, which were then followed by production cycles. The simulation results are shown in Tables 10.1, and 10.2 as well in Figure 4.19, where the simulation results are compared with experimental values [17] and with values obtained from the GEMC simulations using a Lennard-Jones potential.

The results obtained with the Deiters equation of state (D1-EOS) [18] were compared to the simulation results too. This equation of state has the ability of reproducing accurately the phase equilibria of the pure fluid fluorine over wide range of temperature and pressure. The results derived from this equation of state are close to the experimental data [17]. Figures 4.19 and 4.20 show that the simulation values resulting from the GEMC-NVT simulation using *ab initio* pair potentials Eq. 3.5 and Eq. 3.6 agree well with the experimental data [17] and with those calculated with the Deiters equation of state [18].

The vapor pressures are shown in Figure 4.20. From Tables 10.1 and 10.2 it can be seen that the vapor pressures of liquid phase are lower than those of vapor phase. In principle both phases should have the same pressure. This difference may have been caused a too number small of particles in the simulations. It is, however, within the statistical uncertainties for these *ab initio* pair potential types. The influences between the simulation vapor pressures and experimental data [17] are about 3.49% and 9.14% with the *ab initio* pair potentials Eq. 3.5 and Eq. 3.6.
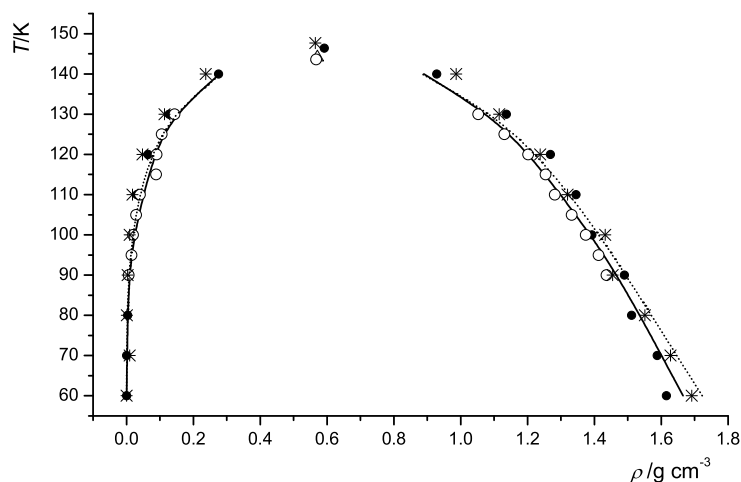
Figure 4.19: Vapor-liquid coexistence diagram of fluorine. Symbols: —, experimental data [17]; ○, Lennard-Jones potential [90]; · · · , Deiters equation of state (D1 EOS) [18]; ●, ∗: *ab initio* pair potentials Eq. 3.5 and Eq. 3.6.

The critical temperature, density and volume were determined directly from the least-square fit of the related formulas of the rectilinear diameter law Eq. 2.93 to the orthobaric densities.

The critical properties of the pure fluid fluorine were given in Table 4.11, which contains the corresponding experimental data [17], and those resulting from the Deiters equation of state [18] and from simulations by Panagiotopoulos [90] using a Lennard-Jones 6-12 potential. The critical pressure was calculated from the Antoine equation 2.94 shown in Table 4.11. The experimental critical values of Table 4.11 can be either directly taken from the cited literature [17, 66] or estimated from the vapor-liquid coexisting phase densities of Panagiotopoulos [90] using the least-square fit of the relations Eq. 2.93. The simulation results are in good agreement with experimental data. Nevertheless there are still some discrepancies. The estimated critical properties in Table 4.11 are higher than the experimental values by about 1.4%-5.8% for the pair potential Eq. 3.5 and 1.2%-4.0% for the pair potential Eq. 3.6. But these discrepancies are not large.
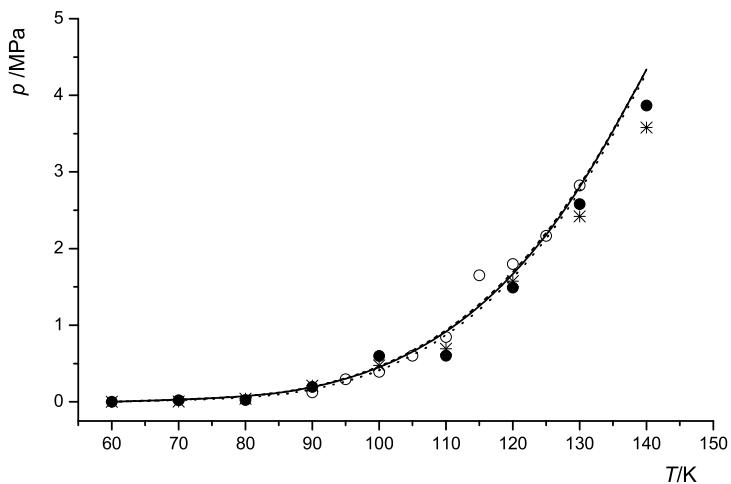
Figure 4.20: Vapor pressure of fluorine. Symbols: —, experimental data [17]; ○, Lennard-Jones potential [90]; ···, Deiters equation of state (D1 EOS) [18]; ●, ∗: *ab initio* pair potentials Eq. 3.5 and Eq. 3.6.
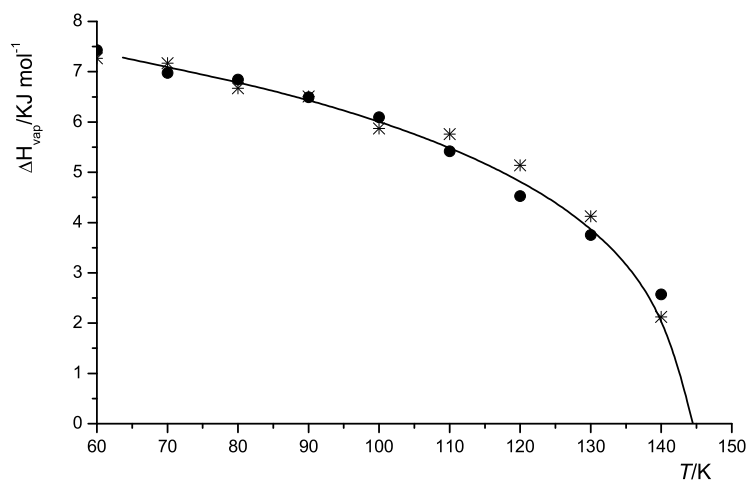
Figure 4.21: Vaporization enthalpy of fluorine. Symbols: —, experimental data [17]; ●, ∗: *ab initio* pair potentials Eq. 3.5 and Eq. 3.6.

Table 4.11: Critical properties of pure fluid fluorine resulting from the simulation results using potentials Eq. 3.5 and Eq. 3.6; D1-EOS : empirical equation of state [18]; Lennard-Jones potential (LJ) [90]; Exp.: experimental values.

method	T_c/K	$\rho_c/\text{g cm}^{-3}$	P_c/MPa	$V_c/\text{cm}^3\text{mol}^{-1}$	ref.
Eq. 3.5	146.405	0.5918	4.9110	64.2073	this work
Eq. 3.6	147.652	0.5646	5.3797	67.2980	this work
Lennard-Jones	143.630	0.5672	5.0386	66.9955	[90]
D1-EOS	144.157	0.5675	5.0493	66.9539	[18]
Exp.	144.300	0.5740	5.2150	66.2003	[66]
Exp.	144.121	0.5710	5.1724	66.5451	[17]

Table 4.12: Enthalpy of vaporization $\Delta_{\text{vap}}H$, entropy of vaporization $\Delta_{\text{vap}}S$ and boiling temperature T_b of the pure fluid fluorine at the standard state $P = 0.1013$ MPa predicted from simulation vapor pressures.

method	$\Delta_{\text{vap}}H/\text{kJmol}^{-1}$	$\Delta_{\text{vap}}S/(\text{kJ/mol.K})$	T_b/K	ref.
Eq. 3.5	6.8045	0.07914	85.9782	this work
Eq. 3.6	7.1596	0.08212	87.1808	this work
Lennard-Jones	7.6461	0.08712	87.7677	[90]
D1-EOS	7.1312	0.08212	86.8353	[18]
Exp.	6.9208	0.08085	85.5970	[66]
Exp.	6.9411	0.08112	85.5695	[17]

Table 4.13: The parameters A, B, β of Ising relations Eq. 2.93, and constants of the Antoine equation Eq. 2.94 for pure fluid fluorine obtained from fits to the simulation results.

method	Ising parameter				Antoine constant			
	A	B	β	ref.	A	B	C	ref.
Eq. 3.5	-0.00050392	0.601798	0.281		3.95617	322.468	-4.035	
Eq. 3.6	-0.00045976	0.718544	0.320		4.02876	326.511	-5.567	
LJ	-0.00052532	0.950152	0.325	[90]	3.46712	198.468	-31.171	[90]
D1-EOS	-0.00060993	0.493808	0.320	[18]	4.07770	325.253	-7.178	[18]
Exp.	-0.00036374	0.605529	0.320	[17]	3.98692	317.191	-5.436	[17]
Exp.	-0.00030476	0.660996	0.320	[116]	4.02355	322.067	-4.748	[115]

Furthermore the enthalpy of vaporization $\Delta_{\text{vap}}H$, entropy of vaporization $\Delta_{\text{vap}}S$ and boiling temperature T_{b} were calculated here from the simulation vapor pressures. The Clausius-Clapeyron equation was also used to test the accuracy of simulation results. These thermodynamic properties were estimated by the least-square fit to the simulation vapor pressures values shown in Table 4.12. The enthalpy of vaporization $\Delta_{\text{vap}}H$ and the entropy of vaporization $\Delta_{\text{vap}}S$ agreed well with the experimental data and data compilations.

Chapter 5

Conclusions

5.1   Conclusions

New potential energy surfaces for the dimers H_2-H_2, H_2-O_2, F_2-F_2 and H_2-F_2 have been constructed, using Møller-Plesset perturbation theory at different levels MPn (n =2, 3, 4) and the coupled-cluster method CCSD(T). The perturbation theory at all levels MPn (n =2, 3, 4) were found to be inadequate for the present computational work. The supermolecular approach was used for calculating the basis set superposition error (BSSE).

The basis sets used for this work were the correlation-consistent sets of Dunning, aug-cc-pVmZ (m = 2, 3, 4, 23) for hydrogen and the three basis sets aug-cc-pVmZ (m = 2, 3, 23) for fluorine, hydrogen-oxygen and hydrogen-fluorine. The potential energy surfaces were built from the extrapolation to the complete basis set limit, which had a significant effect on the convergence of the interaction energies. The interaction energies at 930 different configurations for each of the dimers were computed to determine the 30, 40, 36 and 48 adjustable parameters of the analytical potential functions Eq. 3.3 and Eq. 3.4 used for the dimers H_2-H_2 and H_2-O_2, and the 36, 48, 42, and 56 adjustable parameters of the analytical potential functions Eq. 3.5 and Eq. 3.6 used for the dimers F_2-F_2 and H_2-F_2, respectively, by least-square fits. These fits were carried out combining the Genetic algorithm (GA) and the Levenberg-Marquardt algorithm (LM). The four new *ab initio* analytical potential functions were constructed as 4-dimensional site-site potential functions with five centers per molecule.

The second virial coefficients for the dimers H_2-H_2, F_2-F_2, H_2-O_2 and H_2-F_2 were obtained from the analytical potential functions over a wide range of temperature. It turned out that results agreed very well with the experimental data as well as with the data derived from the empirical correlation equations of Estela-Uribe and the Deiters equation of state. For all dimers containing H_2 the quantum effects were included.

The four accurate *ab initio* pair potential functions were used then to predict the vapor-liquid equilibria of the pure fluids hydrogen and fluorine using global simulation techniques. Computer simulation programs were developed to carry out standard GEMC-NVT and NPT simulations. For hydrogen the phase equilibrium results predicted from the simulations were compared with literature data [139]. In the case of fluorine the Deiters equation of state [18] was used to calculate the phase equilibria. These comparisons were carried out to show the discrepancies of the different simulations. The predicted phase diagrams, critical parameters and thermodynamic properties of the two pure fluids hydrogen and fluorine were in good agreement with experimental data. This also confirmed that the four developed new *ab initio* analytical potential functions of this work are of high quality, accurate and reliable.

5.2   Limitations

Ab initio calculations at high levels of theory with large basis sets require much computation time even on modern large computers; moreover, the requirement of RAM and disk space are high and in some cases caused program and hardware failures. A extension of this work towards larger molecules is therefore difficult at present.

The second limit is that the 5-site analytical potential functions are not simple potential functions. Therefore it was very difficult to fit these potential function to the *ab initio* interaction energies; these fits required very much computation time. The global Monte Carlo simulations in this work using such 5-site analytical potential functions also needed much computation time.

5.3 Suggestion for further work

The *ab initio* quantum chemical methods used in this computational work might be used to construct the intermolecular energy surface of the dimer oxygen. The second virial coefficients of the dimer oxygen should be calculated with the *ab initio* potential functions developed in this thesis. The difficulty is, of cause, that O_2 is a diradical, which introduces some complications into the quantum mechanical computations.

The prediction of thermodynamic behaviors for the phase equilibria for the pure fluid oxygen as well as of the binary mixtures hydrogen-oxygen and hydrogen-fluorine should be then become possible with Gibbs Ensemble Monte Carlo simulations using our *ab initio* potential functions.

Chapter 6

Appendix A

This appendix describes the results of *ab initio* quantum chemical calculations for the dimers H_2-H_2, H_2-O_2, F_2-F_2 and H_2-F_2.

6.1 Predicting single-molecule properties

Table 6.1: Vibrational frequencies, cm^{-1} of the molecules H_2, O_2 and F_2 calculated with different methods and basis sets, respectively. Experimental vibrational data for H_2: 4401.2; O_2: 1580.2 and F_2: 916.6 [47]. The labels pVDZ, pVTZ, pVQZ and pV23Z denote the basis sets aug-cc-pVDZ, aug-cc-pVTZ, aug-cc-pVQZ and extrapolated energies aug-cc-pV23Z, respectively.

	method	6-31G	6-311G	pVDZ	pVTZ	pVQZ	pV23Z
	MP2	4533.6	4458.1	4463.7	4517.7	4515.0	4540.4
H_2	MP3	4459.7	4366.4	4406.0	4464.5	4463.2	4489.1
	MP4	4414.9	4317.5	4380.0	4435.6	4433.7	4459.0
	CCSD(T)	4370.3	4270.6	4347.6	4404.0	4402.8	4427.7
	MP2	918.5	1005.4	1428.2	1454.7	1479.7	1465.9
O_2	MP3	1483.7	1550.3	1721.8	1734.2	1735.5	1739.4
	MP4	1052.5	1104.3	1450.2	1443.5	1464.4	1440.7
	CCSD(T)	1271.8	1339.1	1564.6	1575.4	1596.2	1579.9
	MP2	893.4	838.2	933.4	1003.1	1003.4	1032.4
F_2	MP3	886.8	842.3	957.2	1037.7	1040.3	1071.6
	MP4	773.1	708.7	835.2	908.8	911.6	939.8
	CCSD(T)	729.8	673.7	823.7	914.8	919.9	953.2

Table 6.2: Dissociation energies in kJ/mol of the molecules calculated at 298.15 K and 1.013 bar. Experimental dissociation energy is 432.1 kJ/mol for H_2; O_2: 498.4 kJ/mol and for F_2: 154.5 kJ/mol [47].

	method	6-31G	6-311G	pVDZ	pVTZ	pVQZ	pV23Z
H_2	MP2	360.605	357.346	386.943	407.185	411.041	415.708
	MP3	374.704	371.349	404.070	422.040	424.553	429.607
	MP4	379.204	376.027	408.571	426.069	428.607	433.436
	CCSD(T)	381.422	378.466	410.434	427.552	430.427	434.760
O_2	MP2	363.220	361.309	491.236	522.568	534.662	535.761
	MP3	345.162	254.424	478.678	429.310	443.135	408.523
	MP4	309.107	331.340	457.246	491.022	504.741	505.243
	CCSD(T)	290.970	307.720	436.379	476.347	489.748	493.175
F_2	MP2	87.112	81.942	140.184	169.108	175.029	181.287
	MP3	46.294	46.625	87.058	109.784	114.654	119.353
	MP4	85.422	84.921	125.186	157.772	163.551	171.493
	CCSD(T)	88.569	81.885	120.000	146.776	151.818	158.051

Table 6.3: Bond lengths/Å of the dimers H_2-O_2 and H_2-F_2 in an optimized T configuration, calculated with different methods and basis sets. Experimental bond lengths are 0.7413 Å, 1.2074 Å and 1.418 Å for hydrogen, oxygen and fluorine, respectively [119].

	MP2			MP3		
Basis set	r_{H-H}/Å	r_{O-O}/Å	r_{F-F}/Å	r_{H-H}/Å	r_{O-O}/Å	r_{F-F}/Å
6-31G	0.7375	1.3428	1.5034	0.7418	1.2509	1.4974
6-311G	0.7372	1.3245	1.5054	0.7418	1.2437	1.4928
pVDZ	0.7549	1.2337	1.4269	0.7587	1.2013	1.4137
pVTZ	0.7374	1.2244	1.4014	0.7401	1.1926	1.3874
pVQZ	0.7363	1.2189	1.3975	0.7390	1.1880	1.3828
pV23Z	0.7300	1.2205	1.3907	0.7323	1.1889	1.3763
	MP4			CCSD(T)		
Basis set	r_{H-H}/Å	r_{O-O}/Å	r_{F-F}/Å	r_{H-H}/Å	r_{O-O}/Å	r_{F-F}/Å
6-31G	0.7441	1.3134	1.5342	0.7460	1.2832	1.5460
6-311G	0.7442	1.3054	1.5424	0.7463	1.2748	1.5512
pVDZ	0.7600	1.2312	1.4499	0.7617	1.2334	1.4507
pVTZ	0.7414	1.2267	1.4223	0.7430	1.2234	1.4186
pVQZ	0.7404	1.2216	1.4178	0.7418	1.2081	1.4135
pV23Z	0.7336	1.2248	1.4107	0.7351	1.2192	1.4050

Table 6.4: Potential energies, $10^6 E_{\min}/E_H$ and equilibrium distances, $r_{\min}/\text{Å}$ of the dimers at selected orientations (α, β, ϕ), calculated with CCSD(T) method and basis sets aug-cc-pVmZ (m = 2, 3, 4, 23). The labels pVDZ, pVTZ, pVQZ and pV23Z denote the basis sets aug-cc-pVDZ, aug-cc-pVTZ, aug-cc-pVQZ and extrapolated energies aug-cc-pV23Z, respectively.

| angle/degree | | | H_2-H_2 | | | | | | | |
| | | | pVDZ | | pVTZ | | pVQZ | | pV23Z | |
α	β	ϕ	$r_{\min}$	$E_{\min}$	$r_{\min}$	$E_{\min}$	$r_{\min}$	$E_{\min}$	$r_{\min}$	$E_{\min}$
0	0	0	3.8	-42.355	3.8	-37.490	3.8	-41.713	3.8	-35.444
90	0	0	3.6	-110.267	3.4	-152.745	3.4	-162.130	3.4	-171.825
90	90	0	3.8	-32.638	3.6	-47.309	3.6	-53.117	3.6	-55.246
90	90	90	3.8	-42.715	3.6	-66.931	3.6	-72.606	3.4	-78.158

| angle/degree | | | H_2-O_2 | | | | | |
| | | | pVDZ | | pVTZ | | pV23Z | |
α	β	ϕ	$r_{\min}$	$E_{\min}$	$r_{\min}$	$E_{\min}$	$r_{\min}$	$E_{\min}$
0	0	0	4.0	-176.903	4.0	-225.514	3.8	-247.957
90	0	0	4.0	-167.764	3.8	-237.364	3.8	-268.209
90	90	0	3.4	-200.841	3.2	-332.693	3.0	-398.079
90	90	90	3.6	-84.217	3.4	-156.328	3.2	-196.486

| angle/degree | | | F_2-F_2 | | | | | |
| | | | pVDZ | | pVTZ | | pV23Z | |
α	β	ϕ	$r_{\min}$	$E_{\min}$	$r_{\min}$	$E_{\min}$	$r_{\min}$	$E_{\min}$
0	0	0	4.8	-7.730	4.4	-132.120	4.4	-202.000
90	0	0	3.8	-398.390	3.6	-547.080	3.6	-616.926
90	90	0	3.4	-250.900	3.2	-410.000	3.2	-501.941
90	90	90	3.2	-313.590	3.0	-513.590	3.0	-637.511

| angle/degree | | | H_2-F_2 | | | | | |
| | | | pVDZ | | pVTZ | | pV23Z | |
α	β	ϕ	$r_{\min}$	$E_{\min}$	$r_{\min}$	$E_{\min}$	$r_{\min}$	$E_{\min}$
0	0	0	4.2	-48.392	4.0	-87.010	4.0	-105.413
90	0	0	3.6	-277.244	3.6	-412.361	3.4	-487.530
90	90	0	3.4	-122.528	3.2	-206.950	3.2	-252.737
90	90	90	3.4	-119.035	3.2	-195.925	3.2	-240.953

6.2   Comparison of theoretical levels
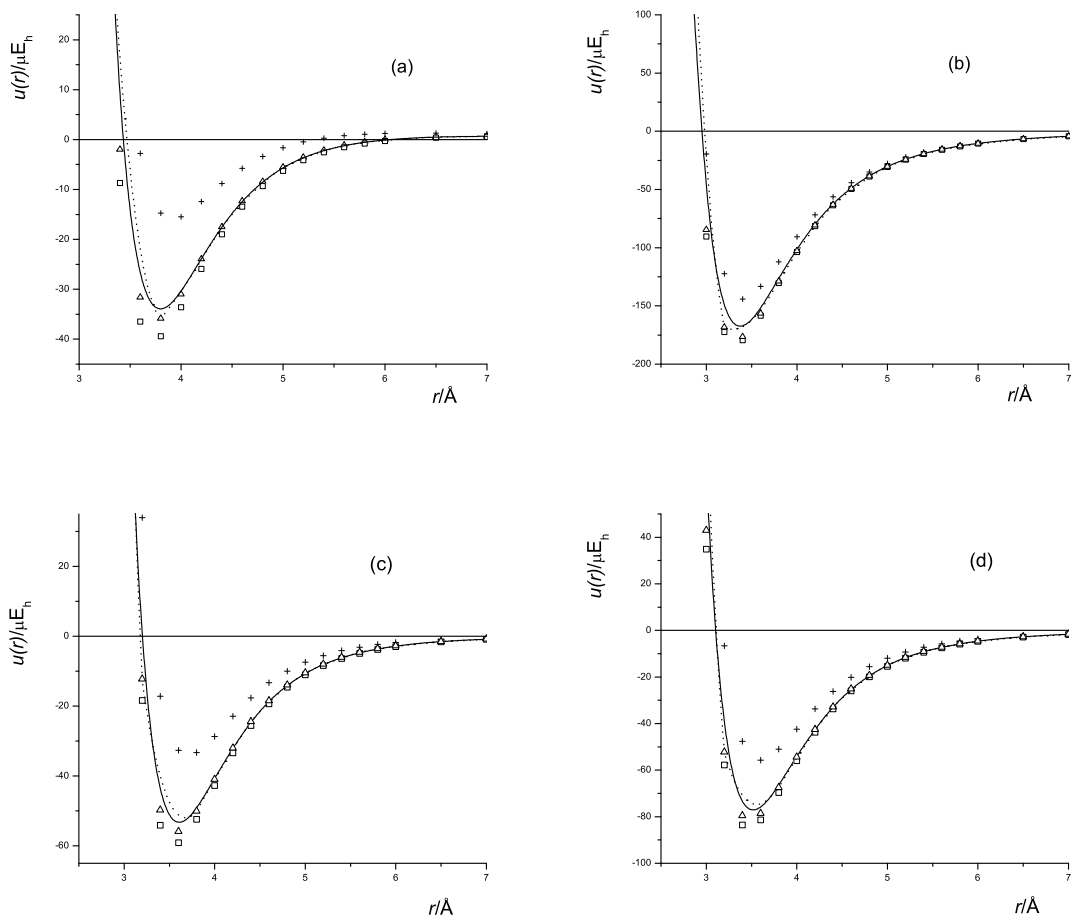
Figure 6.1: Intermolecular potentials of H_2-H_2 calculated with the basis set aug-cc-pV23Z with different post-SCF techniques: +, MP2; △, MP3; □, MP4; —, CCSD(T) (this work); $\cdots$: CCSD(T)/CBS limit by Diep and Johnson [25]; the configurations, L, T, H and X correspond to (a), (b), (c), and (d) in Fig. 3.2.
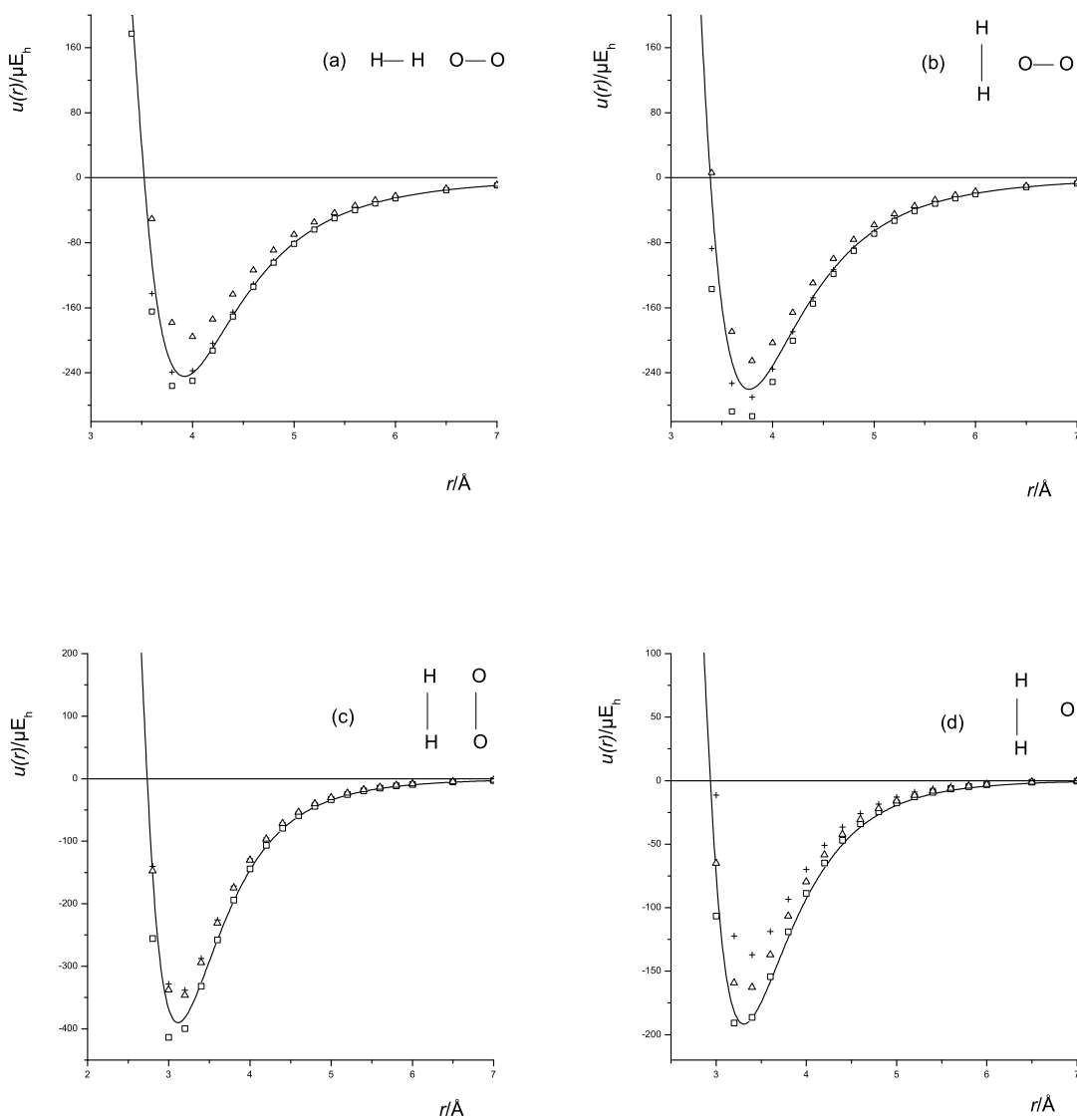
Figure 6.2: Intermolecular potentials of H_2-O_2; for an explanation see Fig. 6.1.
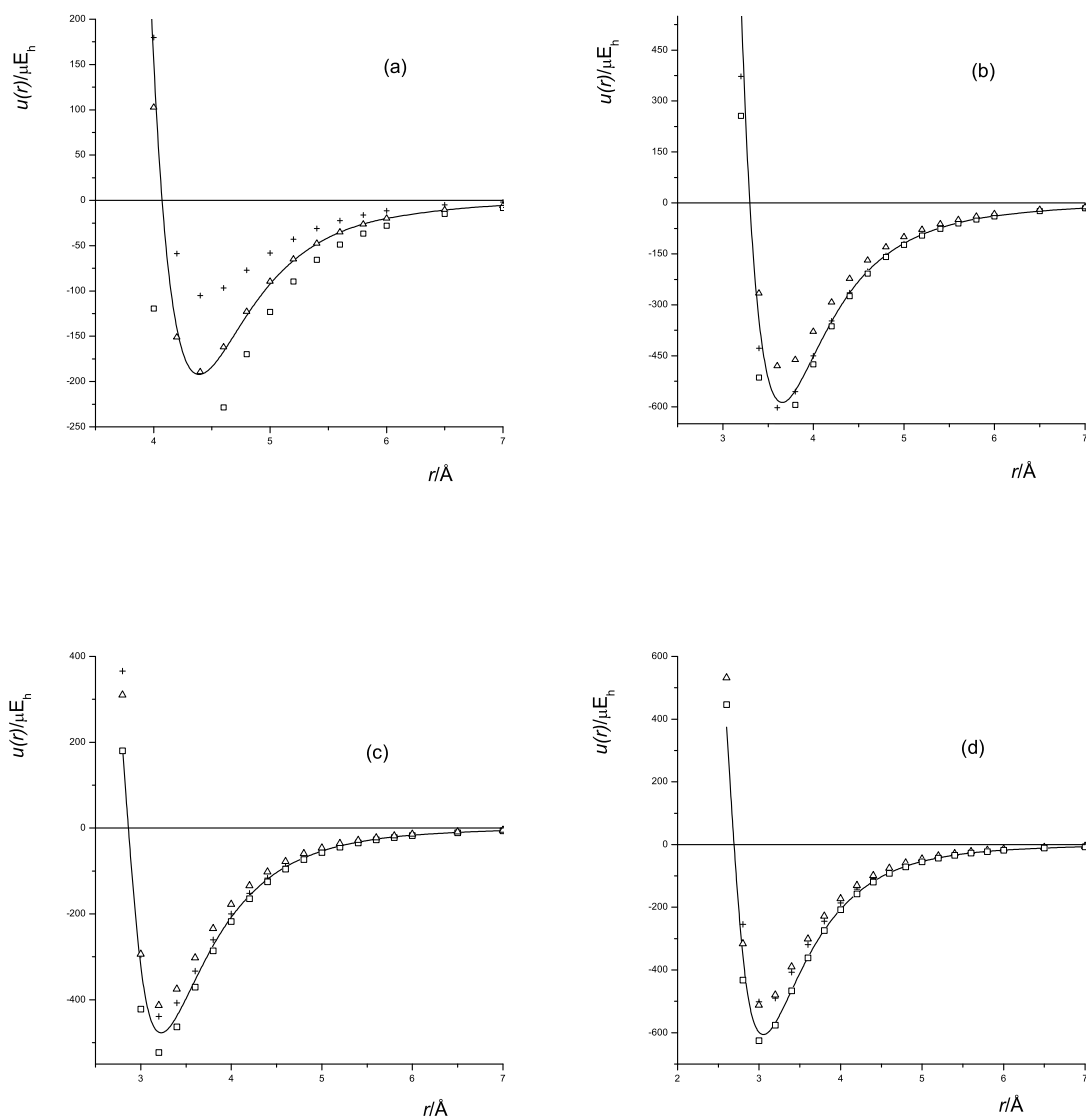
Figure 6.3: Intermolecular potentials of F_2-F_2; for an explanation see Fig. 6.1.
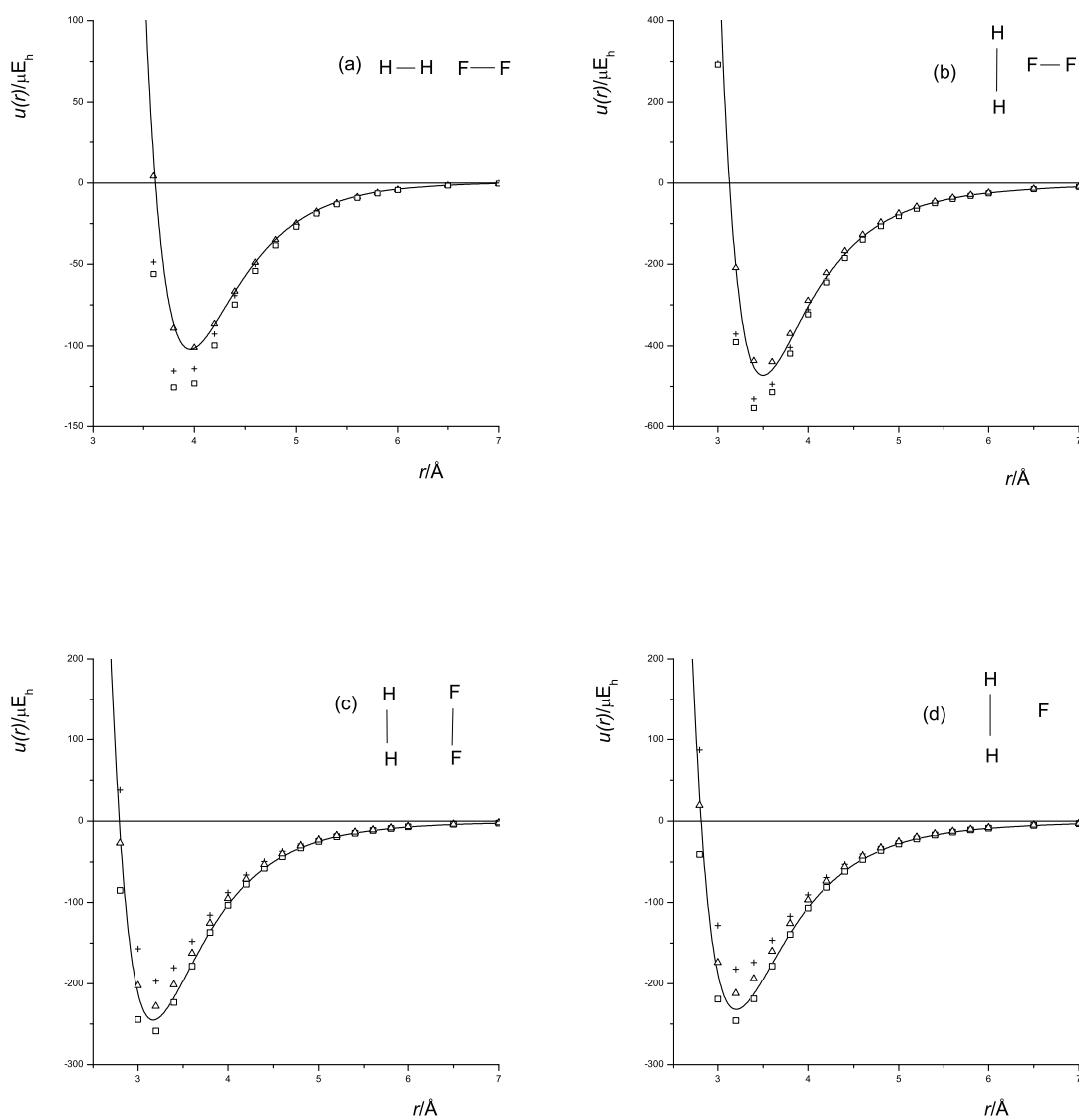
Figure 6.4: Intermolecular potentials of H_2-F_2; for an explanation see Fig. 6.1.

6.3 Comparison of basis sets
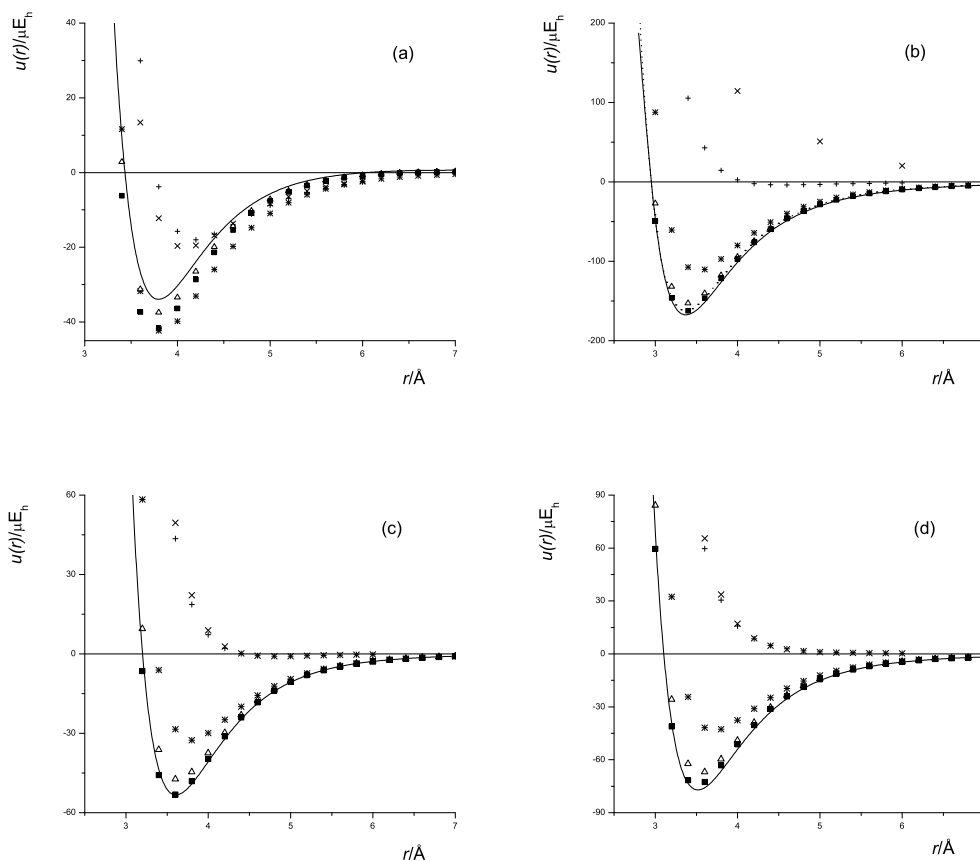
Figure 6.5: Intermolecular potentials of H_2-H_2 calculated with the CCSD(T) method for different basis sets: $\times$, 6-31G; $+$, 6-311G; *, aug-cc-pVDZ; $\triangle$, aug-cc-pVTZ; $\blacksquare$, aug-cc-pVQZ; —, aug-cc-pV23Z; $\cdots$: basis set CBS for T configuration [25]; the configurations L, T, H and X correspond to (a), (b), (c) and (d) in Fig. 3.2.
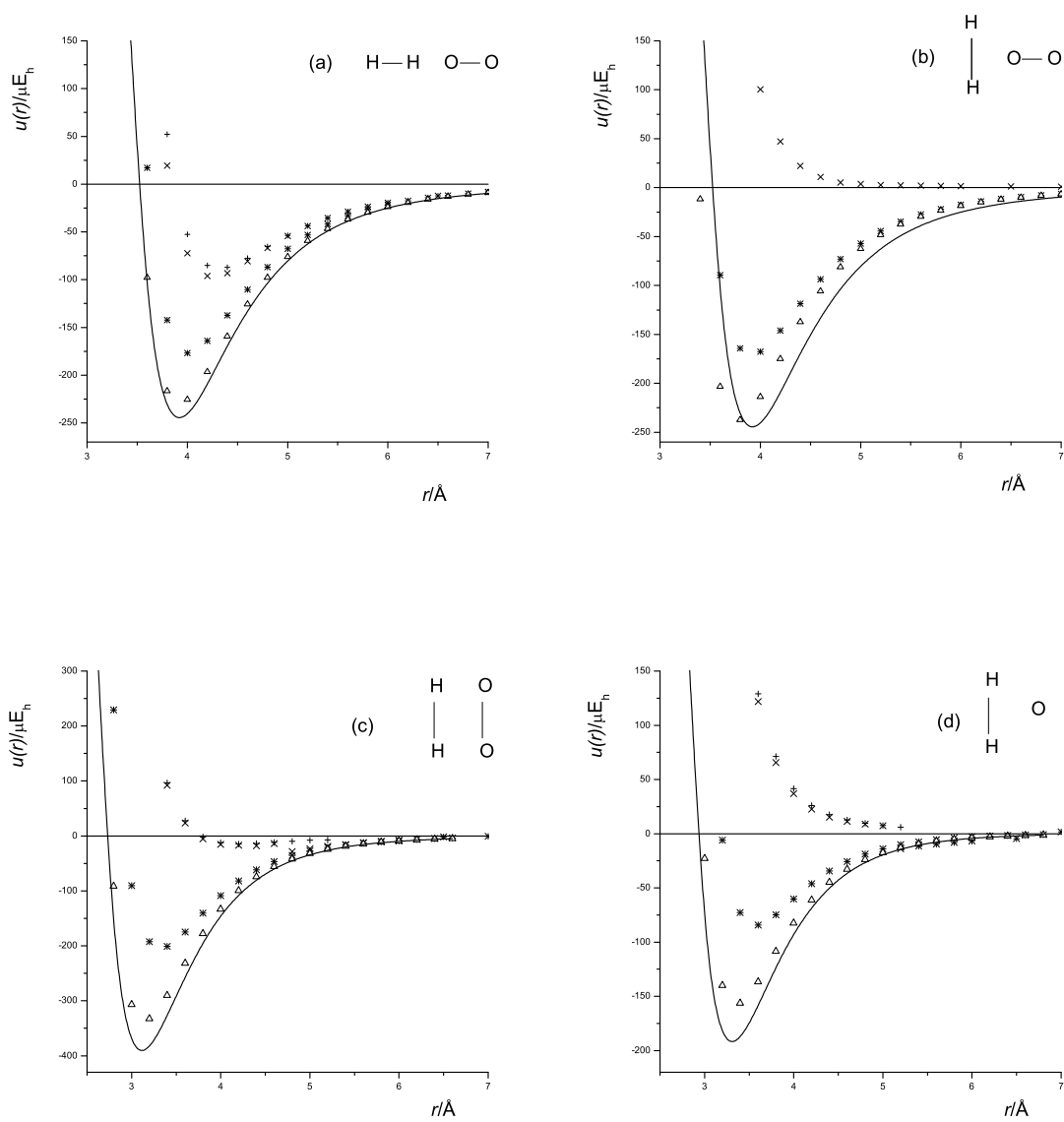
Figure 6.6: Intermolecular potentials of H_2-O_2; for an explanation see Fig. 6.5.
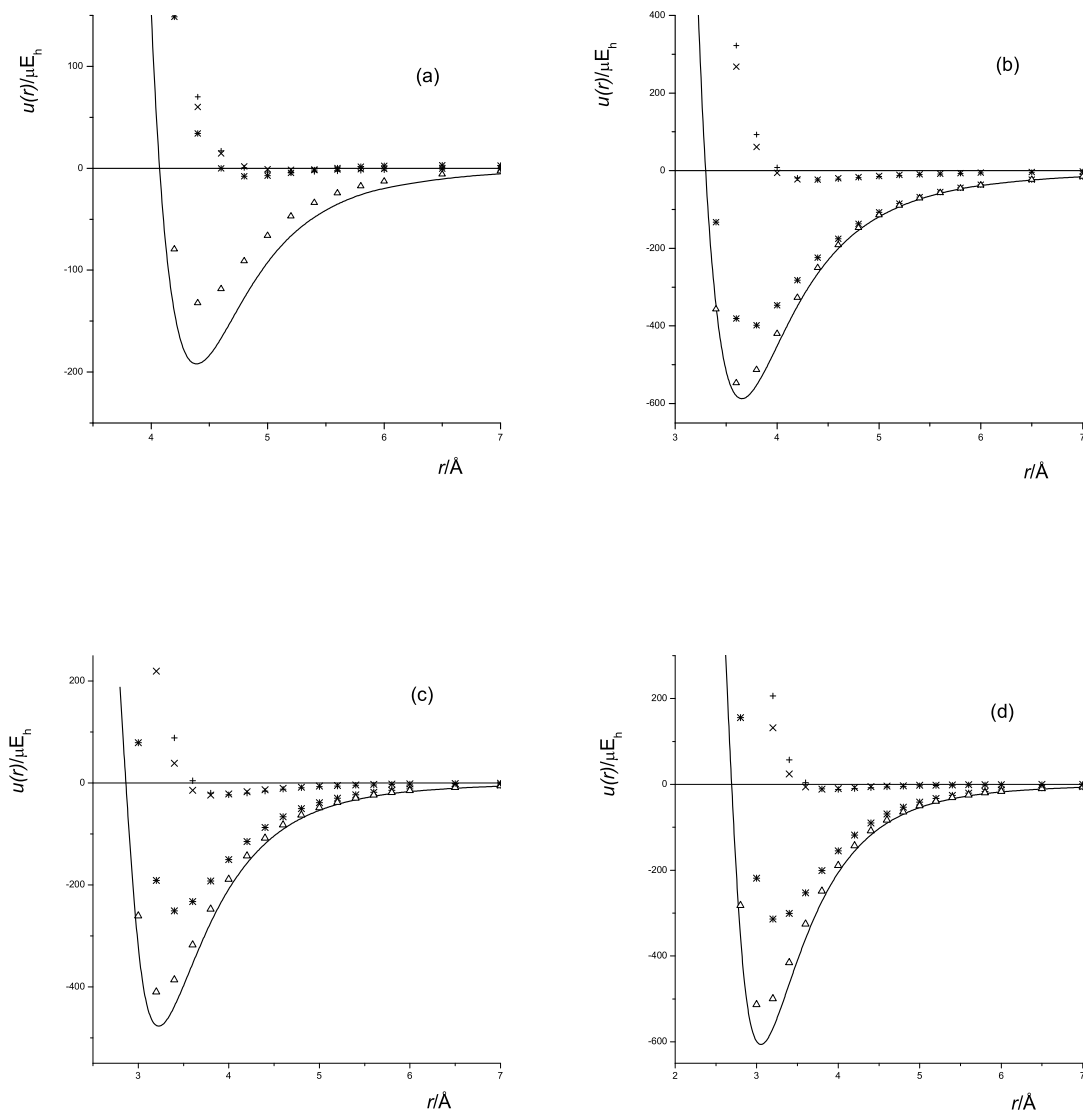
Figure 6.7: Intermolecular potentials of F_2-F_2; for an explanation see Fig. 6.5.
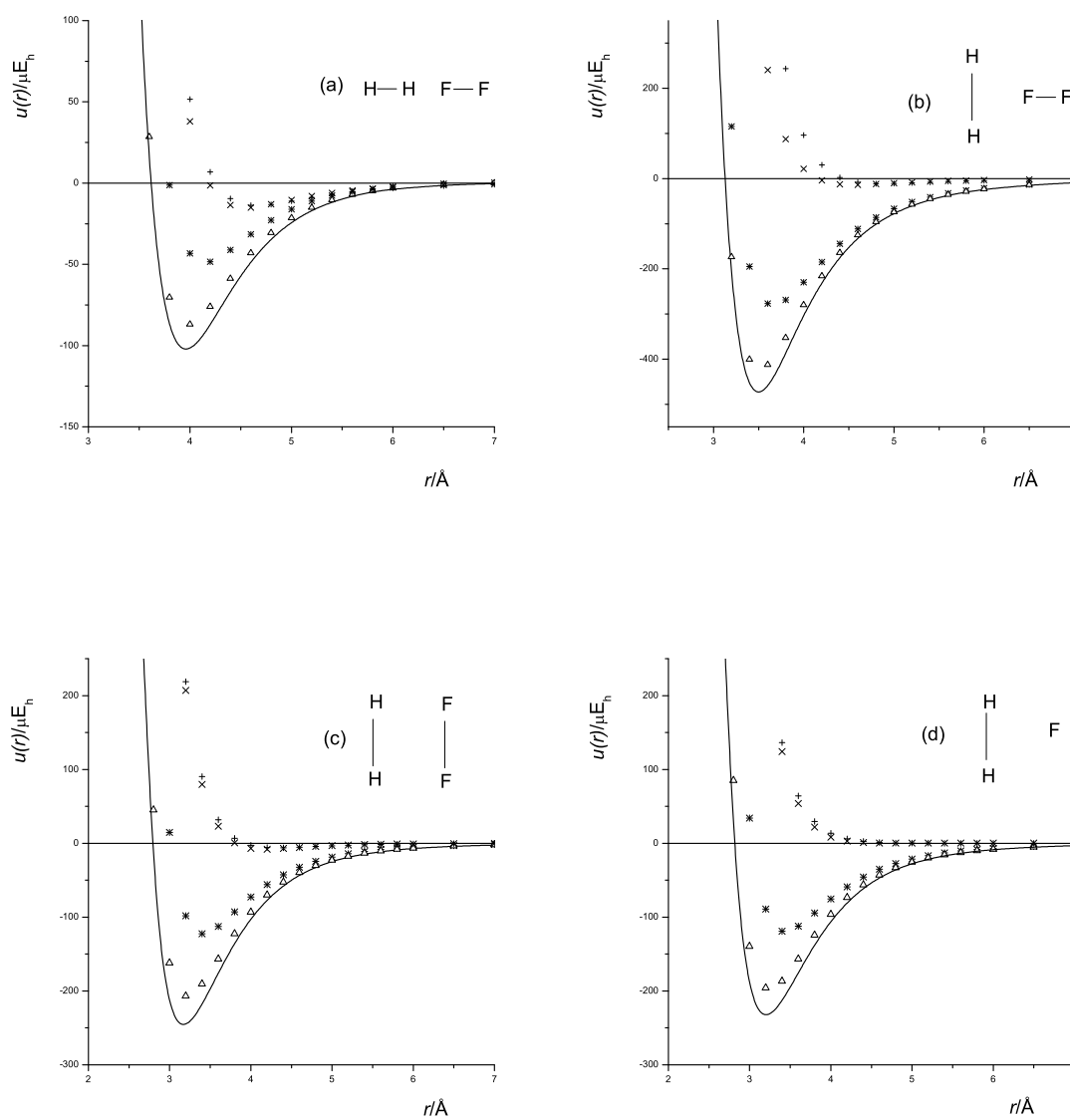
Figure 6.8: Intermolecular potentials of H_2-F_2; for an explanation see Fig. 6.5.

Table 6.5: Pair interaction energies of dimers H_2-H_2 and H_2-O_2 calculated with the CCSD(T) method and the basis sets aug-cc-pVmZ (m = 2, 3, 23) (23 denotes the extrapolation from sets 2 and 3).

α	β	ϕ	r/Å	$10^6 u$ /E_H H_2-H_2				r/Å	$10^6 u$ /E_H H_2-O_2		
				pVDZ	pVTZ	pVQZ	pV23Z		pVDZ	pVTZ	pV23Z
0	0	0	2.8	978.17	877.59	844.38	835.30	3.4	473.71	291.25	214.42
0	0	0	3.0	398.31	342.95	321.76	319.67	3.6	17.12	-98.00	-146.47
0	0	0	3.4	11.64	2.86	-6.19	-0.83	3.8	-142.28	-216.65	-247.96
0	0	0	3.6	-31.77	-31.20	-37.32	-30.96	4.0	-176.90	-225.51	-245.98
0	0	0	3.8	-42.35	-37.49	-41.71	-35.44	4.2	-164.03	-196.57	-210.27
0	0	0	5.0	-10.94	-7.15	-7.58	-12.23	5.0	-67.83	-76.03	-79.48
0	0	0	9.0	0.10	0.31	0.30	-8.36	9.0	-1.82	-2.06	-2.16
0	0	0	10.0	0.10	0.22	0.21	-5.55	10.0	-0.98	-1.10	-1.15
45	0	0	3.0	238.21	144.38	124.32	104.93	3.4	287.21	115.78	43.59
45	0	0	3.2	31.66	-22.89	-35.73	-45.82	3.6	-50.97	-162.59	-209.59
45	0	0	3.4	-49.09	-79.91	-88.17	-92.87	3.8	-160.79	-233.45	-264.04
45	0	0	3.6	-71.87	-89.00	-94.34	-96.20	4.0	-176.12	-223.52	-243.48
45	0	0	4.0	-60.52	-65.57	-67.83	-52.80	4.2	-157.10	-188.29	-201.43
45	0	0	5.0	-18.13	-18.14	-18.30	-23.67	5.0	-62.67	-69.64	-72.58
45	0	0	9.0	-0.38	-0.34	-0.34	-18.14	9.0	-1.21	-1.71	-1.92
45	0	0	10.0	-0.19	-0.16	-0.16	-5.29	10.0	-0.62	-0.67	-0.69
90	0	0	2.8	449.78	265.06	231.32	187.40	3.2	807.44	556.85	451.34
90	0	0	3.0	87.81	-27.16	-49.06	-75.50	3.4	159.81	-11.82	-84.08
90	0	0	3.2	-60.56	-131.85	-146.13	-152.87	3.6	-89.41	-203.25	-251.18
90	0	0	3.4	-107.37	-152.75	-162.13	-100.72	3.8	-164.11	-237.36	-268.21
90	0	0	3.6	-110.27	-140.26	-146.46	-79.08	4.0	-167.76	-213.85	-233.25
90	0	0	3.8	-97.07	-117.62	-121.69	-61.77	4.2	-146.14	-174.93	-187.05
90	0	0	5.0	-24.89	-28.44	-28.54	-10.31	5.0	-57.05	-62.49	-64.78
90	0	0	9.0	-0.84	-0.97	-0.96	-1.02	9.0	-1.34	-1.36	-1.37
90	0	0	10.0	-0.47	-0.54	-0.53	-0.57	10.0	-0.70	-0.25	-0.05
135	45	0	2.8	492.22	292.59	258.77	208.66	3.2	703.34	491.60	402.45
135	45	0	3.0	118.26	-5.71	-28.09	-57.84	3.4	165.69	21.23	-39.59
135	45	0	3.2	-38.94	-115.77	-130.31	-145.14	3.6	-59.89	-156.40	-197.04
135	45	0	3.4	-92.51	-141.03	-150.23	-120.49	3.8	-138.56	-201.86	-228.51
135	45	0	3.6	-100.34	-131.88	-137.53	-96.30	4.0	-151.61	-192.60	-209.85
135	45	0	3.8	-90.50	-111.61	-114.98	-75.57	4.2	-138.06	-164.98	-176.32
135	45	0	4.0	-23.87	-27.03	-27.05	-28.36	5.0	-61.12	-66.61	-68.93
135	45	0	5.0	-0.78	-0.89	-0.88	-0.93	9.0	-1.97	-2.15	-2.23
135	45	0	9.0	-0.43	-0.49	-0.49	-0.51	10.0	-1.07	-1.10	-1.11
90	45	0	2.8	160.83	59.21	34.76	16.48	3.4	401.94	235.32	165.16
90	45	0	3.0	4.84	-56.20	-72.11	-81.87	3.6	125.17	19.35	-25.21
90	45	0	3.2	-52.98	-90.72	-100.88	-106.59	3.8	4.99	-61.15	-89.00
90	45	0	3.4	-66.99	-91.14	-97.54	-101.29	4.0	-40.54	-81.96	-99.40

Table 6.6: Table 6.5 continued

α	β	ϕ	$r/\text{Å}$	$10^6 u$ $/E_\text{H}$ H$_2$-H$_2$				$r/\text{Å}$	$10^6 u$ $/E_\text{H}$ H$_2$-O$_2$		
				pVDZ	pVTZ	pVQZ	pV23Z		pVDZ	pVTZ	pV23Z
90	45	0	3.6	-63.37	-79.31	-83.29	-86.02	4.2	-52.23	-78.68	-89.81
90	45	0	3.8	-54.00	-64.82	-67.25	-69.37	5.0	-28.77	-34.09	-36.33
90	45	0	5.0	-0.49	-0.53	-0.53	-0.55	9.0	-0.66	-0.71	-0.73
90	45	0	9.0	-0.26	-0.28	-0.28	-0.29	10.0	-0.33	-0.33	-0.33
45	45	0	2.8	739.82	595.17	562.62	534.36	3.2	810.42	586.92	492.81
45	45	0	3.0	288.53	205.82	183.92	171.04	3.4	223.04	72.17	8.65
45	45	0	3.2	81.12	36.46	21.83	17.69	3.6	-22.84	-125.08	-168.12
45	45	0	3.4	-5.82	-28.77	-38.40	-38.42	3.8	-110.71	-179.48	-208.43
45	45	0	3.6	-36.22	-47.39	-53.62	-52.09	4.0	-128.82	-175.01	-194.46
45	45	0	3.8	-41.97	-46.92	-50.90	-49.01	4.2	-118.98	-149.99	-163.05
45	45	0	4.0	-38.20	-39.93	-42.44	-40.66	5.0	-50.57	-57.96	-61.07
45	45	0	5.0	-11.35	-10.29	-10.55	-9.85	9.0	-1.21	-1.51	-1.63
45	45	0	10.0	-0.02	0.04	0.04	0.07	10.0	-0.63	-0.72	-0.76
90	90	0	3.0	214.91	132.94	107.33	98.47	2.6	1027.94	576.30	386.14
90	90	0	3.2	58.37	9.44	-6.45	-11.14	2.8	229.37	-91.39	-226.45
90	90	0	3.4	-6.08	-36.17	-45.81	-48.83	3.0	-90.33	-306.90	-398.08
90	90	0	3.6	-28.43	-47.31	-53.12	-55.25	3.2	-192.28	-332.69	-391.81
90	90	0	3.8	-32.64	-44.62	-48.14	-49.66	3.4	-200.84	-290.20	-327.82
90	90	0	4.0	-29.91	-37.48	-39.65	-40.66	3.8	-140.24	-177.70	-193.47
90	90	0	5.0	-9.46	-10.23	-10.55	-10.56	5.0	-27.11	-31.82	-33.80
90	90	0	9.0	-0.15	-0.11	-0.11	-0.09	9.0	-0.38	-0.47	-0.51
90	90	0	10.0	-0.06	-0.03	-0.04	-0.02	10.0	-0.14	-0.19	-0.21
90	45	45	2.8	506.51	330.85	294.77	256.99	3.2	947.10	727.25	634.67
90	45	45	3.2	-2.17	-66.13	-81.70	-93.02	3.4	426.61	244.04	167.17
90	45	45	3.4	-57.96	-97.96	-107.90	-114.78	3.6	145.35	22.64	-29.03
90	45	45	3.6	-70.65	-96.55	-102.79	-107.43	3.8	21.45	-61.22	-96.03
90	45	45	3.8	-66.14	-83.43	-87.29	-90.70	4.0	-26.61	-83.38	-107.28
90	45	45	4.0	-56.14	-68.00	-70.35	-72.98	4.4	-44.83	-66.70	-75.90
90	45	45	5.0	-17.74	-20.14	-20.33	-21.15	5.0	-26.00	-30.60	-32.54
90	45	45	9.0	-0.54	-0.59	-0.59	-0.61	9.0	-0.72	-0.91	-1.00
90	45	45	10.0	-0.29	-0.32	-0.32	-0.33	10.0	-0.31	-0.65	-0.80
45	45	45	3.0	258.05	166.13	144.82	127.49	3.2	680.09	464.30	373.43
45	45	45	3.2	59.68	8.16	-6.05	-13.50	3.4	174.49	28.34	-33.20
45	45	45	3.4	-21.31	-49.49	-58.80	-61.34	3.6	-43.30	-160.77	-210.23
45	45	45	3.6	-47.68	-62.90	-68.86	-69.29	3.8	-119.69	-205.85	-242.13
45	45	45	3.8	-50.64	-58.74	-62.50	-62.15	4.0	-132.43	-196.64	-223.68
45	45	45	4.0	-44.89	-49.08	-51.41	-50.84	4.2	-119.75	-169.44	-190.37
45	45	45	5.0	-13.57	-13.30	-13.51	-13.18	5.0	-53.29	-66.35	-71.84
45	45	45	9.0	-0.22	-0.15	-0.15	-0.12	9.0	-0.78	-2.34	-2.99
45	45	45	10.0	-0.09	-0.05	-0.05	-0.03	10.0	-0.27	-1.30	-1.73

Table 6.7: Table 6.6 continued

α	β	ϕ	$r/\text{Å}$	$10^6 u$ /E_H H$_2$-H$_2$				$r/\text{Å}$	$10^6 u$ /E_H H$_2$-O$_2$		
				pVDZ	pVTZ	pVQZ	pV23Z		pVDZ	pVTZ	pV23Z
90	90	45	2.8	534.90	387.27	348.44	325.20	2.8	445.33	123.89	-11.46
90	90	45	3.2	45.22	-8.38	-23.91	-30.91	3.0	49.63	-164.90	-255.23
90	90	45	3.4	-15.32	-49.32	-58.79	-63.62	3.2	-98.90	-236.46	-294.37
90	90	45	3.6	-35.15	-57.18	-62.92	-66.44	3.4	-136.78	-223.35	-259.81
90	90	45	3.8	-37.67	-52.14	-55.65	-58.23	3.6	-129.43	-184.36	-207.49
90	90	45	4.0	-33.69	-43.29	-45.48	-47.33	4.0	-84.07	-107.88	-117.90
90	90	45	5.0	-10.82	-12.16	-12.48	-12.73	5.0	-20.44	-24.70	-26.49
90	90	45	9.0	-0.23	-0.22	-0.22	-0.21	9.0	-0.12	-0.18	-0.20
90	90	45	10.0	-0.11	-0.10	-0.10	-0.09	10.0	0.01	-0.02	-0.04
90	45	90	2.8	491.26	310.36	275.19	234.30	3.4	444.91	281.94	213.31
90	45	90	3.2	-9.18	-76.07	-91.31	-104.20	3.6	158.97	56.32	13.09
90	45	90	3.4	-62.94	-105.21	-114.93	-122.98	3.8	31.49	-31.62	-58.20
90	45	90	3.6	-74.31	-101.95	-108.04	-113.57	4.0	-19.30	-58.20	-74.58
90	45	90	4.0	-58.29	-71.17	-73.44	-76.58	4.4	-36.08	-51.65	-58.20
90	45	90	5.0	-18.48	-21.17	-21.35	-22.30	5.0	-20.70	-25.18	-27.07
90	45	90	10.0	-0.31	-0.35	-0.35	-0.37	10.0	-0.03	0.00	0.01
45	45	90	2.8	598.82	418.30	387.06	342.40	3.2	558.82	353.11	266.49
45	45	90	3.2	13.24	-51.63	-65.35	-78.90	3.4	120.11	-37.47	-103.82
45	45	90	3.4	-54.81	-93.45	-102.31	-109.70	3.6	-71.12	-185.13	-233.13
45	45	90	3.6	-72.45	-95.90	-101.46	-105.75	3.8	-136.31	-219.43	-254.43
45	45	90	3.8	-69.39	-83.95	-87.37	-90.07	4.0	-143.45	-205.58	-231.74
45	45	90	4.0	-59.36	-68.63	-70.68	-72.53	4.2	-127.99	-174.87	-194.61
45	45	90	5.0	-18.40	-19.77	-19.88	-20.35	5.0	-56.16	-66.44	-70.77
45	45	90	9.0	-0.48	-0.49	-0.49	-0.50	9.0	-1.20	-2.51	-3.06
45	45	90	10.0	-0.25	-0.26	-0.26	-0.26	10.0	-0.54	-0.73	-0.81
90	90	90	2.8	507.94	353.01	314.74	287.87	2.8	661.35	339.17	203.51
90	90	90	3.2	32.44	-25.85	-41.13	-50.35	3.0	189.43	-22.78	-112.13
90	90	90	3.4	-24.45	-62.26	-71.59	-78.16	3.2	-5.97	-140.04	-196.49
90	90	90	3.6	-41.85	-66.93	-72.61	-77.48	3.4	-72.74	-156.33	-191.52
90	90	90	3.8	-42.71	-59.60	-63.09	-66.70	3.6	-84.22	-136.70	-158.80
90	90	90	5.0	-12.18	-14.09	-14.41	-14.89	4.0	-60.13	-82.43	-91.82
90	90	90	9.0	-0.31	-0.33	-0.33	-0.33	5.0	-13.79	-17.56	-19.15
90	90	90	10.0	-0.16	-0.16	-0.16	-0.17	10.0	0.16	0.15	0.14
45	135	45	2.8	519.90	324.36	291.53	242.14	3.2	630.41	423.82	336.84
45	135	45	3.0	137.53	16.77	-4.95	-34.00	3.4	142.78	-15.45	-82.07
45	135	45	3.2	-25.28	-99.40	-113.55	-130.56	3.6	-66.19	-179.49	-227.19
45	135	45	3.4	-82.64	-128.83	-137.83	-148.25	3.8	-138.13	-220.15	-254.68
45	135	45	3.6	-93.04	-122.62	-128.17	-135.05	4.0	-148.27	-208.14	-233.34
45	135	45	3.8	-84.97	-104.47	-107.80	-112.67	4.2	-133.30	-178.43	-197.43
45	135	45	5.0	-22.43	-25.14	-25.17	-26.27	5.0	-60.49	-68.31	-71.61
45	135	45	9.0	-0.70	-0.78	-0.78	-0.82	10.0	-0.99	-0.02	0.39

Table 6.8: Pair interaction energies of dimers F_2-F_2 and H_2-F_2 calculated with the CCSD(T) method and the basis sets aug-cc-pVmZ (m = 2, 3, 23) (23 denotes the extrapolation from sets 2 and 3).

α	β	ϕ	$r/\text{Å}$	$10^6 u$ /E_H F_2-F_2			$r/\text{Å}$	$10^6 u$ /E_H H_2-F_2		
				pVDZ	pVTZ	pV23Z		pVDZ	pVTZ	pV23Z
0	0	0	3.8	1507.75	1057.70	868.47	3.4	505.38	335.88	264.52
0	0	0	4.0	499.98	187.76	56.49	3.6	136.96	28.50	-17.17
0	0	0	4.2	148.60	-79.44	-175.32	3.8	-1.18	-70.33	-99.44
0	0	0	4.4	34.08	-132.12	-202.00	4.0	-43.31	-87.01	-105.41
0	0	0	4.6	0.01	-118.41	-168.20	4.2	-48.39	-75.99	-87.61
0	0	0	4.8	-7.73	-91.01	-126.03	4.4	-41.16	-58.85	-66.30
0	0	0	5.2	-4.55	-47.23	-65.18	4.6	-31.47	-43.10	-48.00
0	0	0	5.4	-1.90	-33.84	-47.27	5.0	-16.05	-21.53	-23.84
0	0	0	5.6	0.19	-24.33	-34.64	6.5	-0.43	-0.97	-1.20
0	0	0	15.0	0.02	-0.03	-0.05	15.0	0.08	0.08	0.08
45	0	0	3.6	536.43	289.26	185.34	3.2	681.25	412.55	299.41
45	0	0	3.8	-182.98	-365.50	-442.24	3.4	116.64	-67.83	-145.50
45	0	0	4.0	-349.40	-490.75	-550.18	3.6	-89.38	-212.51	-264.36
45	0	0	4.2	-334.09	-439.45	-483.75	3.8	-144.70	-224.31	-257.82
45	0	0	4.4	-273.87	-347.76	-378.83	4.0	-141.62	-192.02	-213.24
45	0	0	4.6	-212.72	-262.29	-283.13	4.2	-119.69	-151.53	-164.93
45	0	0	5.0	-122.17	-144.62	-154.06	4.8	-55.62	-64.95	-68.88
45	0	0	8.0	-4.14	-5.02	-5.39	8.0	-1.64	-1.82	-1.90
45	0	0	15.0	-0.17	-0.18	-0.18	15.0	-0.01	-0.01	-0.01
90	0	0	3.2	776.13	472.78	345.24	3.0	965.21	591.55	434.22
90	0	0	3.4	-132.78	-356.72	-450.88	3.2	115.51	-173.79	-295.60
90	0	0	3.6	-380.96	-547.08	-616.93	3.4	-194.63	-400.75	-487.53
90	0	0	3.8	-398.39	-513.15	-561.40	3.6	-277.24	-412.36	-469.25
90	0	0	4.0	-346.68	-420.02	-450.86	3.8	-269.03	-352.55	-387.72
90	0	0	4.2	-282.41	-326.86	-345.55	4.0	-229.62	-280.14	-301.40
90	0	0	4.4	-223.71	-250.28	-261.45	4.2	-184.64	-215.80	-228.92
90	0	0	4.6	-175.26	-191.46	-198.27	4.4	-144.24	-164.44	-172.94
90	0	0	5.4	-67.88	-71.08	-72.43	5.0	-66.65	-73.91	-76.97
90	0	0	8.0	-6.93	-6.79	-6.73	9.0	-1.88	-1.99	-2.03
90	0	0	15.0	-0.34	-0.30	-0.28	15.0	-0.09	-0.10	-0.11
135	45	0	3.5	633.37	382.63	277.21	3.0	1175.25	879.42	754.86
135	45	0	3.7	49.58	-128.62	-203.55	3.2	343.85	137.76	50.99
135	45	0	3.8	-84.33	-230.99	-292.65	3.4	-5.84	-143.00	-200.75
135	45	0	4.0	-198.40	-292.81	-332.51	3.6	-132.56	-220.86	-258.04
135	45	0	4.2	-213.62	-271.31	-295.57	3.8	-161.05	-217.03	-240.60
135	45	0	4.4	-192.62	-227.04	-241.51	4.0	-150.16	-185.87	-200.91
135	45	0	4.6	-161.68	-182.38	-191.08	4.2	-126.84	-150.14	-159.95

Table 6.9: Table 6.8 continued

α	β	ϕ	$r/$Å	$10^6 u$ /E_H F_2-F_2			$r/$Å	$10^6 u$ /E_H H_2-F_2		
				pVDZ	pVTZ	pV23Z		pVDZ	pVTZ	pV23Z
135	45	0	5.0	-105.09	-113.48	-117.01	4.6	-81.36	-92.09	-96.61
135	45	0	6.0	-35.89	-37.09	-37.59	6.0	-16.99	-18.35	-18.92
135	45	0	15.0	-0.32	-0.28	-0.26	15.0	-0.08	-0.08	-0.08
90	45	0	3.0	1343.97	926.04	750.32	3.2	511.89	289.83	196.34
90	45	0	3.2	202.20	-110.38	-241.81	3.4	134.73	-5.71	-64.84
90	45	0	3.4	-182.10	-406.71	-501.15	3.6	-20.27	-106.10	-142.25
90	45	0	3.6	-275.86	-427.25	-490.90	3.8	-72.91	-125.41	-147.51
90	45	0	3.8	-265.86	-363.21	-404.14	4.0	-81.59	-114.64	-128.55
90	45	0	4.0	-224.67	-286.41	-312.37	4.2	-73.79	-95.45	-104.57
90	45	0	4.2	-179.48	-219.45	-236.26	4.4	-61.54	-76.26	-82.46
90	45	0	4.4	-139.68	-166.62	-177.95	4.6	-49.60	-59.84	-64.16
90	45	0	6.0	-20.42	-23.38	-24.62	6.0	-10.19	-11.65	-12.26
90	45	0	15.0	-0.22	-0.20	-0.19	15.0	-0.03	-0.04	-0.05
45	45	0	3.6	1040.07	716.93	581.06	3.2	643.66	452.70	372.30
45	45	0	3.8	302.81	70.83	-26.71	3.4	193.19	64.38	10.15
45	45	0	4.0	31.59	-132.59	-201.62	3.6	9.81	-75.03	-110.75
45	45	0	4.2	-57.02	-169.79	-217.20	3.8	-54.34	-109.17	-132.25
45	45	0	4.4	-76.43	-152.49	-184.47	4.0	-67.93	-103.19	-118.04
45	45	0	4.6	-71.20	-122.86	-144.58	4.2	-62.28	-85.14	-94.76
45	45	0	4.8	-58.88	-94.96	-110.13	4.4	-51.07	-66.18	-72.55
45	45	0	5.0	-46.07	-72.35	-83.40	4.6	-39.84	-50.05	-54.35
45	45	0	6.0	-11.63	-19.21	-22.40	6.0	-5.71	-6.88	-7.38
45	45	0	15.0	-0.07	-0.10	-0.11	15.0	0.04	0.03	0.02
90	90	0	2.8	885.84	394.61	188.07	2.6	1063.97	636.37	456.32
90	90	0	3.0	79.38	-260.74	-403.75	2.8	327.46	45.28	-73.53
90	90	0	3.2	-191.33	-410.00	-501.94	3.0	14.57	-162.09	-236.47
90	90	0	3.4	-250.90	-386.33	-443.27	3.2	-98.21	-206.95	-252.74
90	90	0	3.6	-232.91	-317.69	-353.34	3.4	-122.53	-190.64	-219.31
90	90	0	3.8	-192.13	-247.82	-271.24	3.6	-112.55	-156.73	-175.33
90	90	0	4.0	-150.36	-189.15	-205.46	3.8	-92.74	-122.35	-134.82
90	90	0	4.2	-114.97	-143.25	-155.14	4.0	-72.83	-93.17	-101.74
90	90	0	5.0	-38.78	-48.68	-52.84	5.0	-18.67	-22.85	-24.61
90	90	0	9.0	-0.64	-1.03	-1.19	9.0	-0.22	-0.32	-0.36
90	90	0	15.0	-0.12	-0.12	-0.12	15.0	0.02	0.02	0.02
90	45	45	3.0	1415.68	995.73	819.16	3.0	1260.06	926.92	786.65
90	45	45	3.2	259.31	-54.81	-186.88	3.2	452.07	228.21	133.95
90	45	45	3.4	-147.62	-370.27	-463.88	3.4	94.91	-46.71	-106.35
90	45	45	3.6	-258.25	-405.65	-467.63	3.6	-47.68	-134.33	-170.82
90	45	45	3.8	-258.35	-351.56	-390.75	3.8	-92.26	-145.39	-167.76
90	45	45	4.0	-222.58	-280.90	-305.42	4.0	-95.52	-129.11	-143.25
90	45	45	4.2	-180.06	-217.39	-233.09	4.2	-84.02	-106.14	-115.46

Table 6.10: Table 6.9 continued

α	β	ϕ	$r/\text{Å}$	$10^6 u\ /E_\text{H}$ F$_2$-F$_2$			$r/\text{Å}$	$10^6 u\ /E_\text{H}$ H$_2$-F$_2$		
				pVDZ	pVTZ	pV23Z		pVDZ	pVTZ	pV23Z
90	45	45	4.4	-141.42	-166.49	-177.03	4.4	-69.19	-84.27	-90.62
90	45	45	5.0	-66.47	-76.02	-80.04	5.0	-34.53	-40.19	-42.57
90	45	45	9.0	-2.03	-2.18	-2.24	9.0	-1.00	-1.09	-1.13
90	45	45	15.0	-0.23	-0.20	-0.19	15.0	-0.04	-0.04	-0.04
45	45	45	3.6	703.39	424.76	307.61	3.0	1536.77	1251.85	1131.88
45	45	45	3.8	113.40	-89.12	-174.27	3.2	560.19	365.30	283.24
45	45	45	4.0	-85.14	-227.93	-287.97	3.4	138.73	7.30	-48.04
45	45	45	4.2	-134.25	-231.07	-271.78	3.6	-27.95	-114.36	-150.75
45	45	45	4.4	-130.08	-194.39	-221.43	3.8	-81.66	-137.45	-160.93
45	45	45	4.6	-109.84	-152.88	-170.98	4.0	-88.27	-124.17	-139.29
45	45	45	4.8	-87.44	-117.16	-129.66	4.2	-77.74	-101.09	-110.93
45	45	45	6.0	-18.36	-24.45	-27.01	5.0	-28.93	-34.19	-36.41
45	45	45	9.0	-0.89	-1.45	-1.69	6.0	-7.99	-9.24	-9.76
45	45	45	15.0	-0.12	-0.13	-0.13	15.0	0.02	0.01	0.00
90	90	45	2.6	2058.68	1433.27	1170.31	2.6	1096.04	667.26	486.72
90	90	45	2.8	492.05	29.64	-164.78	2.8	345.28	64.31	-53.99
90	90	45	3.0	-85.33	-400.63	-533.20	3.0	23.76	-151.43	-225.19
90	90	45	3.2	-261.58	-462.23	-546.59	3.2	-93.89	-201.77	-247.19
90	90	45	3.4	-281.30	-405.51	-457.73	3.4	-120.93	-188.80	-217.38
90	90	45	3.6	-246.39	-324.64	-357.54	3.6	-112.53	-156.84	-175.49
90	90	45	3.8	-198.61	-250.41	-272.19	3.8	-93.59	-123.48	-136.06
90	90	45	4.0	-154.02	-190.26	-205.50	4.0	-74.12	-94.77	-103.46
90	90	45	5.0	-40.43	-49.54	-53.37	5.0	-20.04	-24.25	-26.02
90	90	45	9.0	-0.89	-1.21	-1.34	9.0	-0.37	-0.46	-0.50
90	90	45	15.0	-0.14	-0.14	-0.14	15.0	0.00	0.00	0.00
90	45	90	3.0	1516.76	1091.11	912.14	3.0	1167.15	832.18	691.14
90	45	90	3.2	333.99	16.44	-117.08	3.2	392.89	167.47	72.56
90	45	90	3.4	-102.53	-324.38	-417.66	3.4	55.46	-87.24	-147.33
90	45	90	3.6	-234.12	-378.27	-438.88	3.6	-74.88	-162.30	-199.11
90	45	90	3.8	-246.79	-336.34	-373.99	3.8	-111.47	-165.22	-187.85
90	45	90	4.0	-217.93	-273.09	-296.28	4.0	-109.39	-143.49	-157.85
90	45	90	4.2	-179.00	-213.96	-228.66	4.2	-94.20	-116.76	-126.26
90	45	90	4.4	-142.16	-165.43	-175.21	4.4	-76.81	-92.26	-98.76
90	45	90	6.0	-22.98	-25.10	-25.99	6.0	-12.57	-14.13	-14.79
90	45	90	15.0	-0.25	-0.23	-0.22	15.0	-0.05	-0.05	-0.05
45	45	90	3.4	1535.92	1230.87	1102.61	3.0	1302.96	1011.88	889.32
45	45	90	3.6	349.40	124.03	29.27	3.2	418.89	217.25	132.34
45	45	90	3.8	-80.62	-243.68	-312.24	3.4	45.50	-90.18	-147.31
45	45	90	4.0	-207.10	-318.40	-365.20	3.6	-93.77	-182.38	-219.69
45	45	90	4.2	-219.01	-291.14	-321.47	3.8	-130.22	-187.12	-211.07

Table 6.11: Table 6.10 continued

α	β	ϕ	$r/\text{Å}$	$10^6 u$ /E_H F$_2$-F$_2$			$r/\text{Å}$	$10^6 u$ /E_H H$_2$-F$_2$		
				pVDZ	pVTZ	pV23Z		pVDZ	pVTZ	pV23Z
45	45	90	4.4	-192.67	-238.30	-257.49	4.0	-125.11	-161.67	-177.06
45	45	90	5.0	-97.49	-111.03	-116.72	5.0	-40.60	-46.09	-48.40
45	45	90	6.0	-29.46	-32.79	-34.19	6.0	-12.63	-13.95	-14.50
45	45	90	15.0	-0.22	-0.21	-0.21	15.0	-0.03	-0.03	-0.03
90	90	90	2.6	1213.39	622.63	374.24	2.6	1131.78	701.21	519.91
90	90	90	2.8	155.26	-282.02	-465.88	2.8	365.19	85.18	-32.72
90	90	90	3.0	-218.86	-513.59	-637.51	3.0	34.06	-139.66	-212.80
90	90	90	3.2	-313.59	-499.45	-577.60	3.2	-88.98	-195.93	-240.95
90	90	90	3.4	-300.68	-415.54	-463.83	3.4	-119.04	-186.59	-215.03
90	90	90	3.6	-253.00	-325.76	-356.35	3.6	-112.35	-156.70	-175.38
90	90	90	3.8	-200.62	-249.13	-269.53	3.8	-94.36	-124.45	-137.12
90	90	90	4.0	-154.72	-188.82	-203.16	4.0	-75.39	-96.26	-105.04
90	90	90	5.0	-41.59	-49.98	-53.51	5.0	-21.29	-25.64	-27.47
90	90	90	6.0	-13.33	-16.18	-17.38	6.0	-6.82	-8.09	-8.63
90	90	90	15.0	-0.17	-0.16	-0.16	15.0	-0.01	-0.01	-0.01
45	135	45	3.4	1278.50	988.09	865.99	3.0	1190.62	895.85	771.73
45	135	45	3.6	280.21	67.43	-22.03	3.2	352.03	146.78	60.36
45	135	45	3.8	-95.39	-244.21	-306.78	3.4	0.14	-136.98	-194.71
45	135	45	4.0	-210.68	-307.94	-348.83	3.6	-127.35	-216.06	-253.42
45	135	45	4.2	-222.89	-283.13	-308.46	3.8	-156.35	-212.83	-236.61
45	135	45	4.4	-198.65	-235.03	-250.33	4.0	-145.94	-182.07	-197.28
45	135	45	4.6	-165.19	-187.34	-196.65	4.2	-123.10	-146.69	-156.62
45	135	45	6.0	-34.89	-36.53	-37.22	6.0	-15.97	-17.32	-17.89
45	135	45	15.0	-0.30	-0.30	-0.30	15.0	-0.07	-0.07	-0.07
180	135	45	3.6	536.43	289.26	185.34	3.2	453.84	282.23	209.98
180	135	45	3.8	-182.98	-365.50	-442.24	3.4	32.52	-86.41	-136.49
180	135	45	4.0	-349.40	-490.75	-550.18	3.6	-118.49	-198.81	-232.63
180	135	45	4.2	-334.09	-439.45	-483.75	3.8	-153.93	-206.93	-229.25
180	135	45	4.4	-273.87	-347.76	-378.83	4.0	-144.13	-178.95	-193.61
180	135	45	4.6	-212.72	-262.29	-283.13	4.2	-120.20	-143.29	-153.01
180	135	45	4.8	-161.79	-194.75	-208.61	4.6	-73.49	-84.23	-88.75
180	135	45	6.0	-32.12	-37.77	-40.15	6.0	-12.56	-13.73	-14.22
180	135	45	15.0	-0.17	-0.18	-0.18	15.0	-0.01	-0.01	-0.01

Chapter 7

Appendix B

This appendix describes the fitting results of *ab initio* 5-site pair potential functions for the dimers H_2-H_2, H_2-O_2, F_2-F_2 and H_2-F_2.

7.1   Fitting pair potentials of dimers H_2-H_2, H_2-O_2
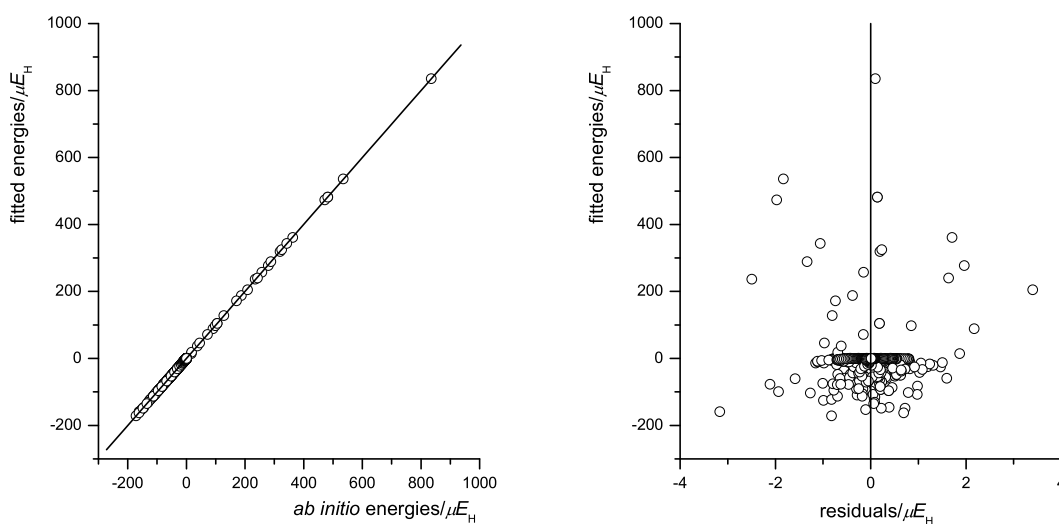
Figure 7.1: Quality of the 5-site *ab initio* analytical potential fit Eq. 3.4 for hydrogen at the theory level CCSD(T)/aug-cc-pV23Z.
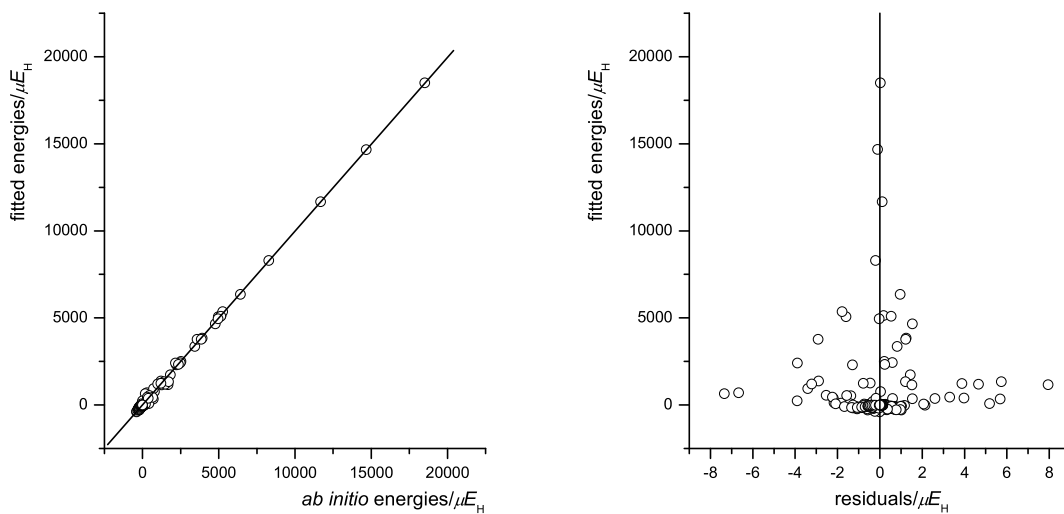
Figure 7.2: Quality of the 5-site *ab initio* analytical potential fit Eq. 3.3 for hydrogen-oxygen at the theory level CCSD(T)/aug-cc-pV23Z.
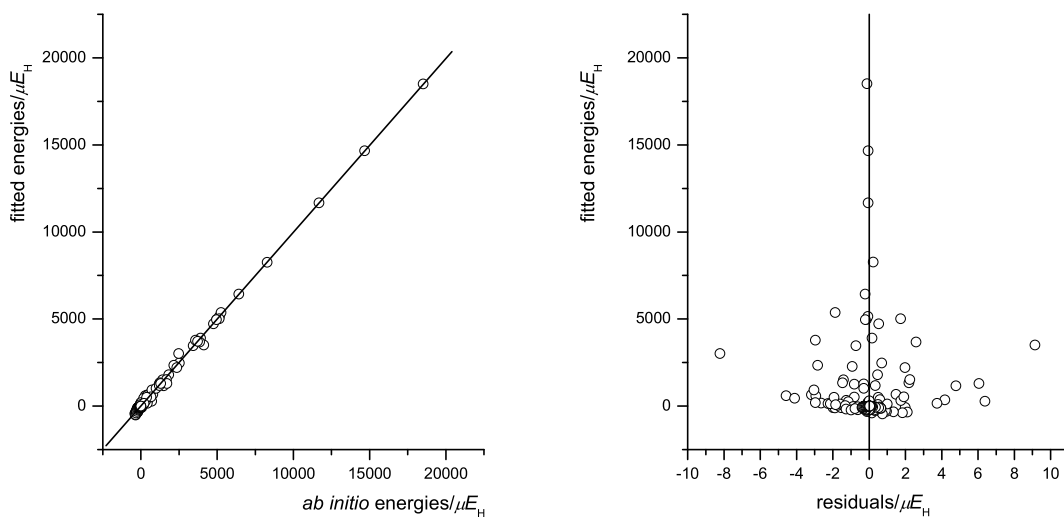

Figure 7.3: Quality of the 5-site *ab initio* analytical potential fit Eq. 3.4 for hydrogen-oxygen at the theory level CCSD(T)/aug-cc-pV23Z.

Table 7.1: Optimized parameters of the 5-site potential function Eq. 3.3 for the dimers H_2-H_2 and H_2-O_2. For all interactions $\delta_{ij} = 2.0$ Å^{-1} and $\beta = 1.0$ Å^{-1} were assumed. Partial charges: hydrogen: $q_N/e = -0.07833$, $q_H = 0$; oxygen: $q_N/e = -0.98630$; $q_M = -2q_N$. $E_H = 4.359782 \times 10^{-18}$J (Hartree energy unit).

	D_e/E_H	α/Å^{-1}	(C_6/E_H)/Å^6	(C_8/E_H)/Å^8	(C_{10}/E_H)/Å^{10}
H-H	1.0227960×10^{-1}	0.572624	1.3331335×10^1	-6.0552638×10^1	1.1426530×10^2
H-N	$-7.6904291 \times 10^{-1}$	2.833929	-4.8925193×10^1	2.2518041×10^2	-4.1995086×10^2
H-M	$-1.9218850 \times 10^{-1}$	0.571454	7.0555940×10^1	-3.2310401×10^2	6.0228738×10^2
M-M	$-4.9351615 \times 10^{-2}$	0.577347	-2.9215876×10^2	1.3811359×10^3	-2.5920488×10^3
M-N	4.1656272×10^0	3.034345	1.9573909×10^2	-9.2093494×10^2	1.7194907×10^3
N-N	5.5668718×10^{-1}	0.572581	4.4157578×10^2	-2.1135278×10^3	3.9998766×10^3
H-O	7.1344072×10^1	2.224363	4.2837184×10^1	-1.7077254×10^2	1.8833419×10^2
H-N	-8.2853629×10^2	3.063894	-4.8770389×10^2	2.5555354×10^3	-3.9233150×10^3
H-M	7.9803402×10^3	3.424206	9.2825459×10^2	-7.7164750×10^3	1.0264176×10^4
N-O	-2.4782492×10^2	2.325012	4.9110956×10^0	-1.2536655×10^2	3.6964806×10^2
N-N	3.1923965×10^2	2.376826	-2.1482107×10^2	2.6808196×10^3	-4.1720911×10^3
N-M	-4.3465863×10^3	3.615596	6.6574171×10^2	-5.8167896×10^3	1.0538800×10^4
M-O	4.0478281×10^2	2.580552	7.6550470×10^1	-1.8143994×10^2	3.2133610×10^2
M-M	-9.4272238×10^2	2.401622	-2.0533920×10^3	1.9203419×10^4	-3.1259521×10^4

Table 7.2: Optimized parameters of the 5-site potential function Eq. 3.4 for the dimers H_2-H_2 and H_2-O_2. For all interactions $\delta_{ij} = 5.0$ Å^{-1} and $\beta = 1.0$ Å^{-1} were assumed. See Table 7.1 for the partial charges.

	D_e/E_H	$\alpha/$Å^{-1}	$(C_6/E_H)/$Å^6	$(C_8/E_H)/$Å^8	$(C_{10}/E_H)/$Å^{10}	$(C_{12}/E_H)/$Å^{12}
H-H	-6.7840793 $\times$ 10^0	1.923067	4.2622953 $\times$ 10^1	-3.1534347 $\times$ 10^1	2.1629628 $\times$ 10^2	-1.6550872 $\times$ 10^2
H-N	-5.8195070 $\times$ 10^1	2.392939	-7.3078210 $\times$ 10^1	2.9865985 $\times$ 10^2	-3.5496098 $\times$ 10^2	6.2763187 $\times$ 10^2
H-M	8.1963312 $\times$ 10^1	2.150854	3.6798154 $\times$ 10^1	-2.8631558 $\times$ 10^2	-1.4576096 $\times$ 10^2	-2.1335450 $\times$ 10^2
M-M	-9.5207702 $\times$10^1	2.106373	-8.1992347 $\times$ 10^2	4.3234831 $\times$ 10^3	-1.6093781 $\times$ 10^4	2.5157521 $\times$ 10^4
M-N	1.1101172 $\times$ 10^2	2.355682	5.2084251 $\times$ 10^2	-2.4776371 $\times$ 10^3	8.0867352 $\times$ 10^3	-1.1975862 $\times$ 10^4
N-N	8.1942167 $\times$ 10^1	1.959511	1.4635001 $\times$ 10^3	-8.5495684 $\times$ 10^3	3.5233328 $\times$ 10^4	-5.7733649 $\times$ 10^4
H-O	8.0308925 $\times$ 10^2	2.544218	-2.4132460 $\times$ 10^2	-6.7476151 $\times$ 10^2	-5.0921066 $\times$ 10^3	2.8012113 $\times$ 10^3
H-N	-2.4427742 $\times$ 10^4	3.971425	6.4791331 $\times$ 10^2	-1.0353963 $\times$ 10^4	5.6572612 $\times$ 10^4	-3.3143922 $\times$ 10^4
H-M	9.7726177 $\times$ 10^4	3.889565	-1.0595428 $\times$ 10^3	2.3569137 $\times$ 10^4	-1.9681587 $\times$ 10^5	9.8966862 $\times$ 10^4
N-O	-3.7381800 $\times$ 10^3	2.600285	5.7004391 $\times$ 10^2	7.7424748 $\times$ 10^3	6.1319897 $\times$ 10^3	7.7395300 $\times$ 10^3
N-N	2.7755945 $\times$ 10^3	2.897540	-6.9532173 $\times$ 10^2	-7.3659667 $\times$ 10^2	6.7221266 $\times$ 10^3	-3.0543881 $\times$ 10^4
N-M	-2.5348859 $\times$ 10^4	3.751627	8.3082816 $\times$ 10^2	7.7658214 $\times$ 10^3	-7.0829484 $\times$ 10^3	8.5697641 $\times$ 10^4
M-O	4.9501410 $\times$ 10^3	2.596322	-7.9205831 $\times$ 10^2	-1.0988081 $\times$ 10^4	-4.7931859 $\times$ 10^3	-1.4496810 $\times$ 10^4
M-M	-5.6542124 $\times$ 10^3	2.820828	-7.4164112 $\times$ 10^2	-1.2615712 $\times$ 10^4	1.8484688 $\times$ 10^5	-3.0812949 $\times$ 10^5

## 7.2 Fitting pair potentials of dimers F_2-F_2, H_2-F_2
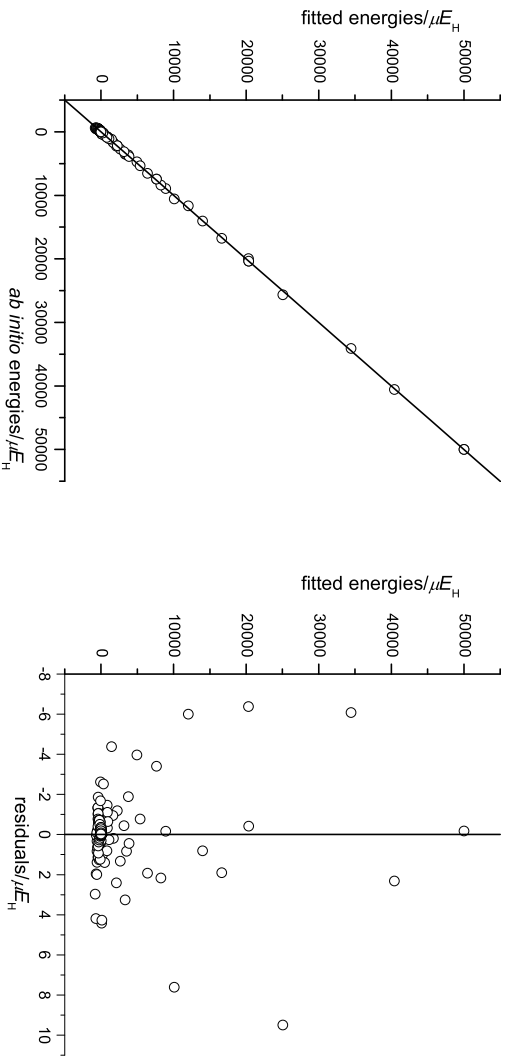
Figure 7.4: Quality of the 5-site *ab initio* analytical potential fit Eq. 3.6 for fluorine at the theory level CCSD(T)/aug-cc-pV23Z.
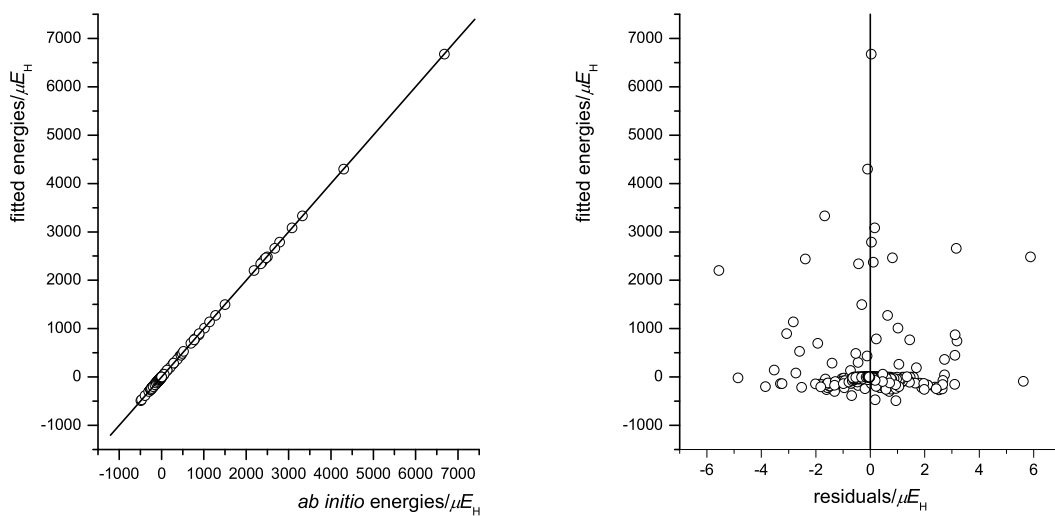
Figure 7.5: Quality of the 5-site *ab initio* analytical potential fit Eq. 3.5 for hydrogen-fluorine at the theory level CCSD(T)/aug-cc-pV23Z.
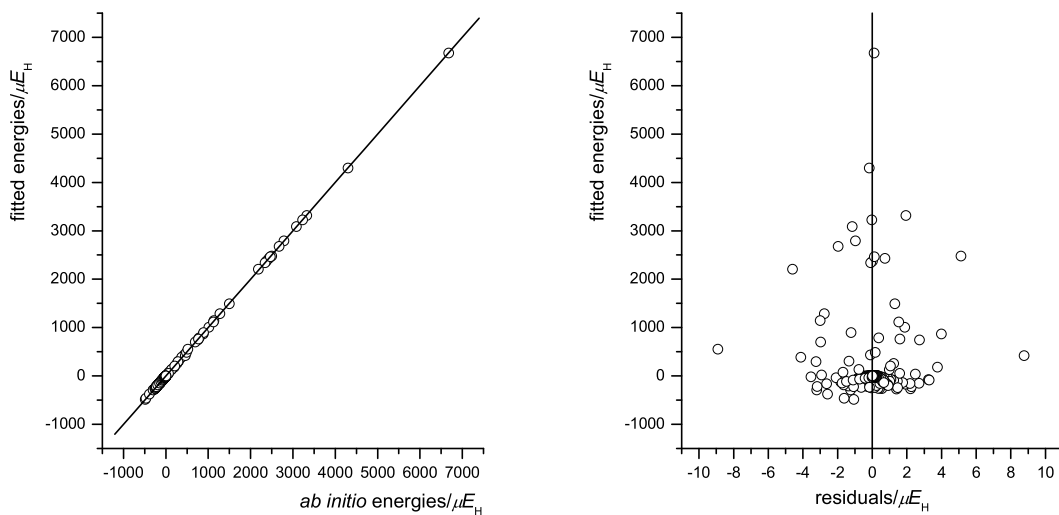

Figure 7.6: Quality of the 5-site *ab initio* analytical potential fit Eq. 3.6 for hydrogen-fluorine at the theory level CCSD(T)/aug-cc-pV23Z.

Table 7.3: Optimized parameters of the 5-site potential function Eq. 3.5 for the dimers F_2-F_2 and H_2-F_2. For all interactions $\delta_{ij} = 2.0$ Å^{-1} was assumed. Partial charges: hydrogen: q_N/e = -0.078329, $q_H = 0$; fluorine: q_N/e = -0.781897132, $q_F = 0$; $q_M = -2q_N$. $E_H = 4.359782 \times 10^{-18}$J (Hartree energy unit).

	D_e/E_H	α/Å^{-1}	β/Å^{-1}	(C_6/E_H)Å^6	(C_8/E_H)Å^8	(C_{10}/E_H)Å^{10}
F-F	4.5974720×10^0	5.278793	1.617556	6.9533045×10^1	-7.8174045×10^2	3.8360409×10^3
F-N	-9.0747157×10^2	5.019366	0.652754	-1.2637218×10^2	1.1234232×10^3	-6.1458463×10^3
F-M	6.6992723×10^1	5.019574	1.245679	1.4521977×10^2	-1.3652884×10^3	8.3442391×10^3
M-M	1.5869262×10^2	3.483313	0.434485	1.5231052×10^1	-1.5841515×10^3	3.6390746×10^3
M-N	-7.6586901×10^1	5.252010	0.688880	5.0245981×10^1	1.0743838×10^3	-2.1705318×10^3
N-N	-3.4793023×10^2	3.431624	0.558077	-1.1051724×10^2	1.6178480×10^3	-5.3087935×10^3
H-F	-1.2998526×10^0	1.359765	-0.081002	-2.5762236×10^0	1.4264490×10^1	-3.5028153×10^1
H-N	$-5.6494975 \times 10^{-2}$	1.286156	-5.148780	-7.1318146×10^1	3.7611779×10^2	-6.5142385×10^2
H-M	2.7802594×10^0	1.070086	-2.073589	1.0897255×10^2	-6.4494812×10^2	1.1979607×10^3
N-F	2.0745652×10^1	1.400898	-1.051550	5.3696452×10^1	-2.5941110×10^2	5.3928707×10^2
N-N	3.1915920×10^1	1.951238	-0.688997	1.7431585×10^2	-9.4371444×10^2	1.5560964×10^3
N-M	-1.6196579×10^1	1.978559	-0.342494	-1.2215049×10^2	7.7225795×10^2	-1.0487256×10^3
M-F	-1.5630681×10^1	1.437144	-0.489872	-1.0978703×10^2	5.2659459×10^2	-1.0794681×10^3
M-M	-4.2454722×10^0	1.095669	-1.479315	-1.2777729×10^2	4.2169046×10^2	-1.6846562×10^3

Table 7.4: Optimized parameters of the 5-site potential function Eq. 3.6 for the dimers F_2-F_2 and H_2-F_2. For all interactions $\delta_{ij} = 5.0$ Å^{-1} was assumed. See Table 7.3 for the partial charges.

	D_e/E_H	$\alpha/$Å^{-1}	$\beta/$Å^{-1}	(C_6/E_H)Å^6	(C_8/E_H)Å^8	(C_{10}/E_H)Å^{10}	(C_{12}/E_H)Å^{12}
F-F	8.8171786×10^2	3.244041	0.077961	-6.2157865×10^1	1.2321451×10^3	5.4513393×10^3	-1.2697245×10^3
F-N	-1.1827787×10^2	3.159481	0.921714	1.3397431×10^2	-3.3368060×10^3	-1.1509838×10^4	6.9397783×10^3
F-M	3.1679473×10^2	3.119872	0.670539	-1.9821670×10^2	4.9441767×10^3	1.1566430×10^4	-3.8524907×10^3
M-M	6.7764210×10^1	2.580436	-0.261325	-5.8754971×10^2	6.4076016×10^3	-5.0988435×10^4	1.0700619×10^5
M-N	6.8749639×10^2	3.241169	0.330852	2.8958183×10^2	-1.9917828×10^3	4.2916608×10^4	-7.1733704×10^4
N-N	-2.9343556×10^2	3.121165	0.803472	1.1596520×10^3	-1.5773995×10^4	6.3144928×10^4	-1.6208326×10^5
H-F	3.0463804×10^1	2.520069	-0.224604	5.0474996×10^1	-2.7938515×10^1	3.6422180×10^2	-2.1159364×10^2
H-N	-2.7806721×10^1	2.269005	-0.042749	-1.7030307×10^2	3.3526431×10^2	-1.5002802×10^3	1.5374112×10^3
H-M	6.5239690×10^1	2.938248	0.279555	1.4483963×10^2	-1.2399348×10^2	2.0678809×10^3	-2.1851258×10^3
N-F	4.2020099×10^1	2.054421	-0.487799	-5.8550342×10^1	3.1625056×10^2	-2.1594953×10^2	2.5251962×10^2
N-N	5.1162888×10^1	2.141455	-0.254528	3.1633506×10^2	-2.6568174×10^2	-2.2587158×10^2	1.4039026×10^3
N-M	-4.4667507×10^1	2.852174	0.128157	-1.9092711×10^2	-6.6195414×10^2	5.2222878×10^3	-8.6454961×10^3
M-F	-2.4889589×10^1	2.104182	0.313304	-8.1709626×10^0	-4.3286727×10^2	-5.4342203×10^2	4.2248237×10^2
M-M	-2.5535101×10^1	1.980672	-0.033874	-6.1411549×10^1	2.2612488×10^3	-1.6238287×10^4	2.4340458×10^4

Chapter 8

Appendix C

This appendix describes the results of second virial coefficient calculations for the dimers H_2-H_2, H_2-O_2, F_2-F_2 and H_2-F_2.

8.1 Virial coefficients of dimers H_2-H_2, H_2-O_2

Table 8.1: Second virial coefficients, B_{el}^0 of hydrogen (given in cm^3/mol) calculated from pair potentials at the level CCSD(T)/aug-cc-pVmZ (m = 2, 3, 4, 23).

T/K	method	aug-cc-pVDZ	aug-cc-pVTZ	aug-cc-pVQZ	aug-cc-pV23Z
60	Eq. 3.3	-6.4360	-17.4870	-18.1200	-23.6538
	Eq. 3.4	-9.2330	-18.0600	-18.0720	-23.1345
70	Eq. 3.3	-0.6200	-10.3070	-10.9220	-15.1003
	Eq. 3.4	-3.5350	-11.2800	-11.3900	-14.6678
80	Eq. 3.3	3.5210	-5.1820	-5.7840	-9.4397
	Eq. 3.4	0.5270	-4.5250	-6.6210	-8.9468
90	Eq. 3.3	6.5930	-1.3640	-1.9550	-5.3277
	Eq. 3.4	3.5350	-2.8520	-3.0680	-4.8632
100	Eq. 3.3	8.9450	1.5740	0.9940	-2.1366
	Eq. 3.4	5.8360	-0.0900	-0.3360	-1.7990
150	Eq. 3.3	15.2640	9.6160	9.0761	7.1616
	Eq. 3.4	11.9980	7.4340	7.1220	6.5967
200	Eq. 3.3	17.6320	13.0130	12.5020	11.1852
	Eq. 3.4	14.4520	10.5760	10.2520	10.2296
400	Eq. 3.3	19.9440	16.4280	15.9480	14.2686
	Eq. 3.4	16.3820	13.6950	13.3900	13.3268

Table 8.2: Second virial coefficients of hydrogen as a function of temperature (given in cm^3/mol). B_{cl}^0: classical result obtained from pair potentials; B_r^1, $B_{a,I}^1$, $B_{a,\mu}^1$: quantum corrections; B: total virial coefficient; Sph.harm: *ab initio* prediction of Diep and Johnson [25, 26] and Etters et al. [32]; exp.: experimental data.

T/K	Method	$B_{cl}^{(0)}$	$B_r^{(1)}$	$B_{a,I}^{(1)}$	$B_{a,\mu}^{(1)}$	B	ref.
	Eq. 3.3	-23.65376	0.33886	0.23818	0.08891	-22.98781	
60.0	Eq. 3.4	-23.13453	0.44618	0.16819	0.10622	-22.41395	
	Sph.harm					-21.3	[32]
	Exp.					-24.0	[66]
	Eq. 3.3	-15.10032	0.82164	0.21554	0.06926	-13.99389	
70.0	Eq. 3.4	-14.66783	0.64801	0.03147	0.01434	-13.97401	
	Sph.harm					-14.11	[32]
	Exp.					-16.0	[66]
	Eq. 3.3	-12.01632	0.46978	0.14782	0.04058	-11.35814	
75.0	Eq. 3.4	-11.54848	0.34957	0.11663	0.02498	-11.05729	
	Sph.harm					-11.93840	[25]
	Exp.					-12.0	[66]
	Eq. 3.3	-9.43967	0.10774	0.04736	0.00877	-9.27580	
80.0	Eq. 3.4	-8.94676	0.16611	0.11432	0.05549	-8.61084	
	Sph.harm					-8.94	[32]
	Exp.					-11.0	[66]
	Eq. 3.3	-5.32774	0.24869	0.03753	0.02708	-5.01445	
90.0	Eq. 3.4	-4.86315	0.09058	0.04461	0.04257	-4.68539	
	Sph.harm					-5.04	[32]
	Exp.					-7.0	[66]
	Eq. 3.3	-2.13663	1.00789	0.30780	0.03499	-0.78595	
100.0	Eq. 3.4	-1.79898	0.95604	0.25957	0.02334	-0.56002	
	Sph.harm					-1.20776	[26]
	Exp.					-1.9±1.0	[28]
	Eq. 3.3	7.16159	0.46291	0.19352	0.05909	7.87712	
150.0	Eq. 3.4	6.59670	0.58708	0.22251	0.07541	7.48170	
	Sph.harm					7.61891	[26]
	Exp.					7.1±0.5	[28]
	Eq. 3.3	11.18517	0.21872	0.08462	0.02026	11.50877	
200.0	Eq. 3.4	10.22962	0.66563	0.19718	0.05211	11.14455	
	Sph.harm					11.52550	[26]
	Exp.					11.3±0.5	[28]
	Eq. 3.3	13.76118	0.37335	0.24436	0.00739	14.38629	
300.0	Eq. 3.4	12.75553	1.24404	0.44549	0.04092	14.48598	
	Sph.harm					14.78800	[26]
	Exp.					14.8±0.5	[28]
	Eq. 3.3	14.26859	0.89985	0.42168	0.03695	15.62707	
400.0	Eq. 3.4	13.32682	1.53453	0.61004	0.06834	15.53973	
	Sph.harm					15.96840	[26]
	Exp.					15.2±0.5	[28]

Table 8.3: Cross second virial coefficient (given in cm^3/mol) of the mixture hydrogen–oxygen; correl.: empirical correlation [30]; exp.: experimental data. For an explanation of the other properties see Table 8.2.

T/K	method	$B^{(0)}$	$B_r^{(1)}$	$B_{a,I}^{(1)}$	$B_{a\mu}^{(1)}$	B	ref.
49.8	Eq. 3.3	-138.33772	0.26696	0.19886	0.01531	-137.85659	
	Eq. 3.4	-136.92058	0.05736	0.03702	0.02815	-136.79804	
	correl.					-142.09728	
	exp.					-110.0	[77]
60.0	Eq. 3.3	-100.68668	0.20949	0.10404	0.04190	-100.33125	
	Eq. 3.4	-99.64381	0.02042	0.01906	0.00957	-99.59477	
	correl.					-106.39316	
80.0	Eq. 3.3	-61.87517	0.28309	0.22841	0.05662	-61.30705	
	Eq. 3.4	-60.90565	0.08494	0.03695	0.03241	-60.75136	
	correl.					-63.88700	
	exp.					-72.9	[124]
85.0	Eq. 3.3	-55.74469	0.40514	0.38766	0.07753	-54.87436	
	Eq. 3.4	-54.67789	0.32468	0.07273	0.05714	-54.22335	
	correl.					-56.80610	
	exp.					-54.0	[124]
86.5	Eq. 3.3	-54.07285	0.31435	0.17659	0.04671	-53.53520	
	Eq. 3.4	-52.97568	0.12753	0.07273	0.01429	-52.76113	
	correl.					-54.88163	
	interpolation					-58.1	Eq. (4.6)
90.0	Eq. 3.3	-50.42771	0.35160	0.34420	0.07032	-49.66159	
	Eq. 3.4	-49.26103	0.19092	0.05388	0.04550	-48.97073	
	correl.					-50.66400	
	exp.					-32.5	[124]
100.0	Eq. 3.3	-41.60513	0.42705	0.40062	0.08012	-40.69733	
	Eq. 3.4	-40.27439	0.29924	0.06562	0.05491	-39.85462	
	correl.					-40.59072	
150.0	Eq. 3.3	-15.83443	0.44923	0.41374	0.08275	-14.88871	
	Eq. 3.4	-14.58003	0.34345	0.07797	0.05879	-14.09982	
	correl.					-13.80439	
200.0	Eq. 3.3	-3.64660	0.42646	0.40027	0.08005	-2.73982	
	Eq. 3.4	-2.74036	0.32290	0.07223	0.05699	-2.28824	
	correl.					-2.78858	
273.15	Eq. 3.3	4.25375	0.40567	0.38797	0.07759	5.12497	
	Eq. 3.4	5.03061	0.30245	0.06652	0.05519	5.45477	
	correl.					4.65614	
400.0	Eq. 3.3	8.11890	0.44770	0.25992	0.08169	8.90821	
	Eq. 3.4	8.98165	0.34470	0.07832	0.05890	9.46358	
	correl.					9.93124	

8.2 Virial coefficients of dimers F_2-F_2, H_2-F_2

Table 8.4: Second virial coefficients, B_{cl}^0 of fluorine (given in cm^3/mol) calculated from pair potentials at the level CCSD(T)/aug-cc-pVmZ ($m = 2, 3, 23$).

T/K	method	aug-cc-pVDZ	aug-cc-pVTZ	aug-cc-pV23Z	exp.	ref.
90.0	Eq. 3.5	-78.3858	-135.459	-191.1797	-208.70	[17]
	Eq. 3.6	-79.4597	-137.5410	-173.0646		
100.0	Eq. 3.5	-63.4378	-111.381	-156.0938	-156.0	[28]
	Eq. 3.6	-64.3069	-113.0929	-142.0271		
110.0	Eq. 3.5	-51.8488	-93.2073	-129.9349	-134.30	[17]
	Eq. 3.6	-52.5591	-94.6399	-119.0659		
125.0	Eq. 3.5	-38.6615	-73.0314	-101.5889	-101.80	[17]
	Eq. 3.6	-39.1912	-74.1539	-94.2294		
140.0	Eq. 3.5	-28.8293	-58.3204	-81.4776	-81.50	[28]
	Eq. 3.6	-29.2243	-59.2168	-76.5069		
145.0	Eq. 3.5	-26.0883	-54.2675	-76.0106	-75.90	[28]
	Eq. 3.6	-26.4457	-55.1016	-71.6566		
150.0	Eq. 3.5	-23.5639	-50.5525	-71.0214	-70.90	[28]
	Eq. 3.6	-23.8867	-51.3295	-67.2143		
165.0	Eq. 3.5	-17.0652	-41.0644	-58.3449	-55.700	[17]
	Eq. 3.6	-17.2990	-41.6956	-55.8495		
200.0	Eq. 3.5	-6.2481	-25.4901	-37.6058	-35.900	[17]
	Eq. 3.6	-6.3337	-25.8819	-37.0192		
230.0	Eq. 3.5	0.0347	-16.5473	-25.7783	-25.100	[17]
	Eq. 3.6	0.0352	-16.8016	-26.2051		
250.0	Eq. 3.5	3.2611	-11.9754	-19.8561	-19.700	[17]
	Eq. 3.6	3.3058	-12.1595	-20.7978		
260.0	Eq. 3.5	4.6587	-9.9978	-17.3484	-17.300	[17]
	Eq. 3.6	4.7225	-10.1515	-18.5141		
300.0	Eq. 3.5	9.1755	-3.6096	-9.6341	-9.700	[17]
	Eq. 3.6	9.3012	-3.6650	-11.5282		

Table 8.5: Second virial coefficients of fluorine (given in cm^3/mol). D1 EOS.: Deiters equation of state [18]. For an explanation of the other properties see Table 8.2.

T/K	method	B_{cl}^0	B_r^1	B_a^1	$B_{\mu a}^1$	B	ref.
	Eq. 3.5	-191.17969	0.18516	0.02538	0.00239	-190.96676	
90.0	Eq. 3.6	-173.06457	0.14564	0.05156	0.00325	-172.86412	
	D1 EOS					-191.50	
	exp.					-208.7	[17]
	Eq. 3.5	-156.09376	0.16025	0.03518	0.00251	-155.89582	
100.0	Eq. 3.6	-142.02710	0.15576	0.02341	0.01064	-141.83729	
	D1 EOS					-154.13	
	exp.					-156	[28]
	Eq. 3.5	-129.93488	0.14767	0.01764	0.00198	-129.76759	
110.0	Eq. 3.6	-119.06590	0.13545	0.02680	0.00749	-118.89616	
	D1 EOS					-126.88	
	exp.					-134.3	[17]
	Eq. 3.5	-101.58895	0.54453	0.05442	0.00301	-100.98699	
125.0	Eq. 3.6	-94.22943	0.26773	0.03244	0.00212	-93.92714	
	D1 EOS					-97.684	
	exp.					-101.8	[17]
	Eq. 3.5	-81.47758	0.79348	0.08608	0.00124	-80.59678	
140.0	Eq. 3.6	-76.50689	0.19292	0.04030	0.00237	-76.27129	
	D1 EOS					-77.164	
	exp.					-81.5	[28]
	Eq. 3.5	-71.02139	0.60294	0.06077	0.00299	-70.35468	
150.0	Eq. 3.6	-67.21430	0.67348	0.04438	0.00554	-66.49090	
	D1 EOS					-66.603	
	exp.					-70.9	[28]
	Eq. 3.5	-58.34490	0.84495	0.06283	0.00926	-57.42787	
165.0	Eq. 3.6	-55.84945	0.18875	0.04876	0.00275	-55.60919	
	D1 EOS					-53.971	
	exp.					-55.7	[17]
	Eq. 3.5	-37.60579	0.81083	0.02856	0.00183	-36.76456	
200.0	Eq. 3.6	-37.01920	0.59788	0.01826	0.00137	-36.40170	
	D1 EOS					-33.878	
	exp.					-35.9	[17]
	Eq. 3.5	-19.85605	0.13516	0.06470	0.00258	-19.65362	
250.0	Eq. 3.6	-20.79783	0.31533	0.05762	0.00226	-20.42263	
	D1 EOS					-17.068	
	exp.					-19.7	[17]
	Eq. 3.5	-9.63409	0.28788	0.07426	0.00247	-9.26948	
300.0	Eq. 3.6	-11.52820	0.63636	0.02146	0.00119	-10.86919	
	D1 EOS					-10.93136	
	exp.					-9.7	[17]

Table 8.6: Cross second virial coefficient (given in cm^3/mol) of the mixture hydrogen-fluorine; correl.: empirical correlation [30]. For an explanation of the other properties see Table 8.2.

T/K	method	B_{cl}^0	B_r^1	B_a^1	$B_{\mu a}^1$	B
	Eq. 3.5	-127.16061	0.25665	0.04059	0.00936	-126.85402
50.0	Eq. 3.6	-130.27400	0.25984	0.02854	0.00122	-129.98440
	correl.					-129.68653
	Eq. 3.5	-94.37193	0.94286	0.03580	0.00627	-93.38700
60.0	Eq. 3.6	-95.57771	0.65438	0.03717	0.00892	-94.87724
	correl.					-96.13747
	Eq. 3.5	-72.52409	0.73608	0.07981	0.00454	-71.70367
70.0	Eq. 3.6	-73.42758	0.75490	0.06559	0.00257	-72.60452
	correl.					-73.03982
	Eq. 3.5	-57.36159	0.84995	0.05766	0.00717	-56.44682
80.0	Eq. 3.6	-58.22628	0.59290	0.07121	0.00512	-57.55704
	correl.					-56.59350
	Eq. 3.5	-46.37209	0.84180	0.09613	0.00919	-45.42496
90.0	Eq. 3.6	-47.30293	0.85496	0.07564	0.00716	-46.36517
	correl.					-44.48640
	Eq. 3.5	-38.06140	0.92346	0.09564	0.00734	-37.03496
100.0	Eq. 3.6	-39.09347	0.81835	0.09038	0.00654	-38.17820
	correl.					-35.30930
	Eq. 3.5	-31.53132	2.17599	0.04835	0.00289	-29.30408
110.0	Eq. 3.6	-32.67128	2.13952	0.09574	0.00619	-30.42984
	correl.					-28.17736
	Eq. 3.5	-26.23363	2.29254	0.07961	0.00268	-23.85880
120.0	Eq. 3.6	-27.47822	2.09754	0.09299	0.00146	-25.28623
	correl.					-22.51585
	Eq. 3.5	-14.88313	2.79728	0.08713	0.00214	-11.99658
150.0	Eq. 3.6	-16.40953	2.88428	0.04793	0.00245	-13.47487
	correl.					-11.05352
	Eq. 3.5	-9.67362	2.32415	0.08126	0.00876	-7.25945
170.0	Eq. 3.6	-11.36799	2.89699	0.08965	0.00436	-8.37699
	correl.					-6.17663
	Eq. 3.5	-4.02889	2.29647	0.08819	0.00190	-1.64233
200.0	Eq. 3.6	-5.95276	2.83244	0.07572	0.00351	-3.04110
	correl.					-1.12520
	Eq. 3.5	1.72024	1.58046	0.04442	0.00192	3.34704
250.0	Eq. 3.6	-0.52143	2.66320	0.07062	0.00372	2.21611
	correl.					3.99524
	Eq. 3.5	4.81646	1.74384	0.07652	0.00842	6.64525
300.0	Eq. 3.6	2.34253	3.06065	0.09833	0.00733	5.50883
	correl.					7.01982

Chapter 9

Appendix D

This appendix describes the simulation results of the pure fluid hydrogen using global Gibbs ensemble simulations.

9.1   pVT data of fluid hydrogen
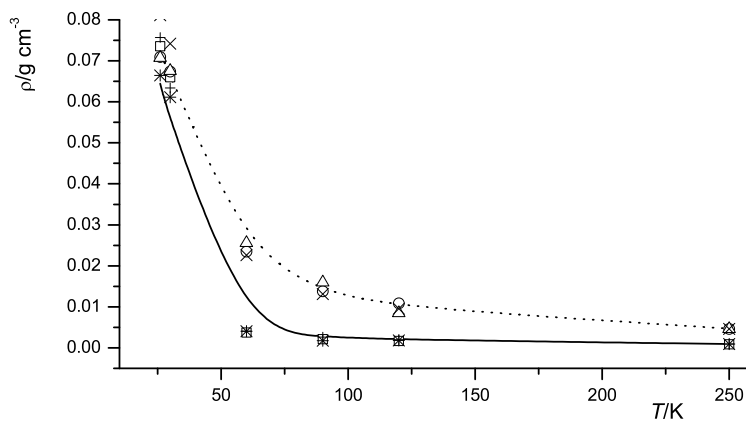
Figure 9.1: Densities of hydrogen at two pressures 1.0 MPa and 5.0 MPa as a function of temperature. Experimental data [76, 75]: —, at 1.0 MPa, and $\cdots$, at 5.0 MPa; equation of state (EOS) [139]: +, at 1.0 MPa, and ×, at 5.0 MPa; calculated with Eq. 3.3 and Eq. 3.4: □, and ∗, at 1.0 MPa; ∘, and △, at 5.0 MPa.

9.2   Site-site pair distribution functions
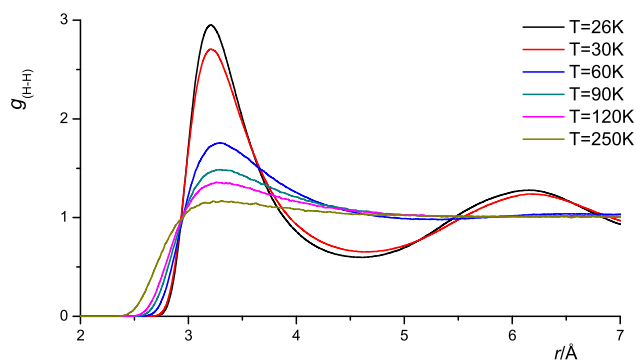
Figure 9.2: Temperature dependence of g_{H-H} for hydrogen at $P = 1.0$ MPa from GEMC NPT simulation using the pair potential Eq. 3.3.
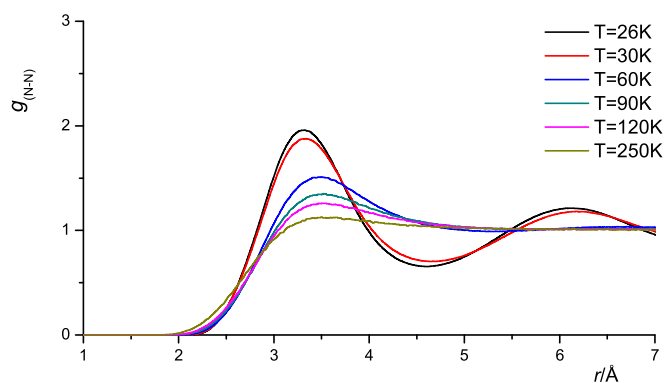

Figure 9.3: Temperature dependence of g_{N-N} for hydrogen at $P = 1.0$ MPa from GEMC NPT simulation using the pair potential Eq. 3.3.
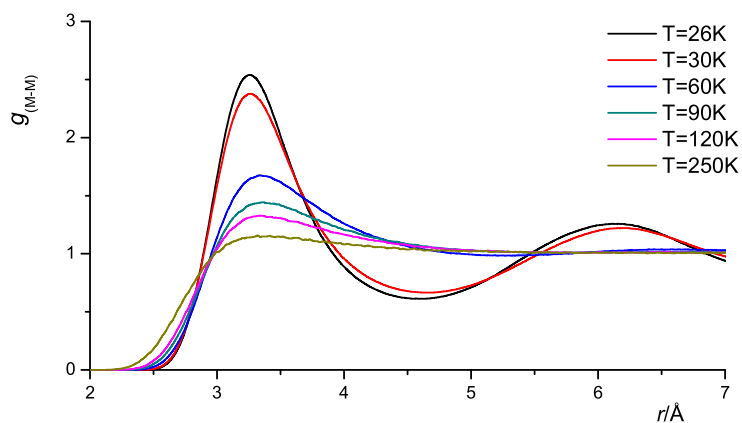
Figure 9.4: Temperature dependence of g_{M-M} for hydrogen at $P = 1.0$ MPa from GEMC NPT simulation using the pair potential Eq. 3.3.
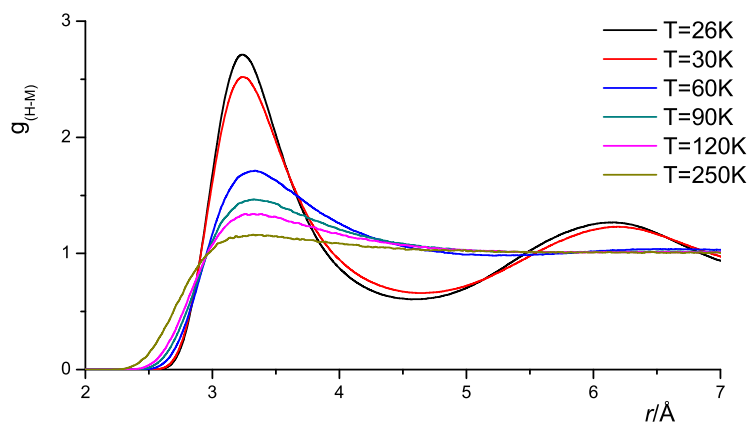
Figure 9.5: Temperature dependence of g_{H-M} for hydrogen at $P = 1.0$ MPa from GEMC NPT simulation using the pair potential Eq. 3.3.
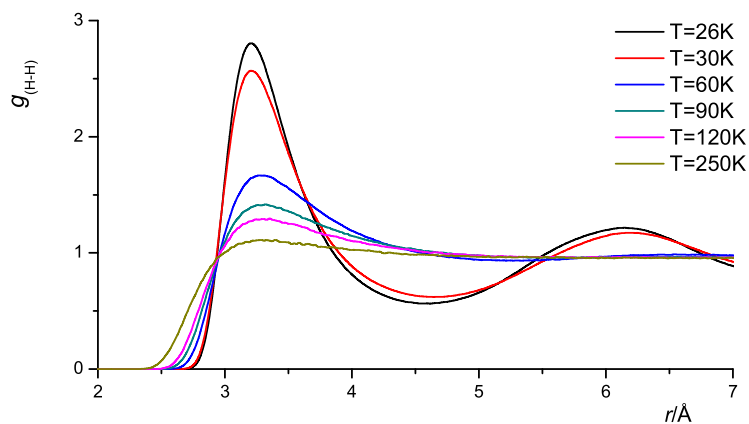
Figure 9.6: Temperature dependence of g_{H-H} for hydrogen at $P = 5.0$ MPa from GEMC NPT simulation using the pair potential Eq. 3.3.
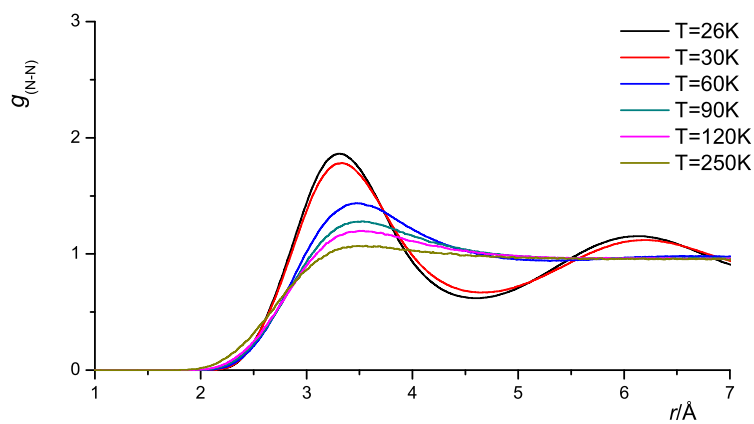
Figure 9.7: Temperature dependence of g_{N-N} for hydrogen at $P = 5.0$ MPa from GEMC NPT simulation using the pair potential Eq. 3.3.
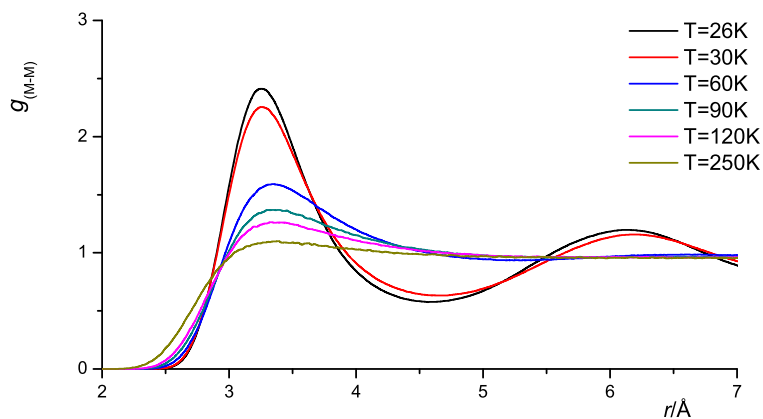
Figure 9.8: Temperature dependence of g_{M-M} for hydrogen at $P = 5.0$ MPa from GEMC NPT simulation using the pair potential Eq. 3.3.
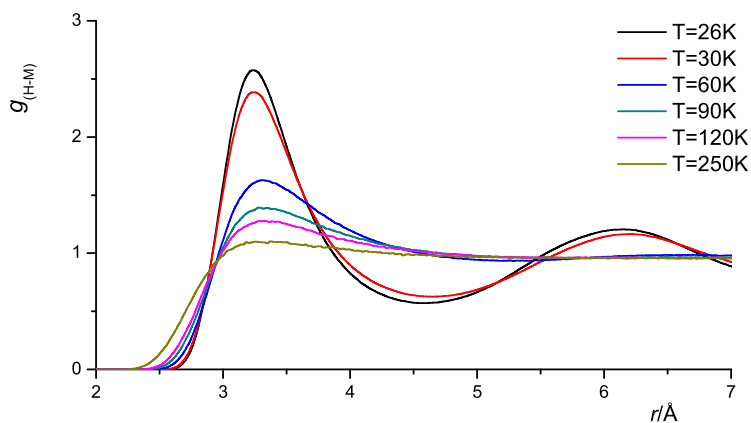

Figure 9.9: Temperature dependence of g_{H-M} for hydrogen at $P = 5.0$ MPa from GEMC NPT simulation using the pair potential Eq. 3.3.
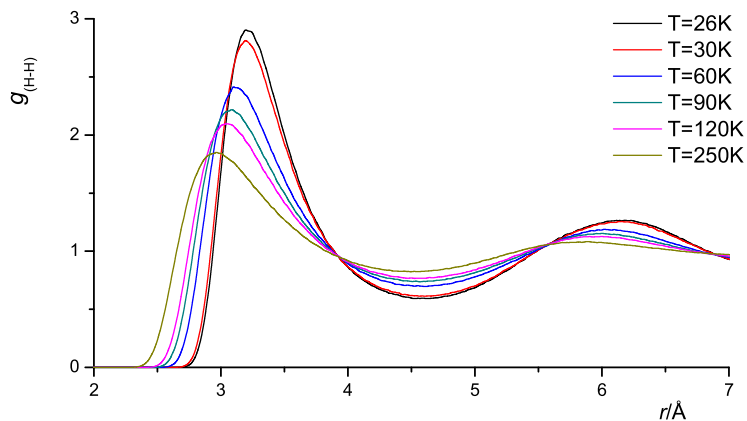
Figure 9.10: Temperature dependence of $g_{\mathrm{H-H}}$ for hydrogen at $P = 1.0$ MPa from GEMC NPT simulation using the pair potential Eq. 3.4.
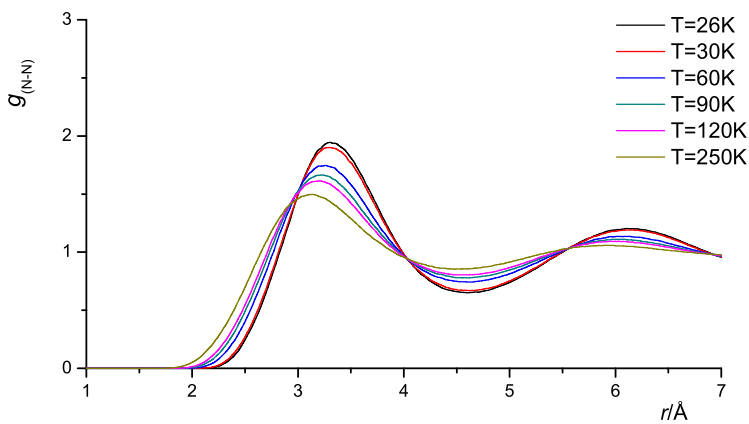

Figure 9.11: Temperature dependence of $g_{\mathrm{N-N}}$ for hydrogen at $P = 1.0$ MPa from GEMC NPT simulation using the pair potential Eq. 3.4.
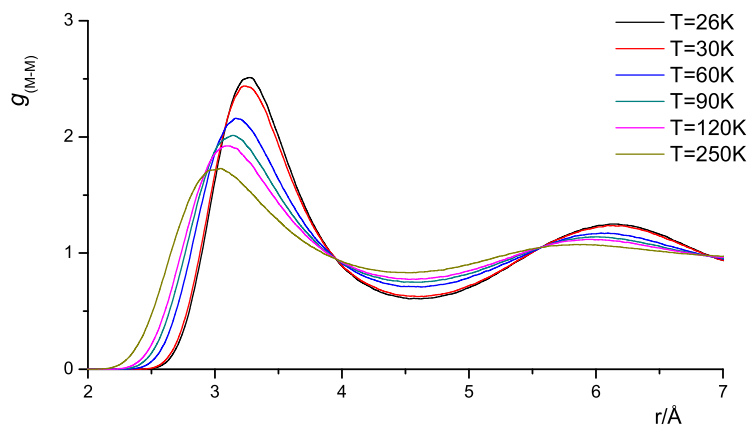
Figure 9.12: Temperature dependence of $g_{\mathrm{M-M}}$ for hydrogen at $P = 1.0$ MPa from GEMC NPT simulation using the pair potential Eq. 3.4.
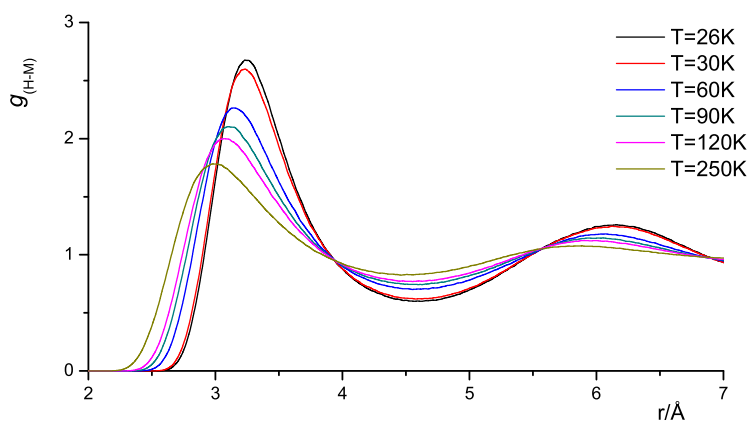
Figure 9.13: Temperature dependence of $g_{\mathrm{H-M}}$ for hydrogen at $P = 1.0$ MPa from GEMC NPT simulation using the pair potential Eq. 3.4.
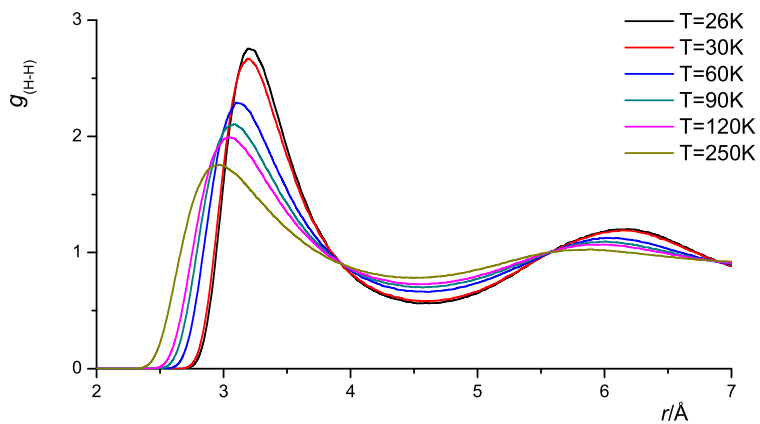
Figure 9.14: Temperature dependence of $g_{\mathrm{H-H}}$ for hydrogen at $P = 5.0$ MPa from GEMC NPT simulation using the pair potential Eq. 3.4.
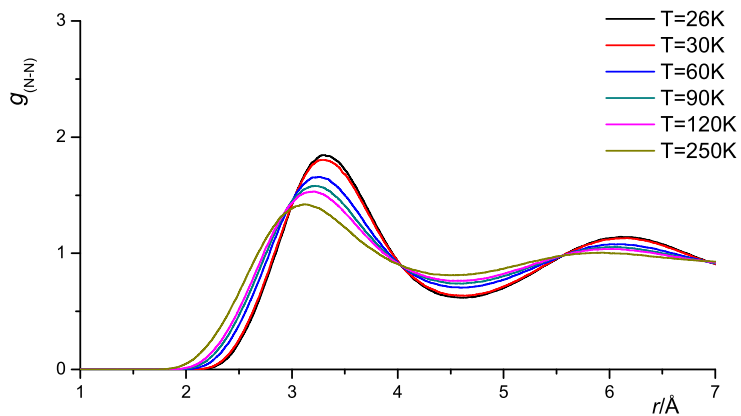
Figure 9.15: Temperature dependence of $g_{\mathrm{N-N}}$ for hydrogen at $P = 5.0$ MPa from GEMC NPT simulation using the pair potential Eq. 3.4.
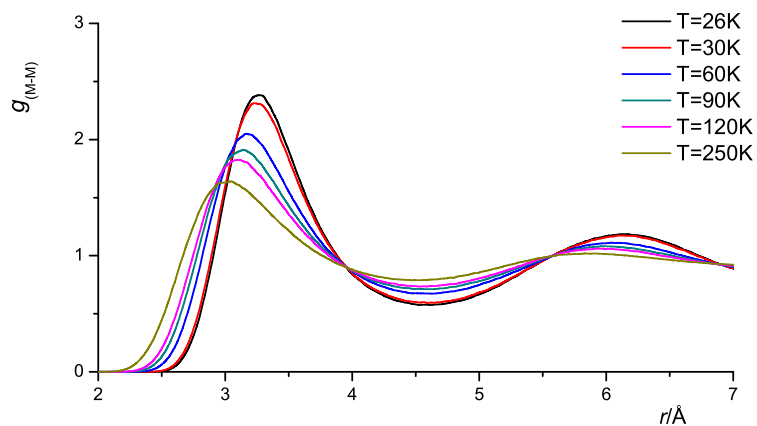
Figure 9.16: Temperature dependence of $g_{\mathrm{M-M}}$ for hydrogen at $P = 5.0$ MPa from GEMC NPT simulation using the pair potential Eq. 3.4.
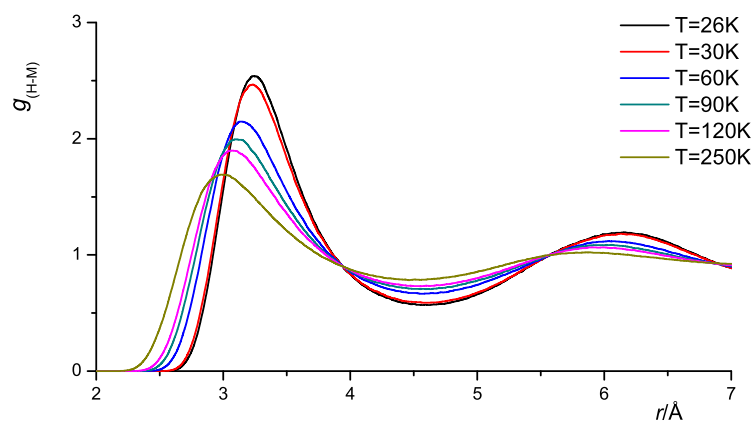

Figure 9.17: Temperature dependence of $g_{\mathrm{H-M}}$ for hydrogen at $P = 5.0$ MPa from GEMC NPT simulation using the pair potential Eq. 3.4.
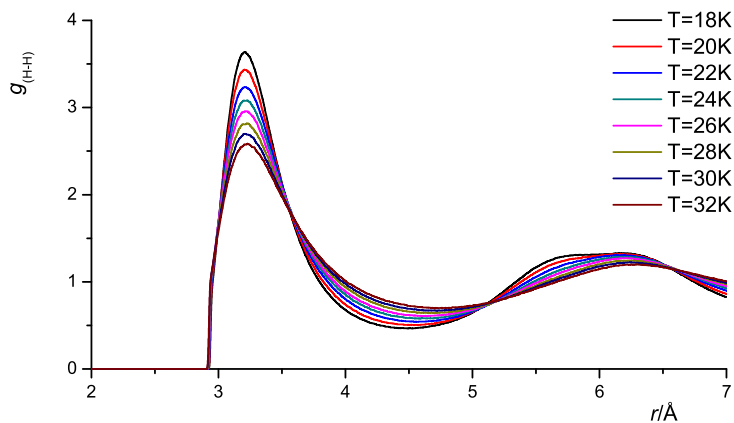
Figure 9.18: Temperature dependence of g_{H-H} for the liquid phase hydrogen from GEMC NVT simulation using pair potential Eq. 3.3.
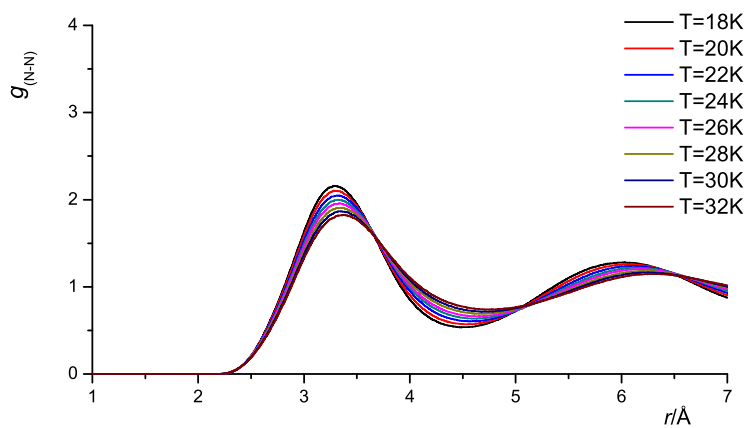
Figure 9.19: Temperature dependence of g_{N-N} for the liquid phase hydrogen from GEMC NVT simulation using pair potential Eq. 3.3.
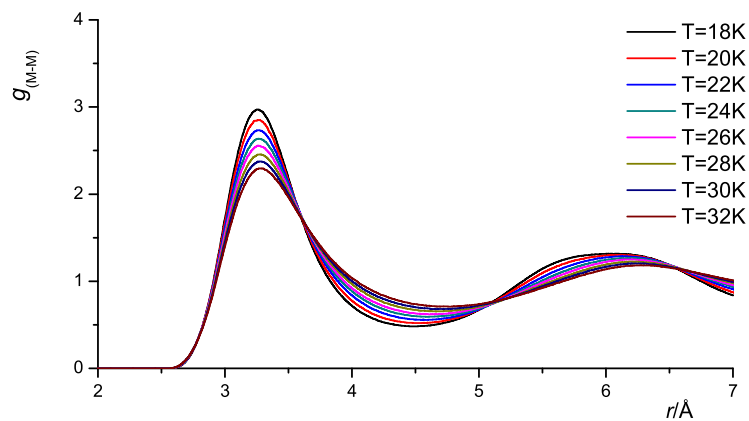
Figure 9.20: Temperature dependence of $g_{\mathrm{M-M}}$ for the liquid phase hydrogen from GEMC NVT simulation using pair potential Eq. 3.3.
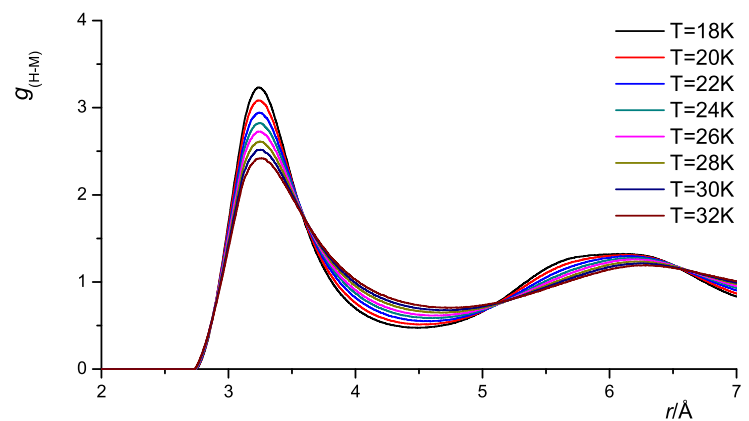
Figure 9.21: Temperature dependence of $g_{\mathrm{H-M}}$ for the liquid phase hydrogen from GEMC NVT simulation using pair potential Eq. 3.3.
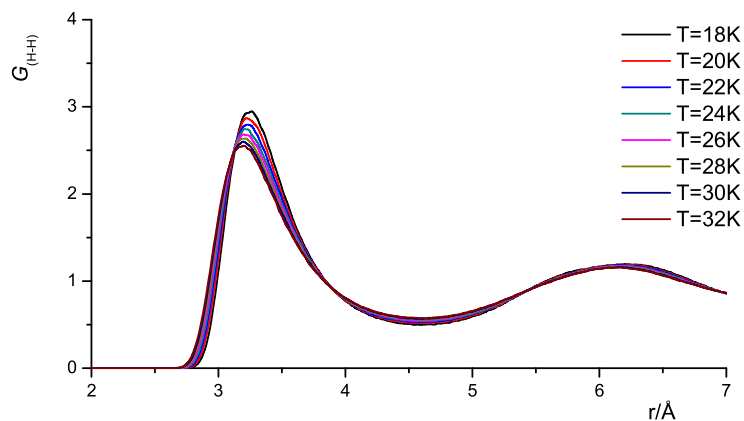
Figure 9.22: Temperature dependence of g_{H-H} for the liquid phase hydrogen from GEMC NVT simulation using pair potential Eq. 3.4.
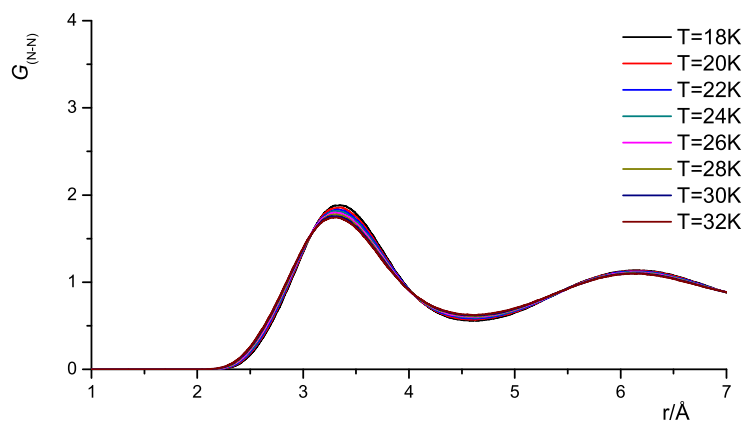
Figure 9.23: Temperature dependence of g_{N-N} for the liquid phase hydrogen from GEMC NVT simulation using pair potential Eq. 3.4.
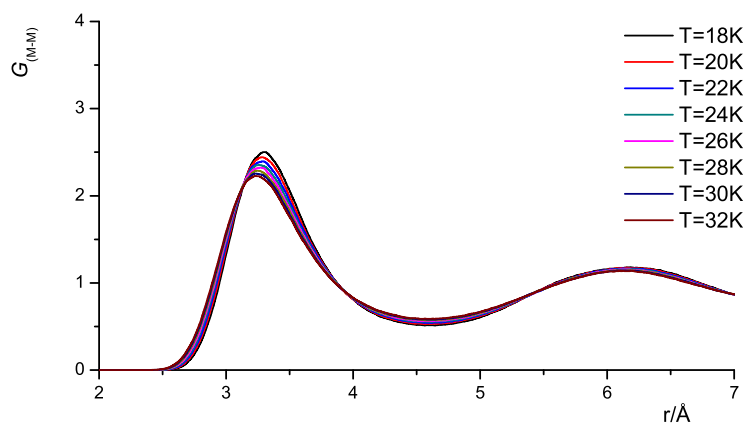
Figure 9.24: Temperature dependence of $g_{\mathrm{M-M}}$ for the liquid phase hydrogen from GEMC NVT simulation using pair potential Eq. 3.4.
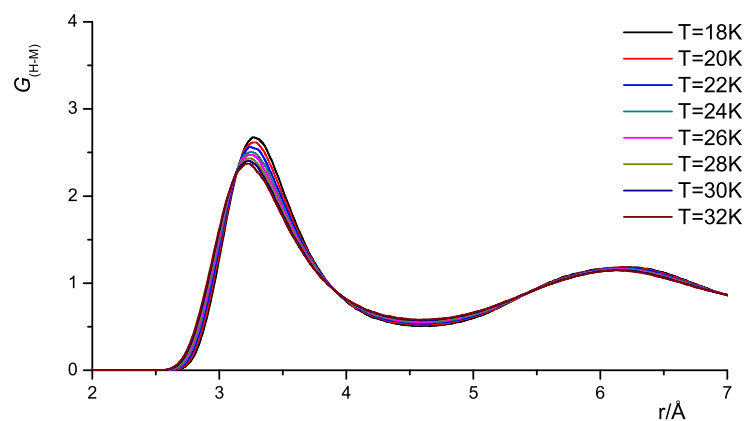

Figure 9.25: Temperature dependence of $g_{\mathrm{H-M}}$ for the liquid phase hydrogen from GEMC NVT simulation using pair potential Eq. 3.4.

Table 9.1: Density results (given in g/cm^3) for the pure liquid estimated at two pressures 1.0 MPa and 5.0 MPa for hydrogen, and 1.0 MPa and 10.0 MPa for fluorine using *ab initio* potentials, respectively; EOS : modified Benedict-Webb-Rubin equation of state [139]; exp.: experimental data [17, 76]; D1 EOS: Deiters equation of state [18].

		H$_2$-H$_2$					F$_2$-F$_2$		
T/K	method	1MPa	5MPa	ref.	T/K	method	1MPa	10MPa	ref.
	Eq. 3.3	0.06642	0.07092			Eq. 3.5	1.44592	1.47111	
	Eq. 3.4	0.07355	0.07078			Eq. 3.6	1.45897	1.53230	
26.0	EOS	0.07570	0.08110	[139]	90.0	D1 EOS	1.49650	1.52210	[18]
	Exp.	0.06442	0.07189	[76]		Exp	1.46890	1.49450	[17]
	Eq. 3.3	0.06113	0.06742			Eq. 3.5	0.04714	1.29150	
	Eq. 3.4	0.06602	0.06755			Eq. 3.6	0.03540	1.26885	
30.0	EOS	0.06340	0.07420	[139]	120.0	D1 EOS	0.04348	1.28990	[18]
	Exp.	0.05528	0.06652	[76]		Exp	0.04346	1.27160	[17]
	Eq. 3.3	0.00406	0.02349			Eq. 3.5	0.03184	0.90295	
	Eq. 3.4	0.00377	0.02564		150.0	Eq. 3.6	0.03091	0.86049	
60.0	EOS	0.00408	0.02260	[139]		D1 EOS	0.03239	0.90258	[18]
	Exp.	0.00423	0.02381	[76]		Exp	0.03235	0.91730	[17]
	Eq. 3.3	0.00175	0.01377			Eq. 3.5	0.02663	0.39237	
	Eq. 3.4	0.00215	0.01380		180.0	Eq. 3.6	0.01866	0.29157	
90.0	EOS	0.00264	0.01310	[139]		D1 EOS	0.02624	0.39667	[18]
	Exp.	0.00271	0.01359	[76]		Exp	0.02622	0.38633	[17]
	Eq. 3.3	0.00178	0.01087			Eq. 3.5	0.02183	0.27879	
120	Eq. 3.4	0.00169	0.00807		210.0	Eq. 3.6	0.02087	0.23933	
	EOS	0.00198	0.00956	[139]		D1 EOS	0.02218	0.27020	[18]
	Exp.	0.00201	0.00985	[76]		Exp	0.02218	0.26290	[17]
	Eq. 3.3	0.00094	0.00463			Eq. 3.5	0.01678	0.17592	
250	Eq. 3.4	0.00088	0.00462		270.0	Eq. 3.6	0.01880	0.19612	
	EOS	0.00095	0.00460	[139]		D1 EOS	0.01704	0.18074	[18]
	Exp.	0.00096	0.00469	[76]		Exp	0.01704	0.17872	[17]

Table 9.2: GEMC simulation results and statistical uncertainties for hydrogen calculated with the CCSD(T)/aug-cc-pV23Z extrapolated potentials Eq. 3.3; exp.: experimental data [76]; EOS : equation of state [139]; the values of parentheses are the uncertainty of the last digits obtained from the simulations, e.g., 0.0746(31) = 0.0746 ± 0.031.

T/K	method	ρ_l/gcm^{-3}	ρ_v/gcm^{-3}	μ_l/kJmol^{-1}	μ_v/kJmol^{-1}	P_l(MPa)	P_v(MPa)	H_l/kJmol^{-1}	H_v/kJmol^{-1}
18	Eq. 3.3	0.07278(31)	0.00045(10)	-2.1001(41)	-2.1065(39)	-0.0269(43)	0.0375(3)	-0.2435(54)	0.6677(3)
	EOS	0.07322	0.00069			0.0481	0.0481	-0.5581	0.3528
	Exp.	0.07320	0.00069			0.0461	0.0461	0.5038	1.4154
20	Eq. 3.3	0.07173(30)	0.00107(2)	-2.0488(43)	-2.0667(57)	-0.0183(7)	0.0703(42)	-0.1968(21)	0.7041(1)
	EOS	0.07111	0.00124			0.0933	0.0933	-0.5215	0.3788
	Exp.	0.07109	0.00125			0.0901	0.0901	0.5409	1.4410
22	Eq. 3.3	0.06943(58)	0.00191(5)	-2.0176(38)	-2.0320(63)	0.0862(11)	0.1364(31)	-0.0827(56)	0.7978(39)
	EOS	0.06873	0.00207			0.1631	0.1631	-0.4793	0.3985
	Exp.	0.06872	0.00207			0.1208	0.1208	0.5830	1.4603
24	Eq. 3.3	0.06672(40)	0.00295(85)	-2.0625(23)	-2.0692(34)	0.1726(183)	0.2465(23)	-0.0624(79)	0.7842(17)
	EOS	0.06600	0.00324			0.2641	0.2641	-0.4307	0.4102
	Exp.	0.06601	0.00325			0.2579	0.2579	0.6316	1.4712
26	Eq. 3.3	0.06358(99)	0.00442(73)	-2.0911(54)	-2.0991(73)	0.2885(525)	0.3326(314)	-0.0373(13)	0.7595(27)
	EOS	0.06280	0.00490			0.4025	0.4025	-0.3743	0.4116
	Exp.	0.06283	0.00492			0.3950	0.3950	0.6878	1.4720
28	Eq. 3.3	0.05796(3)	0.00718(62)	-2.1056(61)	-2.2641(56)	0.5411(484)	0.6196(93)	0.1833(82)	0.9085(31)
	EOS	0.05892	0.00726			0.5852	0.5852	-0.3076	0.3989
	Exp.	0.05897	0.00730			0.5770	0.5770	0.7545	1.4589
30	Eq. 3.3	0.05459(53)	0.01048(122)	-2.1231(59)	-2.1288(61)	0.7878(51)	0.8017(43)	0.0213(36)	0.6399(213)
	EOS	0.05384	0.01081			0.8199	0.8199	-0.2248	0.3632
	Exp.	0.05393	0.01089			0.8116	0.8116	0.8374	1.4230
32	Eq. 3.3	0.04748(75)	0.01654(56)	-2.1458(60)	-2.1483(58)	1.0386(68)	1.0754(75)	0.2988(37)	0.7329(28)
	EOS	0.04564	0.01750			1.1168	1.1168	-0.1046	0.2726
	Exp.	0.04599	0.01750			1.1068	1.1068	0.9569	1.3369

Table 9.3: GEMC simulation results and statistical uncertainties for hydrogen calculated with the CCSD(T)/aug-cc-pV23Z extrapolated potentials Eq. 3.4. For an explanation of the other properties see Table 9.2.

T/K	method	ρ_l/gcm^{-3}	ρ_v/gcm^{-3}	μ_l/kJmol^{-1}	μ_v/kJmol^{-1}	P_l(MPa)	P_v(MPa)	H_l/kJmol^{-1}	H_v/kJmol^{-1}
	Eq. 3.4	0.07380(84)	0.00105(23)	-2.0882(43)	-2.0922(60)	-0.0498(3)	0.0329(8)	-0.2566(10)	0.6451(36)
18	EOS	0.07322	0.00069			0.0481	0.04808	-0.5581	0.3528
	Exp.	0.07320	0.00069			0.0461	0.04610	0.5038	1.4154
	Eq. 3.4	0.07046(85)	0.00126(20)	-2.0384(40)	-2.0498(67)	-0.0109(53)	0.0578(20)	-0.2116(35)	0.6773(152)
20	EOS	0.07109	0.00125			0.0933	0.09325	-0.5215	0.3788
	Exp.	0.07109	0.00125			0.0901	0.09010	0.5409	1.4410
	Eq. 3.4	0.07025(132)	0.00231(16)	-2.0037(37)	-2.0201(63)	0.0216(31)	0.1194(39)	0.0246(43)	0.8881(491)
22	EOS	0.06873	0.00207			0.1631	0.16314	-0.4793	0.3985
	Exp.	0.06872	0.00207			0.1208	0.12080	0.5830	1.4603
	Eq. 3.4	0.06565(237)	0.00314(11)	-2.0472(35)	-2.0606(41)	0.1926(132)	0.2178(348)	-0.1259(94)	0.6956(486)
24	EOS	0.06600	0.00324			0.2641	0.26406	-0.4307	0.4102
	Exp.	0.06601	0.00325			0.2579	0.25790	0.6316	1.4712
	Eq. 3.4	0.06419(13)	0.00536(5)	-2.0899(73)	-2.0905(65)	0.3342(341)	0.3657(104)	0.0939(46)	0.8349(316)
26	EOS	0.06280	0.00490			0.4025	0.40250	-0.3743	0.4116
	Exp.	0.06283	0.00492			0.3950	0.39500	0.6878	1.4720
	Eq. 3.4	0.05813(117)	0.00670(1)	-2.0993(53)	-2.2586(45)	0.4419(65)	0.5376(354)	0.0245(41)	0.6734(25)
28	EOS	0.05892	0.00726			0.5852	0.58524	-0.3076	0.3989
	Exp.	0.05897	0.00730			0.5770	0.57700	0.7545	1.4589
	Eq. 3.4	0.05311(37)	0.01088(18)	-2.1149(60)	-2.1141(87)	0.6655(7)	0.7535(110)	0.0716(25)	0.5805(784)
30	EOS	0.05384	0.01081			0.8199	0.81989	-0.2248	0.3632
	Exp.	0.05393	0.01089			0.8116	0.81160	0.8374	1.4230
	Eq. 3.4	0.04663(35)	0.01736(14)	-2.1454(46)	-2.1321(67)	1.0166(13)	1.0352(68)	0.2014(86)	0.5108(382)
32	EOS	0.04564	0.01750			1.1168	1.11680	-0.1046	0.2726
	Exp.	0.04599	0.01750			1.1068	1.10680	0.9569	1.3369

ρ_l, ρ_v, μ_l, μ_v, ΔH_l, ΔH_v, P_l and P_v parameters of the liquid and vapor phase at the temperature, respectively.

Chapter 10

Appendix E

This appendix describes the simulation results of pure fluid fluorine using the global Gibbs ensemble simulations.

10.1 pVT data of fluid fluorine
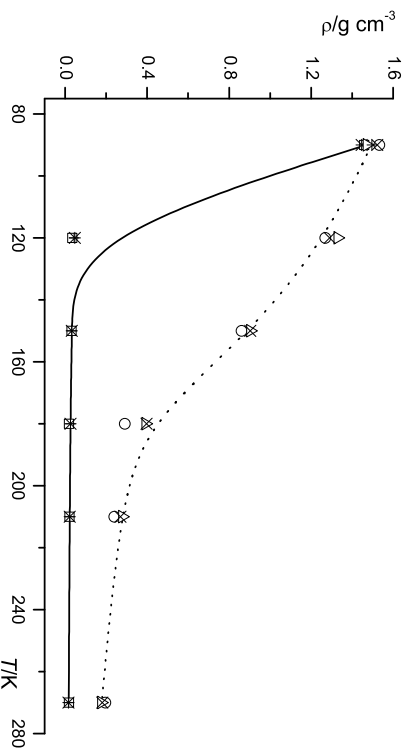
Figure 10.1: Densities of fluorine at two pressures 1.0 MPa and 10.0 MPa as a function of temperature. Experimental data [17]: —, at 1.0 MPa, and $\cdots$, at 10.0 MPa; equation of state (D1 EOS) [18]: $+$, at 1.0 MPa, and $\times$, at 10.0 MPa; calculated with Eq. 3.5 and Eq. 3.6: $\square$, and $*$, at 1.0 MPa; $\circ$, and $\triangle$, at 10 MPa.

10.2   Site-site pair distribution functions
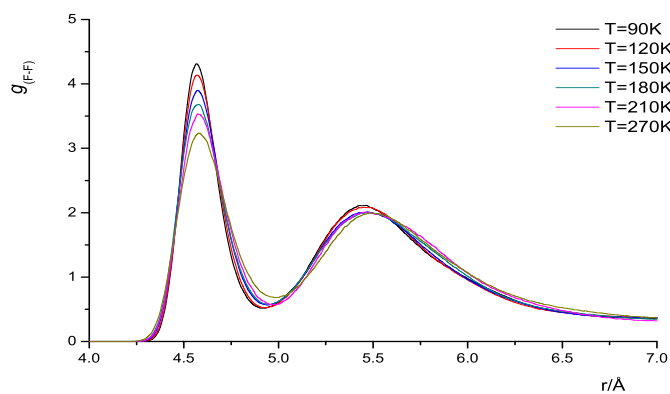
Figure 10.2:   Temperature dependence of g_{F-F} for fluorine at $P = 1.0$ MPa from GEMC NPT simulation using the pair potential Eq. 3.5.
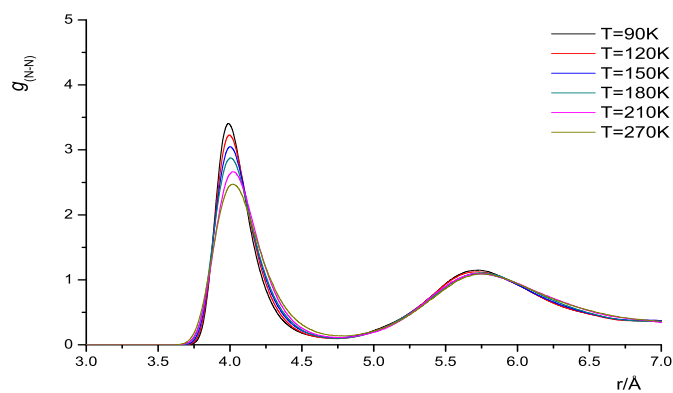
Figure 10.3:   Temperature dependence of g_{N-N} for fluorine at $P = 1.0$ MPa from GEMC NPT simulation using the pair potential Eq. 3.5.
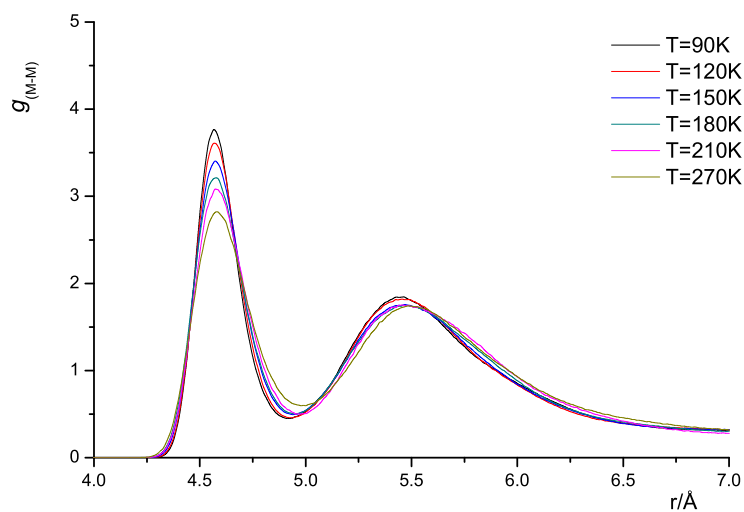
Figure 10.4: Temperature dependence of $g_{\mathrm{M-M}}$ for fluorine at $P = 1.0$ MPa from GEMC NPT simulation using the pair potential Eq. 3.5.
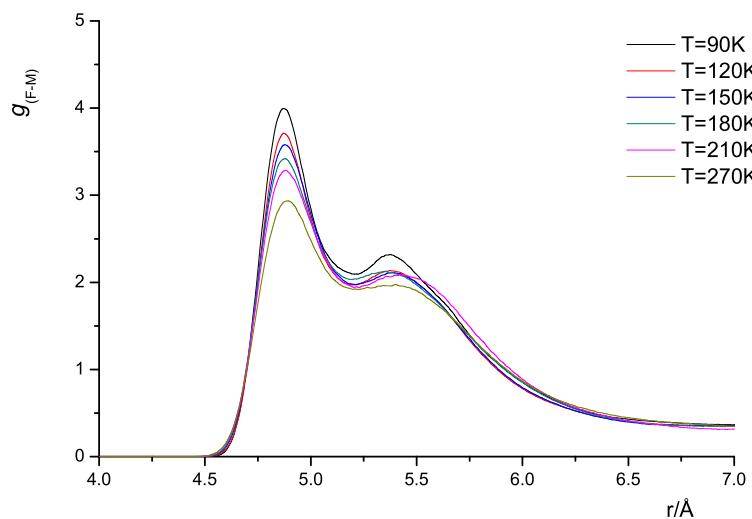
Figure 10.5: Temperature dependence of $g_{\mathrm{F-M}}$ for fluorine at $P = 1.0$ MPa from GEMC NPT simulation using the pair potential Eq. 3.5.
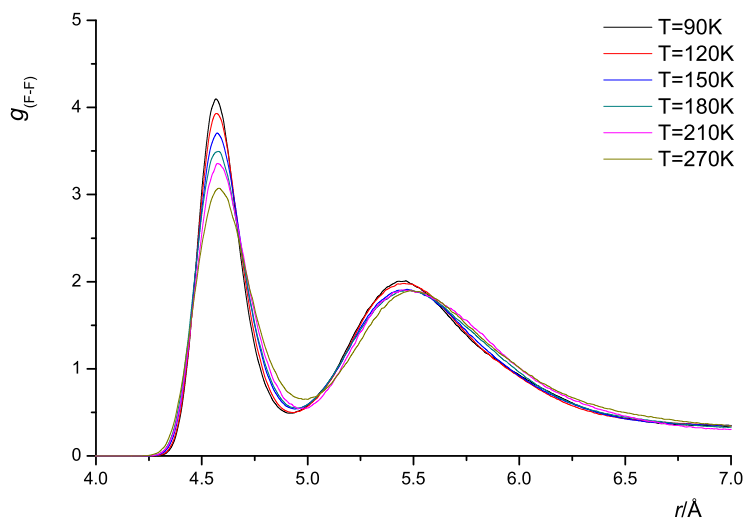
Figure 10.6:   Temperature dependence of $g_{\mathrm{F-F}}$ for fluorine at $P = 10.0$ MPa from GEMC NPT simulation using the pair potential Eq. 3.5.
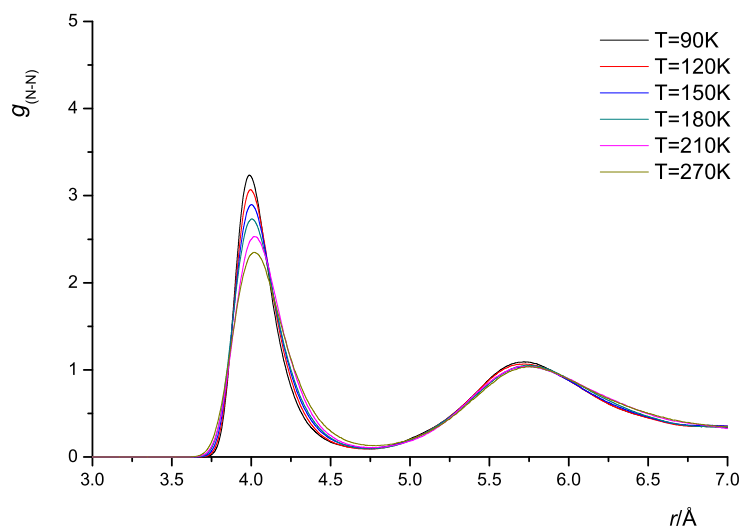
Figure 10.7:   Temperature dependence of $g_{\mathrm{N-N}}$ for fluorine at $P = 10.0$ MPa from GEMC NPT simulation using the pair potential Eq. 3.5.
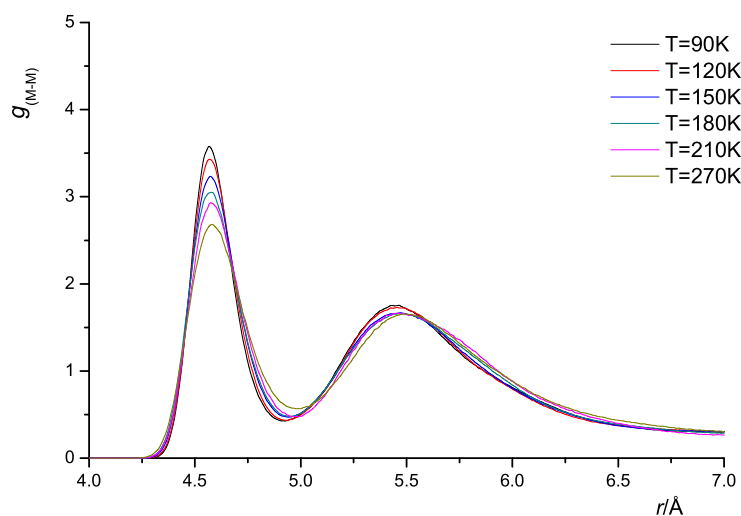
Figure 10.8: Temperature dependence of g_{M-M} for fluorine at $P = 10.0$ MPa from GEMC NPT simulation using the pair potential Eq. 3.5.
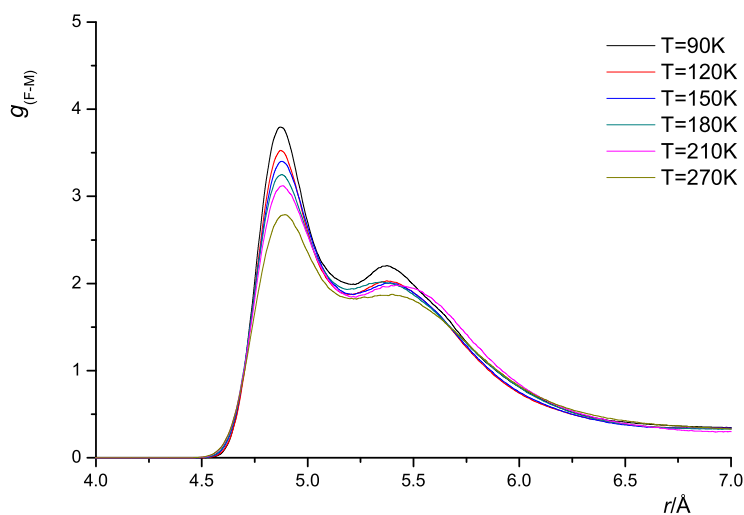

Figure 10.9: Temperature dependence of g_{F-M} for fluorine at $P = 10.0$ MPa from GEMC NPT simulation using the pair potential Eq. 3.5.
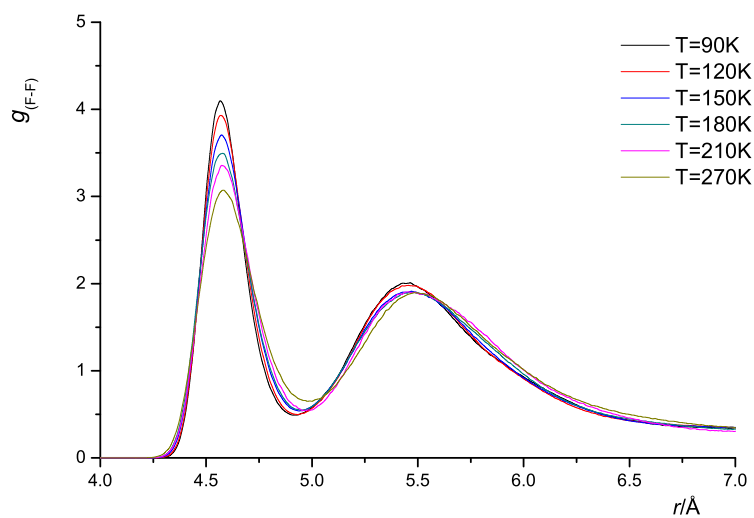
Figure 10.10:   Temperature dependence of $g_{\mathrm{F-F}}$ for fluorine at $P = 1.0$ MPa from GEMC NPT simulation using the pair potential Eq. 3.6.
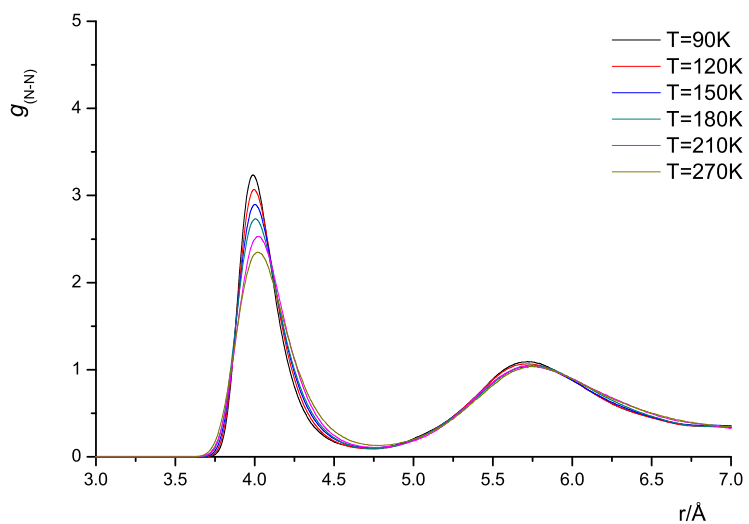
Figure 10.11:   Temperature dependence of $g_{\mathrm{N-N}}$ for fluorine at $P = 1.0$ MPa from GEMC NPT simulation using the pair potential Eq. 3.6.
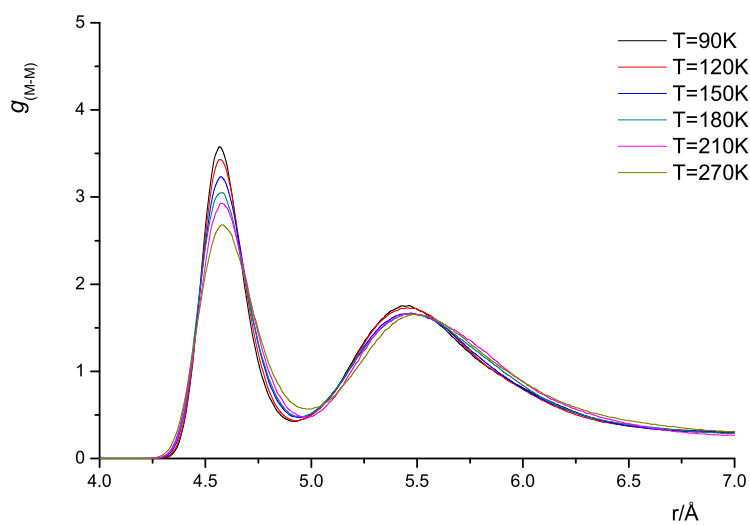
Figure 10.12: Temperature dependence of g_{M-M} for fluorine at $P = 1.0$ MPa from GEMC NPT simulation using the pair potential Eq. 3.6.
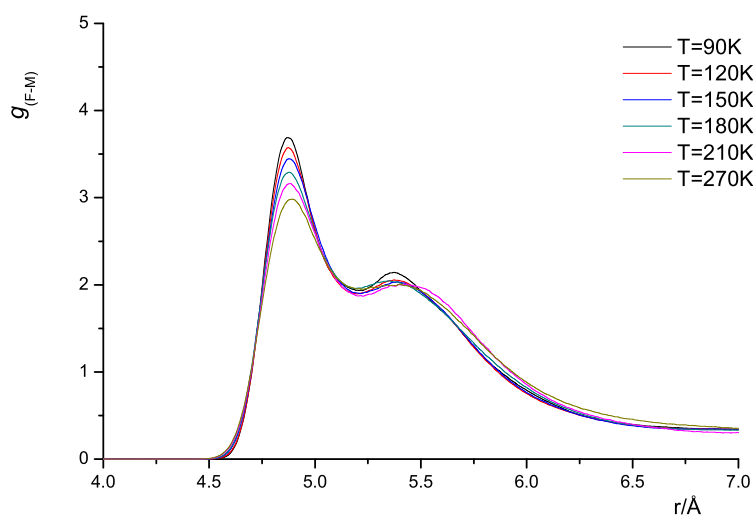

Figure 10.13: Temperature dependence of g_{F-M} for fluorine at $P = 1.0$ MPa from GEMC NPT simulation using the pair potential Eq. 3.6.
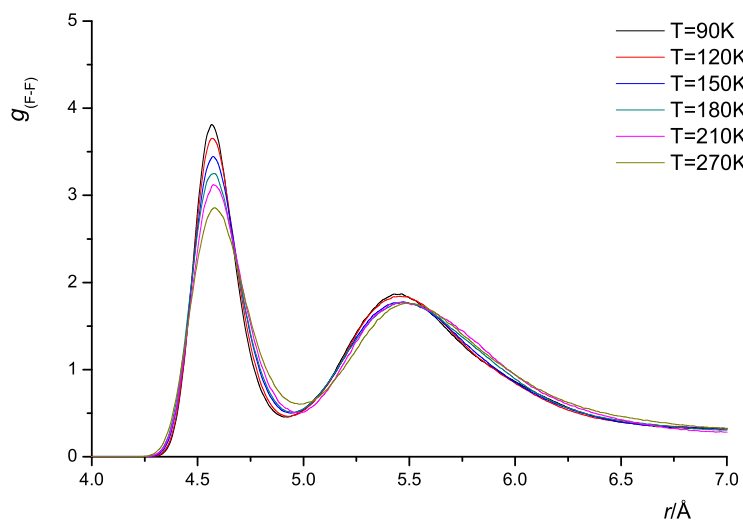
Figure 10.14: Temperature dependence of $g_{\mathrm{F-F}}$ for fluorine at $P = 10.0$ MPa from GEMC NPT simulation using the pair potential Eq. 3.6.
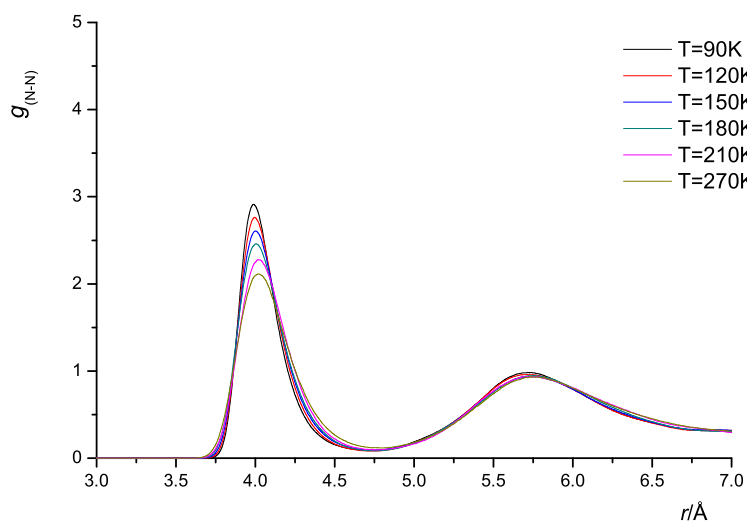
Figure 10.15: Temperature dependence of $g_{\mathrm{N-N}}$ for fluorine at $P = 10.0$ MPa from GEMC NPT simulation using the pair potential Eq. 3.6.
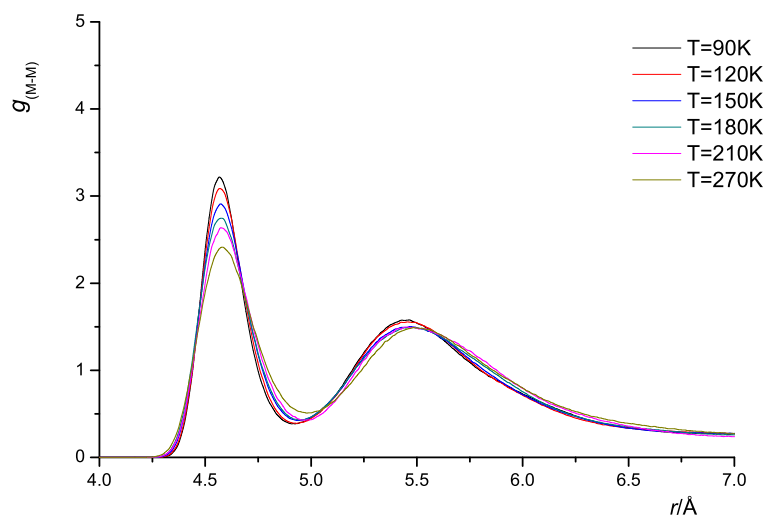
Figure 10.16: Temperature dependence of g_{M-M} for fluorine at $P = 10.0$ MPa from GEMC NPT simulation using the pair potential Eq. 3.6.
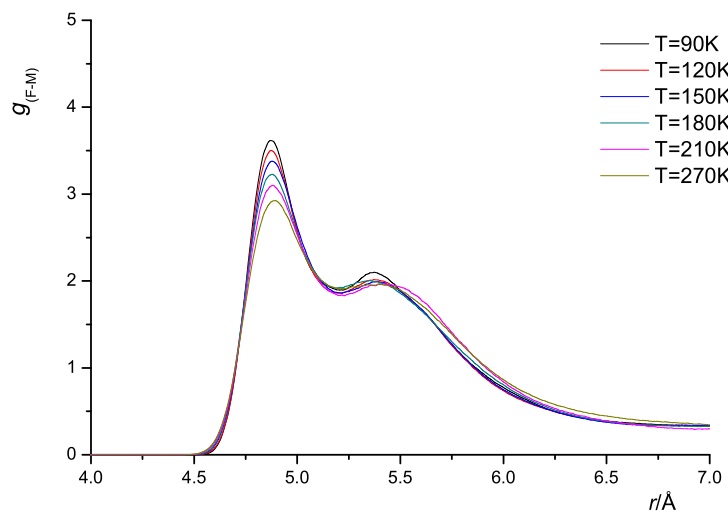


Figure 10.17: Temperature dependence of g_{F-M} for fluorine at $P = 10.0$ MPa from GEMC NPT simulation using the pair potential Eq. 3.6.
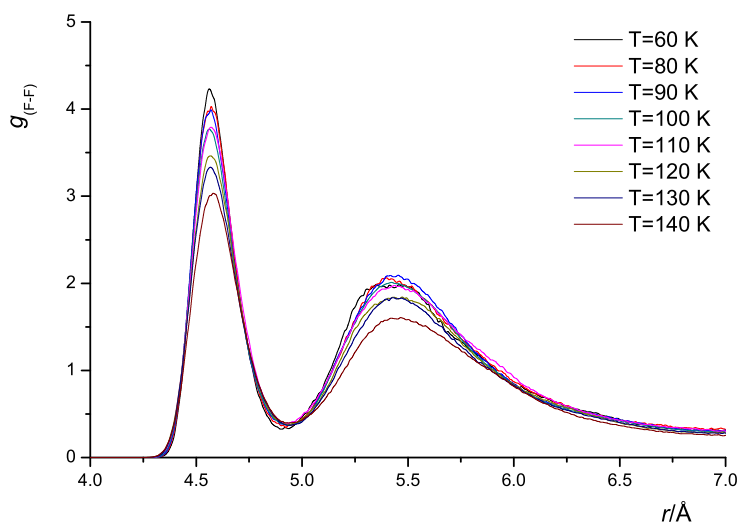
Figure 10.18:   Temperature dependence of $g_{\mathrm{F-F}}$ for the liquid phase fluorine from GEMC NVT simulation using pair potential Eq. 3.5.
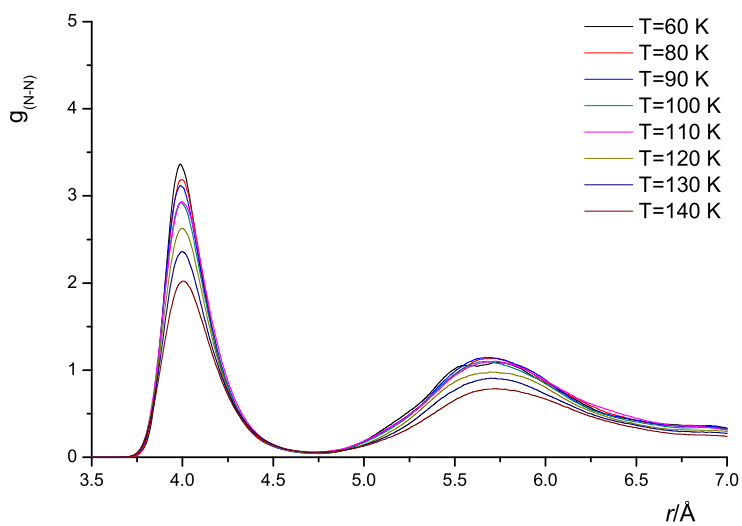
Figure 10.19:   Temperature dependence of $g_{\mathrm{N-N}}$ for the liquid phase fluorine from GEMC NVT simulation using pair potential Eq. 3.5.
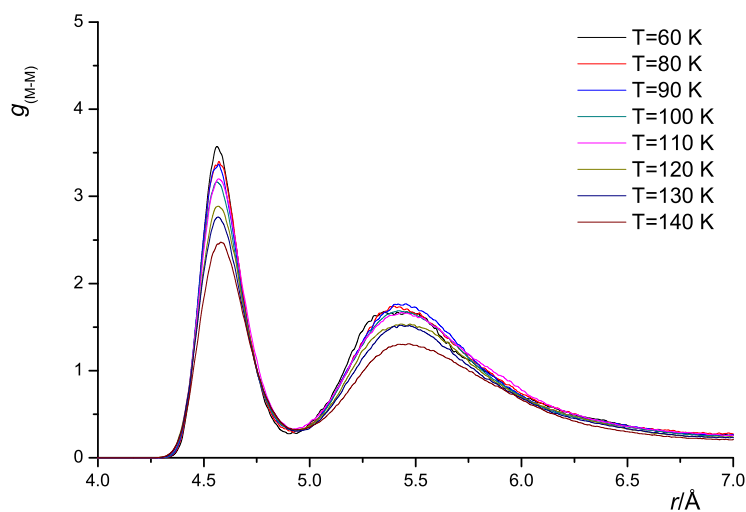
Figure 10.20: Temperature dependence of g_{M-M} for the liquid phase fluorine from GEMC NVT simulation using pair potential Eq. 3.5.
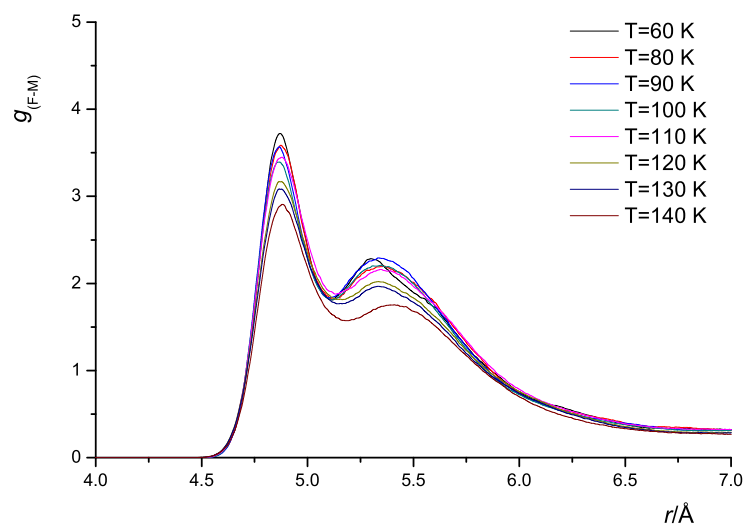
Figure 10.21: Temperature dependence of g_{F-M} for the liquid phase fluorine from GEMC NVT simulation using pair potential Eq. 3.5.
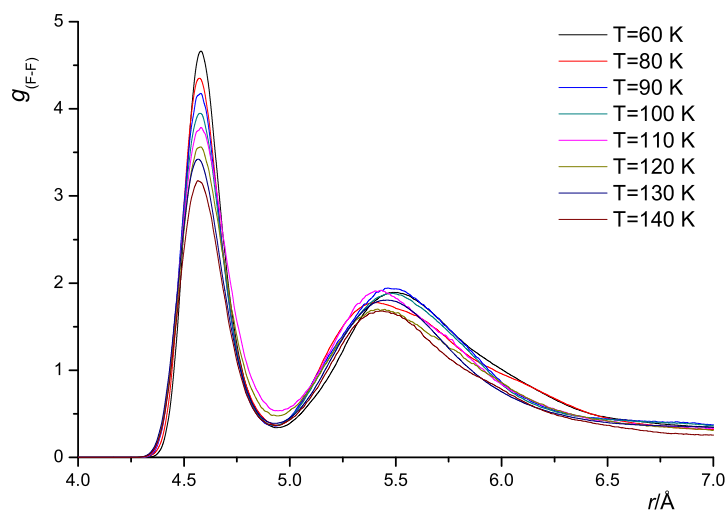
Figure 10.22:   Temperature dependence of $g_{\mathrm{F-F}}$ for the liquid phase fluorine from GEMC NVT simulation using pair potential Eq. 3.6.
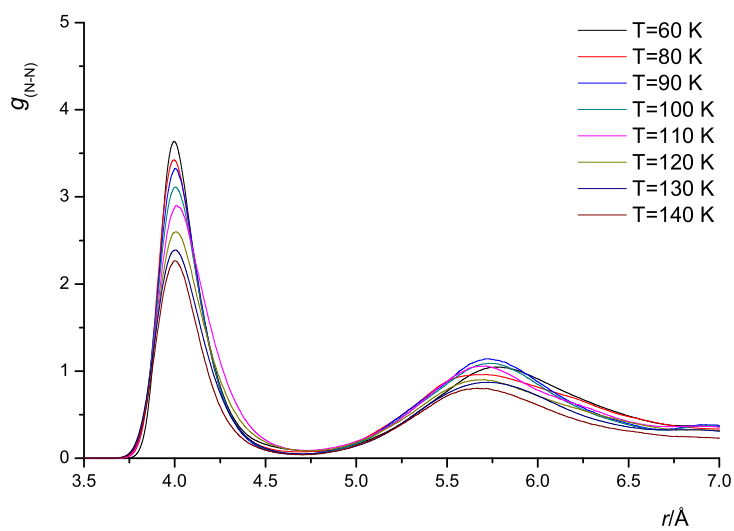
Figure 10.23:   Temperature dependence of $g_{\mathrm{N-N}}$ for the liquid phase fluorine from GEMC NVT simulation using pair potential Eq. 3.6.
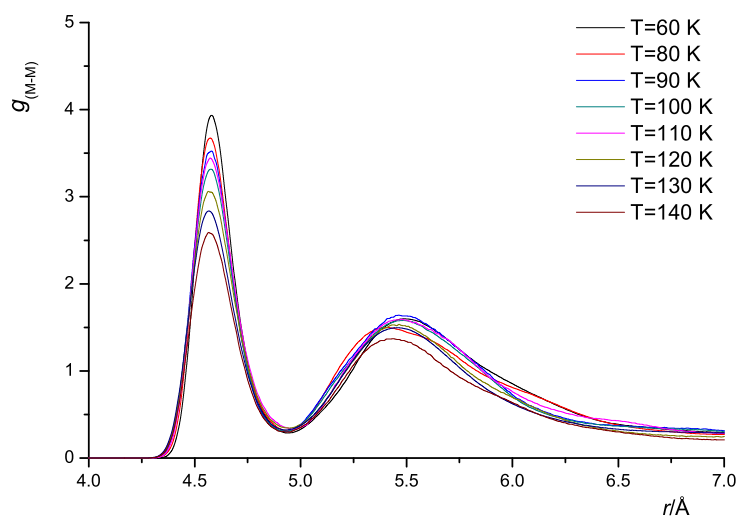
Figure 10.24: Temperature dependence of g_{M-M} for the liquid phase fluorine from GEMC NVT simulation using pair potential Eq. 3.6.
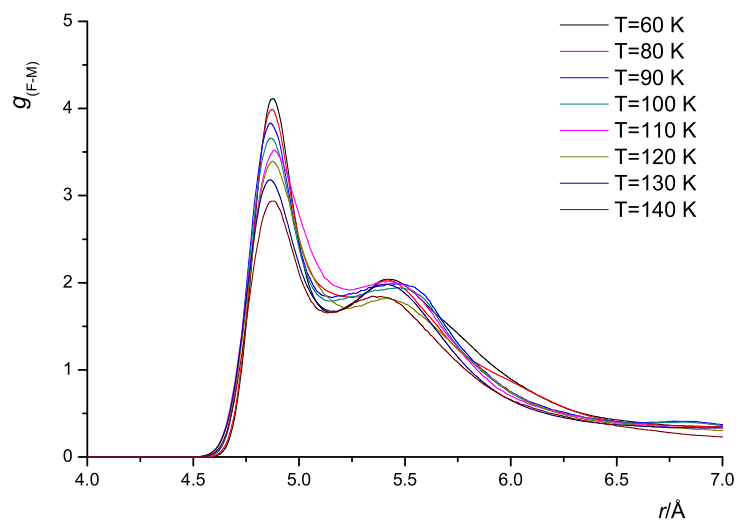
Figure 10.25: Temperature dependence of g_{F-M} for the liquid phase fluorine from GEMC NVT simulation using pair potential Eq. 3.6.

Table 10.1: GEMC simulation results and statistical uncertainties for fluorine calculated with the CCSD(T)/aug-cc-pV23Z extrapolated potentials: Eq. 3.5; D1-EOS: Deiters equation of state [18]; exp.: experimental data [17]; the values of parentheses are the uncertainty of the last digits obtained from the simulations, e.g., 1.6152(63) = 1.6152±0.063.

T/K	method	ρ_l/gcm^{-3}	ρ_v/gcm^{-3}	μ_l/kJmol^{-1}	μ_v/kJmol^{-1}	P_l(MPa)	P_v(MPa)	H_l/kJmol^{-1}	H_v/kJmol^{-1}
	Eq. 3.5	1.61519(63)	0.00019(27)	-8.8204(35)	-10.8407(60)	-0.0042(30)	0.0014(96)	-5.4496(58)	1.9787(35)
60	D1-EOS	1.72234	0.00003			0.0004	0.0004	-0.0006	
	Exp.	1.6654	0.00011			0.0015	0.0015	-14.4730	-7.0847
	Eq. 3.5	1.58789	0.00023	-8.8507	-10.9019	0.0092(10)	0.0198(51)	-4.7651(31)	2.2106(19)
70	D1-EOS	1.64554	0.00041			0.0062	0.0062	-0.0065	
	Exp.	1.6023	0.00079			0.012	0.012	-13.9130	-6.8055
	Eq. 3.5	1.51096(25)	0.00328(23)	-9.3138(31)	-10.9157(41)	0.0210(27)	0.0242(100)	-4.3515(11)	2.4944(71)
80	D1-EOS	1.57021	0.00222			0.0383	0.0383	-7.9760	
	Exp.	1.5365	0.0032			0.0547	0.0547	-13.3470	-6.5489
	Eq. 3.5	1.48944(5)	0.00477(22)	-9.4682(91)	-10.9205(61)	0.1842(11)	0.1948(82)	-2.5156(19)	3.9791(89)
90	D1-EOS	1.49391	0.00744			0.1409	0.1409	-7.3171	
	Exp.	1.4663	0.00924			0.173	0.173	-12.7710	-6.3291
	Eq. 3.5	1.39254(17)	0.02124(21)	-9.8436(35)	-10.9840(73)	0.5850(9)	0.5984(17)	0.2090(39)	6.3059(11)
100	D1-EOS	1.41382	0.0187			0.3778	0.3778	-6.7718	
	Exp.	1.39	0.02149			0.4275	0.4275	-12.1760	-6.1587
	Eq. 3.5	1.34524(41)	0.03124(61)	-10.0076(45)	-10.9921(61)	0.6001(33)	0.6025(119)	1.2867(21)	6.7036(33)
110	D1-EOS	1.3263	0.03947			0.823	0.823	-6.2783	
	Exp.	1.3052	0.04334			0.8891	0.8891	-11.5540	-6.0512
	Eq. 3.5	1.26821(69)	0.06494(15)	-10.0472(72)	-11.3155(83)	1.4848(20)	1.4919(312)	-1.2886(73)	3.2402(18)
120	D1-EOS	1.22523	0.0752			1.5563	1.5563	-5.7855	
	Exp.	1.2074	0.08017			1.6342	1.6342	-10.8850	-6.0325
	Eq. 3.5	1.13623(105)	0.12716(10)	-10.4162(45)	-11.3946(23)	2.5770(9)	2.5798(72)	1.5523(23)	5.3061(51)
130	D1-EOS	1.09674	0.13828			2.6677	2.6677	-1.0499	
	Exp.	1.0848	0.14372			2.7475	2.7475	-10.1310	-6.1654
	Eq. 3.5	0.92818(139)	0.27524(3)	-11.0212(40)	-12.9982(81)	3.8628(22)	3.8680(102)	2.3925(87)	4.9666(13)
140	D1-EOS	0.88452	0.28238			4.2882	4.2882	-4.3746	
	Exp.	0.89017	0.27828			4.3357	4.3357	-5.9299	-6.6740

Table 10.2: GEMC simulation results and statistical uncertainties for fluorine calculated with the CCSD(T)/aug-cc-pV23Z extrapolated potentials Eq. 3.6. For an explanation of the other properties see Table 10.1

T/K	method	ρ_l/gcm^{-3}	ρ_v/gcm^{-3}	μ_l/kJmol^{-1}	μ_v/kJmol^{-1}	P_l(MPa)	P_v(MPa)	H_l/kJmol^{-1}	H_v/kJmol^{-1}
	Eq. 3.6	1.69145(143)	0.00014(160)	-8.1897(52)	-9.7181(16)	-0.0185(21)	0.0013(84)	-8.8349(52)	-1.5660(84)
60	D1-EOS	1.72234	0.00003			0.0004	0.0004	-0.0006	
	Exp.	1.66540	0.00011			0.0015	0.0015	-14.4730	-7.0847
	Eq. 3.6	1.55135(23)	0.00102(40)	-8.6130(32)	-9.6250(63)	0.0370(31)	0.0397(88)	-4.1439(56)	2.5257(271)
80	D1-EOS	1.57021	0.00222			0.0383	0.0383	-7.9760	
	Exp.	1.53650	0.00320			0.0547	0.0547	-13.3470	-6.5489
	Eq. 3.6	1.45475(247)	0.00358(39)	-8.8154(43)	-9.5023(7)	0.1870(12)	0.2095(71)	-0.9748(53)	5.5354(12)
90	D1-EOS	1.49391	0.00744			0.1409	0.1409	-7.3171	
	Exp.	1.46630	0.00924			0.1730	0.1730	-12.7710	-6.3291
	Eq. 3.6	1.43215(128)	0.00975(37)	-8.8164(13)	-10.9369(73)	0.4587(35)	0.4754(14)	-2.7207(53)	3.1519(47)
100	D1-EOS	1.41382	0.01870			0.3778	0.3778	-6.7718	
	Exp.	1.39000	0.02149			0.4275	0.4275	-12.1760	-6.1587
	Eq. 3.6	1.31980(4)	0.01798(31)	-8.8441(78)	-10.0485(93)	0.6858(43)	0.6938(28)	-1.8011(71)	3.9569(10)
110	D1-EOS	1.32630	0.03947			0.8230	0.8230	-6.2783	
	Exp.	1.30520	0.04334			0.8891	0.8891	-11.5540	-6.0512
	Eq. 3.6	1.23790(157)	0.04778(24)	-9.1228(25)	-10.1876(8)	1.5565(7)	1.5745(30)	-0.9526(84)	4.1848(64)
120	D1-EOS	1.22523	0.07520			1.5563	1.5563	-5.7855	
	Exp.	1.20740	0.08017			1.6342	1.6342	-10.8850	-6.0325
	Eq. 3.6	1.11521(148)	0.11410(9)	-9.5307(51)	-10.7251(9)	2.4091(51)	2.4199(221)	-0.6153(13)	3.5110(131)
130	D1-EOS	1.09674	0.13828			2.6677	2.6677	-1.0499	
	Exp.	1.08480	0.14372			2.7475	2.7475	-10.1310	-6.1654
	Eq. 3.6	0.98638(100)	0.23747(21)	-9.9894(34)	-11.7404(7)	3.5516(37)	3.5814(199)	-2.8499(36)	-0.7263(15)
140	D1-EOS	0.88452	0.28238			4.2882	4.2882	-4.3746	
	Exp.	0.89017	0.27828			4.3357	4.3357	-1.6536	-6.6740

ρ_l, ρ_v, μ_l, μ_v, ΔH_l, ΔH_v, P$_l$ and P$_v$ parameters of the liquid and vapor phase at the temperature, respectively.

Bibliography

[1] M. Abramowitz and A. Stegun. *Handbook of Mathematical Functions*. Dover Publications, New York, 1964.

[2] European Space Agency. liquid hydrogen from http://en.wikipedia.org/wiki/Liquid-hydrogen.

[3] European Space Agency. liquid hydrogen and liquid oxygen from http://www.daviddarling.info/encyclopedia/A/Ariane.html.

[4] M. P. Allen and D. J. Tildesley. *Computer Simulation of Liquids*. Clarendon Press, Oxford, 1991.

[5] S. Bock, E. Bich, and E. Vogel. A new intermolecular potential energy surface for carbon dioxide from *ab initio* calculations. *J. Chem. Phys.*, 257:147–156, 2000.

[6] S. F. Boys and F. Bernardi. The calculation of small molecular interactions by the differences of separate total energies. Some procedures with reduced errors. *Mol. Phys.*, 19:553–566, 1970.

[7] J. López Cacheiro. Coupled cluster calculations of the ground state potential and interaction induced electric properties of the mixed dimers of helium, neon and argon. *J. Mol. Phys.*, 102:101–110, 2004.

[8] P. S. Y. Cheung and J. G. Powles. Properties of liquid-nitrogen. 4. Computer-simulation. *Mol. Phys.*, 30:921–949, 1975.

[9] P. S. Y. Cheung and J. G. Powles. Properties of liquid-nitrogen. 5. Computer-simulation with quadrupole interaction. *Mol. Phys.*, 32:1383–1405, 1976.

[10] J. Cioslowski. *Quantum-Mechanical Prediction of Thermochemical Data.* Kluwer Academic Publishers, New York, 2001.

[11] J. Cizek. Calculation of wavefunction components in ursell-type expansion using quantum-field theoretical methods. *J. Chem. Phys.*, 45:4256, 1966.

[12] CPC-X Software company. Auto2Fit v.3.0, CPC-X Software: http://www.geocities.com/neuralpower.

[13] C. J. Cramer. *Essentials of Computational Chemistry, Theories and Models.* John Wiley and Sons, New York, 2002.

[14] C. Y. David. *Computational chemistry: A Practical Guide for Applying Techniques to Real-World Problems.* John Wiley and Sons, New York, 2001.

[15] P. J. Davis and P. Rabinowitz. *Methods of Numerical Integration.* Academic Press, New York, 1984.

[16] V. P. Dawson. *Ideas into hardware, A History of the Rocket Engine Test Facility at the NASA Glenn Research Center.* National Aeronautics and Space Administration NASA, Glen Research Center, Cleveland, 2004.

[17] K. M. de Reuck. *Fluorine international thermodynamic Tables of the Fluid State, vol-11.* IUPAC Chemical Data series No. 36, Oxford, 1990.

[18] U. K. Deiters. *ThermoC* project homepage: http://thermoc.uni-koeln.de/index.html.

[19] U. K. Deiters. A new semiempirical equation of state for fluids. I. Derivation. *Chem. Eng. Sci.*, 36:1139–1146, 1981.

[20] U. K. Deiters. A new semiempirical equation of state for fluids. II. Application to pure substances. *Chem. Eng. Sci.*, 36:1146–1151, 1981.

[21] U. K. Deiters. A new semiempirical equation of state for fluids. III. Application to phase equilibria in binary mixtures. *Chem. Eng. Sci.*, 37:855–861, 1982.

[22] U. K. Deiters. A modular program system for the calculation of thermodynamic properties of fluids. *Chem. Eng. Technol.*, 23:581–584, 2000.

[23] U. K. Deiters, M. Hloucha, and K. Leonhard. Experiments? — no, thank you! In T. M Letcher, editor, *Chemistry for the 21st Century: Chemical Thermodynamics*, IUPAC Monograph Series, pages 187–195. Blackwell Science, Oxford, 1999.

[24] U. K. Deiters, M. Neichel, and E. U. Franck. Prediction of the thermodynamic properties of hydrogen-oxygen mixtures from 80 to 373 K and to 100 MPa. *Ber. Bunsenges. Phys. Chem.* 97(5):505–649, 1993.

[25] Phong Diep and J. K. Johnson. An accurate H_2–H_2 interaction potential from first principles. *J. Chem. Phys.*, 112(10):4465–4473, 2000.

[26] Phong Diep and J. K. Johnson. An accurate H_2–H_2 interaction potential from first principles. *J. Chem. Phys.*, 113(10):3480–3481, 2000.

[27] K. B. Domanski, O. Kitao, and K. Nakanishi. A new potential model for carbon-dioxide from *ab-initio* calculations. *J. Mol. Sim.*, 12:343–353, 1994.

[28] J. H. Dymond and E. B. Smith. *The Virial Coefficients of Pure Gases and Mixtures.* Clarendon Press, Oxford, 1980.

[29] R. Eggenberger, S. Gerber, H. Huber, and M. Welker. A new *ab initio* potential for the neon dimer and its application in molecular dynamics simulations of the condensed phase. *Mol. Phys.*, 82:689–699, 1994.

[30] J. F. Estela-Uribe and J. Jaramillo. Generalised virial equation of state for natural gas systems. *Fluid Phase Equilib.*, 231:84–98, 2005.

[31] J. F. Estela-Uribe, J. Jaramillo, M. A. Salazar, and J. P. M. Trusler. Virial equation of state for natural gas systems. *Fluid Phase Equilib.*, 204:169–182, 2003.

[32] R. D. Etters, R. Danilowicz, and W. England. Properties of solid and gaseous hydrogen, based upon anisotropic pair interactions. *Phys. Rev. A*, 12(5):2199–212, 1975.

[33] P. L. Fast, M. L. Sanchez, and D. G. Truhlar. Infinite basis limits in electronic structure theory. *J. Chem. Phys.*, 111:2921–2926, 1999.

[34] J. B. Foresman and A. Frisch. *Exploring Chemistry with Electronic Structure Methods.* Second Edition, Gaussian, Wallingford, 1996.

[35] D. Frenkel. *Understanding Molecular Simulation, A Division of Harcourt.* Academic Press, London, 2002.

[36] E. Frischmand and et al. *GAUSSIAN 03, Revision B.02, Gaussian.* Wallingford, USA, 2003.

[37] S. L. Garrison and S. I. Sandler. On the use of *ab initio* interaction energies for the accurate calculation of thermodynamic properties. *J. Chem. Phys.*, 117:10571–10580, 2002.

[38] D. A. Goldberg. *Genetic Algorithms in Search, Optimization, and Machine Learning.* Addison-Wesley, 1989.

[39] M. Head Gordon. Quantum chemistry and molecular processes. *J. Phys. Chem.*, 100:13213–13225, 1996.

[40] C. G. Gray and K.E. Gubbins. *Theory of Molecular Fluids, vol. 1: Fundamentals.* Oxford University Press, Oxford, 1984.

[41] T. Haarmann and W. Koschel. Numerical simulation of heat loads in a cryogenic H_2/O_2 rocket combustion chamber. *PAMM (Proc. Appl. Math. Mech.)*, 2:360–361, 2003.

[42] J. G. Hayden and J. P. O' Connell. A generalized method for predicting second virial coefficients. *Ind. Eng. Chem. Process Des. Dev.*, 14(3):209–216, 1975.

[43] T. Helgaker, P. Jorgensen, and J. Olsen. *Molecular Electronic - Structure Theory.* John Wiley and Sons, New York, 2000.

[44] A. Hinchliffe. *Modelling Molecular Structures.* John Wiley and Sons, New York, 2000.

[45] J. O. Hirschfelder, C. F. Curtiss, and R. B. Bird. *Molecular Theory of Gases and Liquids.* John Wiley, New York, 1954.

[46] J. Hord. *Is Hydrogen Safe?* Department of Commerce, USA, Washington, 1976.

[47] K. P. Huber and G. Herzberg. *Molecular Spectra and Molecular Structure IV: Spectroscopic Constants of Diatomic Molecules*. Van Nostrand Reinhold, New York, 1979.

[48] F. Jensen. *Introduction to Computational Chemistry*. John Wiley and Sons, New York, 1999.

[49] B. Jeziorski and W. Kolos. *in Molecular Interactions*. Wiley, New York, 1982.

[50] B. Jeziorski and W. Kolos. Intermolecular interactions. *J. Quantum. Chem.*, 12:91, 1997.

[51] T. H. Dunning Jr. Gaussian basis functions for use in molecular calculations. I. Contraction of (9s5p) atomic basis sets for the first-row atoms. *J. Chem. Phys.*, 53:2823, 1970.

[52] T. H. Dunning Jr. Gaussian basis sets for use in correlated molecular calculations. I. The atoms boron through neon and hydrogen. *J. Chem. Phys.*, 90:1007–1023, 1989.

[53] T. H. Dunning Jr and D. E. Woon. Gaussian basis sets for use in correlated molecular calculations. IV. Calculation of static electrical response properties. *J. Chem. Phys.*, 100:2975–2988, 1994.

[54] R. A. Kendall, T. H. Dunning Jr, and R.J. Harrison. Electron affinities of the first-row atoms revisited. systematic basis sets and wave functions. *J. Chem. Phys.*, 96:6796–6806, 1992.

[55] W. Klopper. *Modern Methods and Algorithms of Quantum Chemistry*. Edited by J. Grotendorst, NIC series, John-von-Neumann Institute for Computing, Juelich, 2000.

[56] T. Korona, H. L. Williams, R. Bukowski, B. Jeziorski, and K. Szalewicz. Helium dimer potential from symmetry-adapted perturbation theory calculations using large gaussian geminal and orbital basis sets. *J. Chem. Phys.*, 106:5109–5122, 1997.

[57] J. A. Krumhansl and S. Y. Wu. Quantum theory of the equation of state for solid hydrogen. *Phys. Rev. B*, 5(10):4155–4170, 1972.

[58] L. J. Krzycki. *How to design, build and test small liquid-fuel rocket engines.* Rocketlab, Oregon, 1967.

[59] E. Larry. Homebrew fuel cell and hydrogen electrolyser. *Home Power*, 85:52–59, 2001.

[60] A. R. Leach. *Molecular Modelling Principles and Applications.* Edinburgh Gate, United Kingdom, 2001.

[61] B. I. Lee and M. G. Kesler. Generalized thermodynamic correlation based on 3-parameter corresponding states. *AIChE. J*, 21:510–527, 1975.

[62] M. L. Leininger, W. D. Allen, H. F. Schaefer, and C. D. Sherrill. Is Møller-Plesset perturbation theory a convergent *ab initio* method ? *J. Chem. Phys.*, 112:9213–922, 2000.

[63] J. E. Lennard-Jones. *Proc. Royal. Soc.*, 106:463, 1924.

[64] K. Leonhard and U. K. Deiters. Monte Carlo simulations of neon and argon using *ab initio* potentials. *Mol. Phys.*, 98:1603–1616, 2000.

[65] K. Leonhard and U. K. Deiters. Monte Carlo simulations of nitrogen using an *ab initio* potential. *Mol. Phys.*, 100:2571–2585, 2002.

[66] D. R. Lide. *Handbook of Chemistry and Physics, CRC Press, 82nd Edition.* Boca Raton, 2002.

[67] A. N. Lowan. Table of the zeros of the Legendre polynomials of order 1-16 and the weight coefficients for Gauss mechanical quadrature formula. *Bull. Amer. Math. Soc.*, 48:739–743, 1942.

[68] D. E. Makarov and H. Metiu. Fitting potential-energy surfaces: A search in the function space by directed genettic programming. *J. Chem. Phys.*, 2:590–598, 1998.

[69] A. Malijevský. Monte Carlo simulations of thermodynamic properties of argon, krypton and xenon in liquid and gas state using new *ab initio* pair potentials. *Mol. Phys.*, 101:3335–3340, 2003.

[70] J. J. Martin. Cubic equations of state — which. *Ind. Eng. Chem. Fundam.*, 18(2):81–97, 1979.

[71] M. G. Martin and J. I. Siepmann. Calculating Gibbs free energies of transfer from Gibbs ensemble Monte Carlo simulations. *Theor. Chem. Acc.*, 99:347–350, 1998.

[72] M. G. Martin and J. I. Siepmann. Novel configurational-bias Monte Carlo method for branched molecules. Transferable potentials for phase equilibria. 2. United-atom description of branched alkanes. *J. Phys. Chem.*, B 103:4508–4517, 1999.

[73] P. M. Mathias. The second virial coefficient and the Redlich-Kwong equation. *Ind. Eng. Chem. Res.*, 42:7037–7044, 2003.

[74] R. D. McCarty. *Hydrogen Technological Survey — Thermophysical Properties.* NASA Lewis Research Center, Washington, October 1975.

[75] R. D. McCarty, J. Hord, and H. M. Roder. *Selected Properties of Hydrogen (Engineering Design Data).* Department of Commerce, USA, Washington, 1981.

[76] R. D. McCarty and L. A. Weber. *Thermophysical properties of parahydrogen from the freezing liquid line to 5000 °R for pressures to 10000 PSia.* Government Printing Office, Washington, 1972.

[77] C. McKinley and J. Brewer. *Adv. Cryogen. Eng.*, 7:114–124, 1961.

[78] N. Metropolis, M. Rosenbluth A. Rosenbluth, and A. Teller. Equation of state calculations by fast computing machines. *J. Chem. Phys.*, 21:1087–1092, 1953.

[79] A. M. Michels, W. de Graaf, and C. A. ten Seldam. Virial coefficients of hydrogen and deuterium at temperatures between -175 °C and +150 °C conclusion from the 2nd virial coefficient with regards to the intermolecular potential. *Physica*, 26:393, 1960.

[80] K. K. Mon and K. Binder. Finite size effects for the simulation of phase coexistence in the Gibbs ensemble near the critical point. *J. Chem. Phys.*, 96:6989–95, 1992.

[81] P. M. Morse. Diatomic molecules according to the wave mechanics. II. Vibrational levels. *Phys. Rev.*, 34:57–64, 1929.

[82] S. Nagel, R. Redmer, G. Röpke, M. Knaup, and C. Toepfer. Proton-proton pair distribution in dense fluid hydrogen. *Phys. Rev.*, 57:5572–5577, 1998.

[83] P. K. Naicker, A. K. Sum, and S. I. Sandler. *Ab initio* pair potential and phase equilibria predictions for hydrogen chloride. *J. Chem. Phys.*, 118:4086–4093, 2003.

[84] A. E. Nasrabad and U. K. Deiters. Prediction of thermodynamic properties of krypton by Monte Carlo simulation using *ab initio* interaction potentials. *J. Chem. Phys.*, 119:947–952, 2003.

[85] A. E. Nasrabad, R. Laghaei, and U. K. Deiters. Prediction of the thermophysical properties of pure neon, pure argon, and the binary mixtures neon–argon and argon–krypton by Monte Carlo simulation using *ab initio* potentials. *J. Chem. Phys.*, 121:6423–6434, 2004.

[86] S. K. Nath and J. J. de Pablo. Simulation of vapour-liquid equilibria for branched alkanes. *Mol. Phys.*, 98:231–238, 2000.

[87] S. K. Nath, F. A. Escobedo, and J. J. de Pablo. On the simulation of vapor-liquid equilibria for alkanes. *J. Chem. Phys.*, 108:9905–9911, 1998.

[88] M. R. Noorbala and H. Sabzyan. A MP2/6-31G* intermolecular potential energy surface for the F_2–F_2 system. *J. Mol. Structure (Theochem)*, 678:67–76, 2004.

[89] R. T. Pack. First quantum correction to second virial coefficients for anisotropic interactions: simple, corrected formula. *J. Chem. Phys.*, 78:7217–7222, 1983.

[90] A. Z. Panagiotopoulos. Computational Methodologies and Potentials for Phase Equilibria project homepage: http://kea.princeton.edu /ppe/index.html.

[91] A. Z. Panagiotopoulos. Direct determination of phase coexistence properties of fluids by Monte Carlo simulation in a new ensemble. *Mol. Phys.*, 61:813–826, 1987.

[92] A. Z. Panagiotopoulos. Monte Carlo methods for phase equilibria of fluids. *J. Phys. Condensed Matter*, 12:25–52, 2000.

[93] A. Z. Panagiotopoulos, M. Baus, L. R. Rull, and J. P. Ryckaert. *Gibbs Ensemble Techniques in Observation, Prediction and Simulation of Phase Transitions in Complex Fluids, NATO ASI Series C*, volume 460. Kluwer Academic Publishers, Dordrecht, 1994.

[94] A. Z. Panagiotopoulos, N. Quirke, M. Stapleton, and D. J. Tildesley. Phase equilibria by simulation in the Gibbs ensemble. Alternative derivation, generalization and application to mixture and membrane equilibria. *Mol. Phys*, 63:527–545, 1988.

[95] W. R. Parrish, R. O. Voth, J. G. Hust, T. M. Flynn, C. F. Sindt, and N. A. Olien. *Selected Topics on Hydrogen Fuel.* Department of Commerce, USA, Washington, 1975.

[96] S. V. Patrick, R. Liapine, B. Kirchner, J. D. Anthony, H. Huber, G. Marcellib, and J. S. Richard. Molecular simulation of the vapour-liquid phase coexistence of neon and argon using *ab initio* potentials. *Phys. Chem. Chem. Phys*, 3:1297–1302, 2001.

[97] H. Popkie, H. Kistenmacher, and E. Clementi. Study of the structure of molecular complexes. IV. The Hartree-Fock potential for the water dimer and its application to the liquid state. *J. Chem. Phys.*, 59:1325–1336, 1973.

[98] K. Raghavachari and J. B. Anderson. Electron correlation effects in molecules. *J. Phys. Chem.*, 100:12960–12973, 1996.

[99] A. Ralston. *A First Course in Numerical Analysis.* McGraw-Hill, New York, 1964.

[100] J. R. Recht and A. Z. Panagiotopoulos. Finite-size effects and approach to criticality in Gibbs ensemble simulations. *Mol. Phys.*, 80:843–852, 1993.

[101] J. R. Recht and A. Z. Panagiotopoulos. Molecular simulation of phase coexistence: Finite -size effects and determination of critical parameters for two- and three dimensional Lennard-Jones fluids. *Int. J. Thermophys.*, 15:1057–1072, 1994.

[102] C. R. Robert, J. M. Prausnitz, and T. K. Sherwood. *The Properties of Gases and Liquids.* McGRaw-Hill, New York, 1977.

[103] H. M. Roder. *The Thermodynamic Properties of Slush Hydrogen and Oxygen.* NBSIR 77-859. National Bureau, Boulder, 1977.

[104] J. S. Rowlinson and F. L. Swinton. *Liquids and Liquid Mixture, 3rd Ed.* Butterworth, London, 1982.

[105] H. Sabzyan and M. R. Noorbala. Basis set effects on the intermolecular interaction of the F_2–F_2 system. *J. Mol. Structure (Theochem)*, 636:185–193, 2003.

[106] A. D. Santis, A. Gregson, and D. Rocca. Models of orientational correlations in fluids: applications to liquid fluorine. *J. Phys. Condens. Matter*, (7):483–497, 1995.

[107] B. Smit. *Computer Simulation in Chemical Physics, NATO ASI Ser. C*, volume 397. Kluwer Academic Publishers: Dordrecht, 1993.

[108] B. Smit, Ph. de Smedt, and D. Frenkel. Computer simulations in the Gibbs ensemble. *Mol. Phys.*, 68:931–50, 1989.

[109] B. Smit and D. Frenkel. Calculation of the chemical potential in the Gibbs Ensemble. *Mol. Phys.*, 68:951–8, 1989.

[110] B. Smit, S. Karaborni, and J. I. Siepmann. Computer simulations of vapor-liquid equilibria of n-alkanes. *Chem. Phys.*, 102:2126, 1995.

[111] B. Smit and C. P. Williams. Vapour-liquid equilibria for quadrupolar Lennard-Jones fluids. *J. Phys. Condens. Matter*, 2:4281–4288, 1990.

[112] T. Spyriouni, I. G. Economou, and D. N. Theodorou. Molecular simulation of the pure n-hexadecane vapor-liquid equilibria at elevated temperature. *Macromolecules*, 31:1430 – 1431, 1998.

[113] W. Squire. *Integration for Engineers and Scientists.* Elsevier, New York, 1970.

[114] A. Stone. *Intermolecular Forces.* Clarendon Press, Oxford, 2004.

[115] G. C. Straty and R. Prydz. The vapor pressure of liquid fluorine. *Adv. Cryog. Eng.*, 15:36–41, 1970.

[116] D. R. Stull. Vapor pressure of pure substances organic compounds. *Ind. Eng. Chem.*, 39:517–540, 1947.

[117] A. K. Sum and S. I. Sandler. *Ab initio* pair potentials and phase equilibria predictions of halogenated compounds. *Fluid Phase Equilib.*, 199:5–13, 2002.

[118] A. K. Sum, S. I. Sandler, and P. K. Naicker. *Ab initio* pair potential and phase equilibria predictions for the refrigerant methyl fluoride. *Mol. Phys.*, 100:2433–2447, 2002.

[119] L. E. Sutton and H. J. Bowen. *Tables of interatomic distances and configuration in molecules and ions: 1956-1959.* Number 18 in Special publication, Royal Chemical Society, London, 1965.

[120] K. Szalewicz and B. Jeziorski. *Symmetry-Adapted Perturbation Theory of Intermolecular Interactions, in S. Scheiner (Ed.), Molecular Interactions.* Wiley, New York, 1997.

[121] K. T. Tang and J. P. Toennies. An improved simple model for the van der waals potential based on universal damping functions for the dispersion coefficients. *J. Chem. Phys.*, 80:3726–3741, 1984.

[122] S. D. Tse, D. L. Zhu, and C. K. Law, editors. *Morphology and Burning Rates of Expanding Spherical Flames in H_2/O_2 /Inert Mixtures up to 60 Atmospheres*, volume 76. NASA Glenn Research Center, London, 2000.

[123] P. Ungerer, C. Beauvais, and J. Delhommelle. Optimization of the anisotropic united atoms intermolecular potential for n-alkanes. *J. Chem. Phys.*, 112:5499–5510, 2000.

[124] A. van Itterbeek and W. van Doninck. Measurements on the velocity of sound in mixtures of hydrogen, helium, oxygen, nitrogen and carbon monoxide at low temperatures. In *Proc. Phys. Soc., London*, number Sect. B, 1949.

[125] A. van Itterbeek, O. Verbeke, F. Theewes, K. Staes, and J. de Boelpaep. The difference in vapour pressure between normal and equilibrium hydrogen.

Vapour pressure of normal hydrogen between 20 K and 32 K. *Physica*, 30:1238–1244, 1964.

[126] M. Venkatraj, C. Bratschi, H. Huber, and R. J. Gdanitz. Monte Carlo simulations of vapor-liquid equilibria of neon using an accurate *ab initio* pair potential. *Fluid Phase Equilib.*, 218:285–289, 2004.

[127] F. Vesely. *Computerexperimente an Flüssigkeiten*. Physik Verlag, Weinheim, 1978.

[128] A. Vetere. An improved method to predict second virial coefficients of pure compounds. *Fluid Phase Equilib.*, 164:49–59, 1999.

[129] A. Vetere. An improved method to predict second cross virial coefficients. *Fluid Phase Equilib.*, 204:15–20, 2005.

[130] G. W. M. Vissers, A. Hesselmann, G. Jansen, P. E. S. Wormer, and A. van der Avoird. New CO-CO interaction potential tested by rovibrational calculations. *J. Chem. Phys.*, 122:54306, 2005.

[131] Q. Wang, J. K. Johnson, and J. Q. Broughton. Thermodynamic properties and phase equilibrium of fluid hydrogen from path integral simulations. *Mol. Phys.*, 89:1105–1119, 1996.

[132] W. F. Wang. Atomic potential parameters for H_2 and D_2: quantum corrections in the calculation of second-virial coefficients. *J. Quanti. Spectr. and Radia. Tran.*, 76:23–30, 2003.

[133] B. Widom. Some topics in theory of fluids. *J. Chem. Phys.*, 39(11):2808, 1963.

[134] F. C. Wiliam, F. R. Luiz, R. Gargano, and M. S. Geraldo. Fitting potential energy surface of reactive system via genetic algorithm. *Comput. Physics, eprint arXiv:physics/0511131*, 1:1–10, 2005.

[135] H. P. William, S. A. Teukolsky, T. V. William, and B. P. Flannery. *Numerical Recipes in C: The Art of Scientific Computing*. Cambridge, New York, 1992.

[136] D. E. Winterbone. *Advanced Thermodynamics for Engineers*. John Wiley and Sons. New York, 1997.

[137] P. E. S. Wormer. Second virial coefficients of asymmetric top molecules. *J. Chem. Phys.*, 122:184301–184307, 2005.

[138] P. Sun Yong and J. Shin Lee. Basis set limit binding energies of dimers derived from basis set convergence of monomer energies. *J. Chem. Phys.*, 116:5389–5394, 2002.

[139] B. A. Younglove. Thermophysical properties of fluids. I. argon, ethylene, parahydrogen, nitrogen, nitrogen trifluoride, and oxygen. *J. Phys. Chem. Ref. Data*, 11(1):1–161, 1980.

Erklärung

Ich versichere, dass ich die von mir vorgelegte Dissertation selbständig angefertigt, die benutzten Quellen und Hilfsmittel vollständig angegeben und die Stellen der Arbeit - einschließlich Tabellen, Karten und Abbildungen -, die anderen Werken im Wortlaut oder dem Sinn nach entnommen sind, in jedem Einzelfall als Entlehnung kenntlich gemacht habe; dass diese Dissertation noch keiner anderen Fakultät oder Universität zur Prüfung vorgelegen hat; dass sie noch nicht veröffentlicht worden ist sowie, dass ich eine solche Veröffentlichung vor Abschluss des Promotionsverfahrens nicht vornehmen werde. Die Bestimmungen der Promotionsordnung sind mir bekannt. Die von mir vorgelegte Dissertation ist von Prof. Dr. U. K. Deiters betreut worden.

Name: Tat Pham Van

Köln, Datum . . . . Unterschrift: . . . .

Lebenslauf

Name: Tat Pham Van; Vorname: Tat
Geschlecht: Männlich
Geburstsdatum: 30 . 11. 1966
Geburstort: Namdinh, Vietnam
Familienstand: Verheiratet
Deutschland e-mail: phamvant@uni-koeln.de

Ausbildung

Promotion: Von Juni. 2004 bis Dez. 2006
Institut für Physikalische Chemie
Universität zu Köln, Deutschland
Betreuer: Prof Dr. U. K. Deiters
Titel der Dissertation:"*Ab initio* calculation of intermolecular potentials, prediction
of second virial coefficients for dimers H_2-H_2, H_2-O_2, F_2-F_2 and H_2-F_2, and Monte
Carlo simulations of the vapor-liquid equilibria for hydrogen and fluorine"

M. Sc. (Diplom): Von Sept. 2000 bis Dez. 2002
Chemistry Department Faculty of Science
University of Dalat
Dalat, Vietnam
Betreuer: Prof. Dr. Dang Van Giap
Titel der Diplomarbeit: "Quantitative structure activity relationships (QSAR) of a
set of anti-cancer flavonoid compounds"

B. Sc: Von Sept. 1984 bis July. 1989; National University of Hanoi, Vietnam.